RADAR CHARACTERISTICS OF TORNADIC AND NON-TORNADIC QUASI-LINEAR CONVECTIVE SYSTEMS OVER THE CENTRAL UNITED STATES

A Thesis Presented to the Faculty of the Graduate School at the University of Missouri

In Partial Fulfillment of the Requirements for the Degree of Masters of Science

by

SARAH GRANA

Dr. Neil Fox, Thesis Advisor

JULY 2014

The undersigned, appointed by the dean of the Graduate School, have examined the thesis entitled

RADAR CHARACTERISTICS OF TORNADIC AND NON-TORNADIC QUASI-LINEAR CONVECTIVE SYSTEMS OVER THE CENTRAL UNITED STATES

Presented by Sarah Grana,

a candidate for the degree of master of science,

and hereby certify that, in their opinion, it is worthy of acceptance.

_____

Associate Professor Neil Fox

_____

Professor Patrick Market

_____

Professor Anthony Lupo

_____

Associate Professor Allen Thompson

ACKNOWLEDGEMENTS

I would like to start off by thanking Dr. Patrick Market, Dr. Anthony Lupo, and especially Dr. Neil Fox for all they have taught me, their guidance, and for all of the help they have given me over the past five years, especially in regards to this thesis. I have learned a lot about meteorology and myself throughout this time and was able to push myself farther than I thought possible. I will always appreciate and never forget the extra time taken out of your days to assist me. In addition, I would like to thank Dr. Allen Thompson for joining my committee and supporting me through this process. I would also like to thank Josh Kastman, Adam Hirsch, Laurel McCoy, Brett Williams, Katie Crandall, and other students who gave advice, support, and the past five years. My success would not have been possible without all those who are listed above.

Finally, I would like to thank my family and friends for all of their support and encouragement. None of this would have been possible without them. They have always believed in me even when I did not and pushed me to be the best I could be. I could not have had a better support system behind me. Thank you.

Table of Contents

Figures

Tables

Abstract

Quasi-Linear Convective Systems (QLCS) are linear convective systems known to produce a variety of severe weather threats including damaging winds, hail, flooding, and even tornadoes. Previous studies have found that QLCSs are most common in the Ohio and Mississippi River Valleys and produce roughly 18% of tornadoes across the United States. In addition, it has been shown that QLCS tornadoes spawn from low-level circulations called mesovortices. Mesovortices build quickly from the ground up making it very difficult to accurately identify them on radar, especially at long distances. Therefore, it is imperative that more research be done to distinguish between QLCSs that produce tornadoes and those that do not. Fifty-seven QLCS events were selected to investigate how radar parameters differ between tornadic and non-tornadic QLCSs. These events were broken into the following categories: warm season tornadic, warm season non-tornadic, cold season tornadic, and cold season non-tornadic. Tornadic cases produced one or more tornadoes, while non-tornadic cases had tornado warnings issued without a tornado actually being produced. These events were chosen based on their geographical location and the data available. The goal was to find radar parameters that were statistically significantly different between tornadic events and non-tornadic events.

Chapter 1 Introduction

Mesoscale convective systems (MCSs) are the largest of the convective systems and are defined to be 100 km or more length in at least one direction (Houze, 2004). They can be either linear or circular. The linear MCS is also known as a Quasi-Linear Convective System (QLCS). These systems have a variety of organizational modes based on their distribution of stratiform precipitation, which depends on the thermodynamics and dynamics in the QLCS environment (Parker and Johnson, 2000; Gallus et al., 2008). In addition, they have a way of propagating and maintaining their life that is different from other convective systems such as supercells (Rotunno et al, 1988). Furthermore, QLCSs exist with relative frequency and are responsible for a large portion of severe weather threats in the United States, making them very important to understand, especially for forecasting purposes.

Operational radar data is the primary tool used to classify convective systems and to identify severe weather threats. It has been found that it can be very difficult to accurately identify tornadic circulations in QLCSs. QLCS tornadoes spawn from mesovortices, a low-level circulation associated only with QLCSs. This thesis work analyzed radar parameters for 57 events to discover significant differences between tornadic and non-tornadic QLCSs. The domain of the events evaluated is shown in Figure 1.1.

Figure 1.1 This is the domain used for this research. The red line represents the NWS County Warning Areas (CWA) included.

1.1 Purpose

The purpose of this research was to develop a better understanding of QLCSs, more specifically, the differences between tornadic and non-tornadic QLCSs. The expectation was to increase the accuracy of tornado recognition; in other words, increase the probability of detection and decrease false alarm rates. An analysis of radar parameters was executed on 57 QLCS events (warm season tornadic, warm season non-tornadic, cold season tornadic, and cold season non-tornadic) to determine which parameters are statistically significantly different between the tornadic and non-tornadic cases.

1.2 Objectives

To accomplish the purpose of this study, the following hypotheses were posed:

- Tornadic QLCSs contain greater azimuthal shear, divergence, and spectrum width values than non-tornadic QLCSs.
- Tornadic QLCSs tend to be oriented in a more north-south direction than non-tornadic QLCSs.
- Tornadic QLCSs tend to be characterized by areas with supercellular characteristics. These supercellular characteristics are co-located with high reflectivity (>45 dBZ) areas.
- The QLCS events fulfill the QLCS definition set by Trapp et al. (2005): a contiguous reflectivity area of 40 dBZ or greater is at least 100 km in length.

Chapter 2 Literature Review

An in-depth literature review was performed to accomplish the objectives of this research and to understand the physical processes responsible for QLCS development, specifically, between tornadic and non-tornadic QLCSs. Sections 2.1 discusses the structure and dynamics of MCSs in detail. Sections 2.2 through 2.4 of this review converses about QLCS maintenance, features, organizational modes, and structure and dynamics; while section 2.5 focuses on QLCS climatology. Section 2.6 will detail mesovortices and the differences between tornadic and non-tornadic mesovortices, and differences between mesovortices and mesocyclones. Finally, section 2.7 will be a summary that leads into the research of this thesis.

2.1 Mesoscale Convective System (MCS) Structure and Dynamics

A Mesoscale Convective System (MCS) is a long-lived "cumulonimbus cloud system that produces a contiguous precipitation area ~100 km or more in at least one direction" (Houze, 2004). These systems can be displayed either linearly (quasi-linear convective system: QLCS) or in a circular (mesoscale convective complex) manner and are the largest of the convective systems (Figure 2.1). Severe weather threats posed by this type of system are hail, strong winds, flooding, and tornadoes. The MCS is on the mesoscale time and space scale. The average area of the cold cloud tops associated with MCSs is roughly 10^5 km^2. Also, the precipitation and circulations within an MCS

develops on a scale similar to the cloud tops. Typically, the precipitation area is divided into a stratiform region and a convective region. Where these regions are in a MCS depends mostly on the vertical wind field and the dynamics of the system.

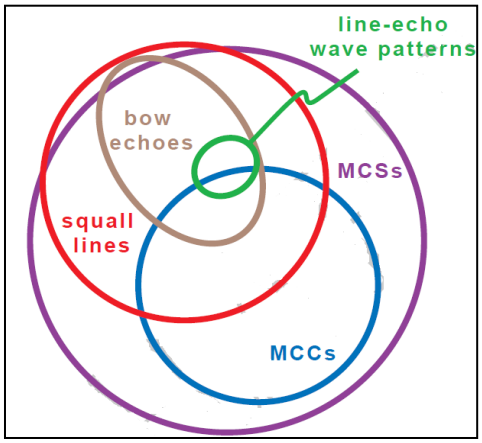

Figure 2.1 Fig. 9.4 from Markowski and Richardson (2010) – Venn diagram of MCS subclassifications. The position and overlap of the circles and ellipses only indicates relationships among the subclassifications; the sizes of the circles and ellipses should not be taken too literally to infer the relative frequencies of the various types of MCS. A small fraction of squall lines and bow echoes is not classified as MCSs because of their horizontal length scale is less than 100 km.

2.1.1 Layer lifting, overturning, and gravity wave response within MCSs

Houze (2004) reviewed MCSs and presented new insights regarding MCS structure and dynamics. Many have viewed convective clouds as forming from parcels of air originating from the planetary boundary layer. This theory describes all smaller convective clouds well, but Houze (2004) suggested that layer lifting theory would represent MCSs better because of their large size and different type of organization. "The upward air motion in an MCS may begin in the form of buoyant convective-scale parcels

rooted in the boundary layer and rising high into the upper troposphere; however, after the MCS matures, a layer of air much deeper than the boundary layer enters and rises on a slantwise path through the system" (Houze, 2004). Additionally, the rising layer is frequently potentially unstable and overturns, but stays a coherent unit as it rises through the system. The overturning of the rising layer is still undergoing further research. What is known so far is the overturning in the layer permits the highest ϑ_e air to rise to the top of the system. Modeling also proposes that at the nose of the cold pool, buoyant elements develop features of trapped gravity waves as they propagate rearward into the stratiform region. These buoyant elements can also develop a lateral component of overturning in the form of longitudinal rolls. Moreover, in the convective region of an MCS, the slantwise layer ascent seems to be part of a gravity wave response to the mean latent heat release. This layer lifting then encourages the formation of the upper stratiform region (Houze, 2004).

Another gravity wave response to heating in the convective region is mid-level inflow entering the stratiform region just below the cloud base. The direction of the mid-level inflow into the stratiform region is mandated by the large scale environmental wind. The inflow accelerates into the MCS due to the pressure gradient forces within the system and then feeds the mesoscale downdraft. An MCS may not always be textbook but in general there is always a mid-level inflow into the stratiform region guided by environmental relative wind. A good example of this is the rear inflow behind a trailing stratiform QLCS.

2.1.2 Mesoscale Convective Vortices

The mesoscale convective vortex (MCV) can greatly affect the appearance of QLCSs. MCVs forms in the mid-levels at the base of the stratiform region. In some cases, MCVs initiate a "bookend" vortex, which are seen in QLCSs. In the midlatitudes, the Coriolis force has a large influence on MCVs and enhances the bookend vortex. The enhancement causes the structure of the system to be asymmetrical. This is seldom seen in the tropics due to the minor influence of the Coriolis force. MCVs are more prominent in longer-lived MCSs and tend to be inertially stable. This is due to static stability being reduced by the saturated conditions in the stratiform upper-level cloud deck. In turn, this decreases the Rossby radius of deformation. The inertial stability of the MCV suggests the vortex becomes a quasi-balanced flow maintained by a secondary vertical circulation. The secondary circulation can extend the life of an MCS by triggering new convection (Houze, 2004).

2.1.3 MCS propagation

Understanding how MCSs propagate is another important characteristic to discuss. Direct lifting of unstable air by an advancing cold pool and wave dynamics affect a system's propagation. For example, the heating profile of an MCS produces mass divergence which creates bores that move at gravity wave speed. The slower bores initiate new convection at a distance from the cold pool and give an MCS a feature of discrete propagation. The new convection can join the current convective line or form a whole new line as the older convection weakens and becomes stratiform precipitation.

Phase locking between externally generated waves and an MCS can also help MCS propagation. The velocity of movement of the MCS becomes one with the external waves but the direction of this velocity can be different from the cold pool propagation. Therefore, "some MCSs bifurcate, with one portion directed by the wave propagation and the other directed by cold pool propagation" (Houze, 2004).

2.1.4 Spatial size of MCSs

The spatial size of an MCS is established by the development and continual regeneration of the stratiform region. As convective cells weaken, the material becomes a part of the stratiform region; therefore, the size of the stratiform region is determined by the ability of an MCS to regenerate new convection. For growth of the stratiform region, the stratiform elements must have a dissipation time that is greater than the lifetime of the active cell. Overtime, a balance can be reached between the old stratiform precipitation and the generation rate of new convective precipitation. The maximum size of an MCS is limited to the number of convective cells possible at a certain time. It can be reached as long as the MCS is in an environment with "sustainability." This means the environment must be able to sustain the most convective cells as possible over a long period of time.

Sustainability can be enhanced by "a boundary layer that has a favorable thermodynamic structure that remains in place over a long period of time in the vicinity of the MCS" (Houze, 2004). A warm moist boundary layer exists over an extensive area over the oceans which allows for the greatest fraction of stratiform precipitation to be found. Over land, stratiform development is limited because the warm moist boundary

typically becomes stable at night. However, the boundary layer can be replenished with moisture through the night with the presence of a low level jet. A continually replenished boundary layer is capable of sustaining an MCS for longer period of time allowing it to grow in size. In conclusion, the size of an MCS is determined by the balance stage between the rate of dissipating stratiform precipitation and the rate of generating convective cells and that old convection is changing to stratiform precipitation.

2.1.5 Vertical redistribution of momentum within MCSs

Houze (2004) also identified two methods in which MCSs vertically redistribute momentum: 1) horizontal acceleration by pressure gradient forces that develop within the system 2) vertical eddy fluxes associated with their internal circulation. For QLCSs, two-dimensional, steady state idealizations describe the redistribution of momentum well. However, the idealizations have trouble illustrating momentum redistribution in all the various MCS structures that transpire. Dividing the QLCS into its respective convective and stratiform regions allows one to separate the redistribution of momentum into the fundamental components that vary from one system to the next. The stratiform region can greatly influence the net change in the environmental momentum profile, while the size of the stratiform region in relation to the convective area affects the final vertical profile of momentum in the environment (Houze, 2004).

2.1.6 Vertical profile of heating within MCSs

In an MCS, the vertical heating profile also displays systematic differences between the convective and stratiform areas and is independent of organizational mode (i.e., Leading/trailing/parallel stratiform structure). Due to the difference in heating profiles of the two areas, two distinct wavelengths of forcing are identified; one for convective heating, 2*H*, and one for the stratiform heating, *H*. The variable *H* is the depth of the troposphere. "These two wavelengths of forcing produce distinct effects on the large-scale environment of the MCS; as the stratiform component of heating becomes greater, the more the net heating by an MCS intensifies and shifts to the upper levels" (Houze, 2004). In addition, these two modes dominate the divergent response of the environment to the MCS. This can be confirmed by an analysis of wind data within the MCS and surrounding the MCS. For that reason, including additional categories like radar echo structure is not essential to comprehend the heating impact of MCSs on the large-scale wind field (Houze, 2004).

2.2 Quasi-Linear Convective Systems (QLCS)

A Quasi-Linear Convective System (QLCS) is a subclassification of an MCS. More specifically it is "a linear region of radar reflectivity greater than or equal to 40 dBZ continuously distributed over a horizontal distance of 100 km or greater" (Trapp et al., 2005). Severe weather hazards associated with QLCSs are severe hail, wind, flooding, and tornadoes; with the primary focus here being tornadoes. The following will discuss

QLCS maintenance, general features, organizational modes, structure and dynamics, climatology, and mesovortices.

2.2.1 QLCS maintenance

Understanding QLCS maintenance has been a topic of research for at least the past 50 years. It wasn't until the early 80's when Thorpe et al. (1982) postulated that in order to get an accurate two-dimensional simulation of long-lived linear convection, there needed to be sufficient strength of low-level shear (0-2.5 km) perpendicular to the line. Rotunno et al. (1988) were able to generate numerical simulations to confirm this theory.

Rotunno et al. 1988 performed four basic simulations to test how a line of nonsupercellular convection can become long-lived (Figure 2.2). The simulations included: no low-level shear or cold pool, only a cold pool present, only low-level shear present, and with both a cold pool and low-level shear in equilibrium. In the case where just a cold pool is present, negative vorticity dominates and causes the updraft to tilt rearward over the cold pool (upshear). This compels the system to weaken because the "outflow from a prior cell induces a circulation above it that inhibits convection" (Rotunno et al, 1988). For the scenario with only environmental low-level shear present, positive vorticity dominates and causes the updraft to tilt in the downshear direction, hence "their energy is drained by the shear and/or they deposit their rain into their inflow stream" (Rotunno et al., 1988). This also eventually kills a convective system. However, these two situations can be seen in the real world to a certain extent, but it would more or less be in an environment where the low-level shear or cold pool is weak instead of

completely absent (Markowski and Richardson, 2010). Finally, when the low-level shear and cold pool are both present and in equilibrium, the positive and negative vorticity are balanced generating a strong and erect updraft. Droegemeier (1985) established that when there is enough low-level shear present, a cold pool produces deeper lifting. Markowski and Richardson (2010) noted that for most thunderstorm outflows, the optimal shear value is somewhere between 17 and 25 ms^{-1}.

Essentially, in the beginning, a system has a weak cold pool and the low-level shear dominates so the updraft will tilt downshear. However, as precipitation falls, evaporation produces a cold pool which then initiates new convection. Sufficient low-level shear alters the cold pool circulation creating a balance between the two; which is crucial for maintaining and creating new convection. Next, the simulations showed the cold pool always getting colder as time progressed. Therefore, the system lives until the cold pool gets cold enough to overcome the influence of the low-level shear. The cold pool then rushes outward underneath the updraft in the downshear direction. The updraft begins to tilt upshear and it becomes harder for new cells to be triggered causing the line to weaken.

In conclusion, the strength and longevity of a QLCS is dictated by the balance between the horizontal vorticity associated with the environmental low-level shear and the system's horizontal vorticity produced by the buoyancy gradient across the cold pool. This only ensues when there is a strong enough value for the wind shear in comparison to the depth and coldness of the cold pool. Lastly, the cold pool also helps govern the motion of QLCSs, except some individual cells may have a motion different from the QLCS system.

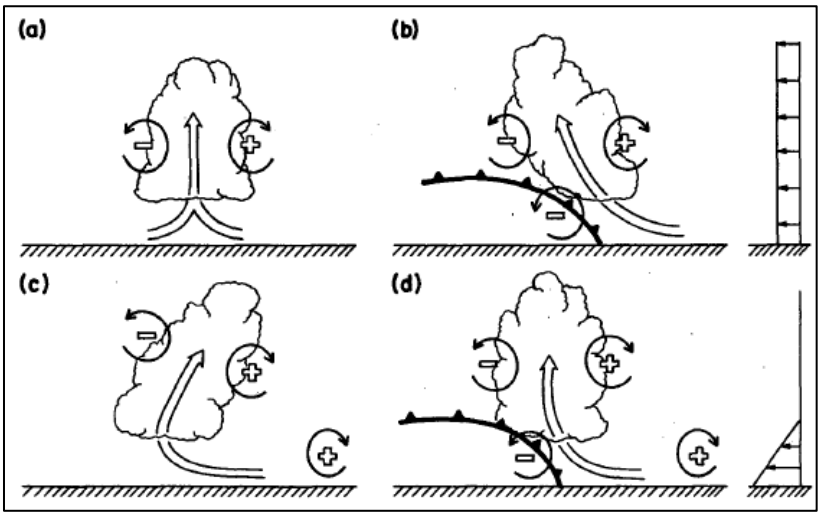

Figure 2.2 Fig. 18 from Rotunno et al. (1988) – Schematic diagram showing how a buoyant updraft may be influenced by wind shear and/or a cold pool. (a) With no shear and no cold pool, the axis of the updraft produced by the thermally created, symmetric vorticity distribution is vertical. (b) With a cold pool, the distribution is biased by the negative vorticity of the underlying cold pool and causes the updraft to lean upshear. (c) With shear, the distribution is biased toward positive vorticity and this causes the updraft to lean back over the cold pool. (d) With both a cold pool and shear, the two effects may negate each other, and allow and erect updraft.

2.2.2 QLCS features

There are many different features associated with QLCSs such as, gust fronts and downdrafts. Additional features have been established to be associated only with QLCSs; for example, the jump updraft, overturning updraft, mesovortices, bookend vortices, and the rear inflow jet. Figure 2.3 depicts the airflow of a basic linear system. The jump draft is responsible for ascending inflow air from front-to-rear, while the overturning updraft transports some of the inflow up and back over itself. Typically one updraft is dominant over the other but that depends on which QLCS organizational mode is present, which will be discussed later in Section 2.3 (Parker and Johnson, 2004). Mesovortices are the

low-level circulations found within QLCSs. They form within the lowest 2.5 km AGL and build quickly upwards. The diameter of such circulations is typically 2-9 km. Lastly, mesovortices are responsible for producing damaging straight-line winds and tornadoes but can be difficult to see on radar especially at far distances. Mesovortices will be discussed further in Section 2.7.

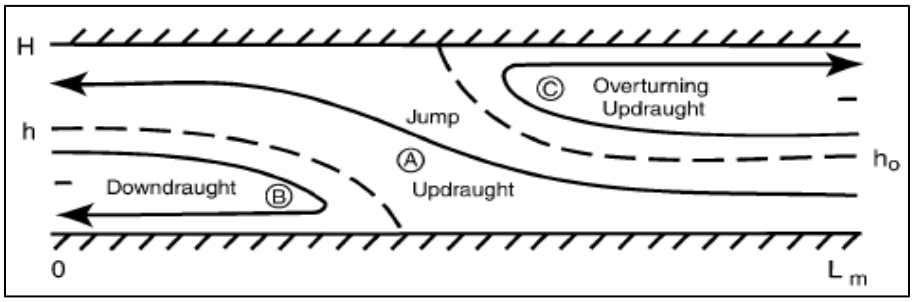

Figure 2.3 Fig. 3 from Parker and Johnson (2004) – Schematic diagram of the airflow in Moncrieff's (1992) stationary dynamical model for two-dimensional convection.

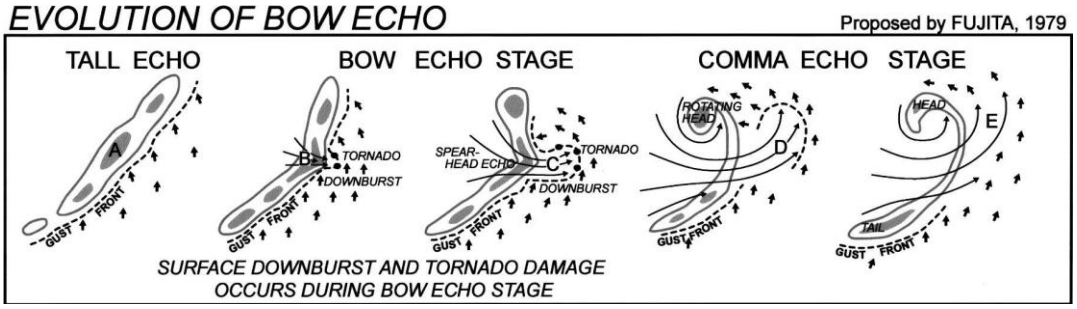

Figure 2.4 Fig. 1 from Atkins et al. (2005) – Schematic diagram illustrating bow echo evolution. Figure adapted from Fujita (1979).

Bookend (midlevel) vortices are a circulation feature found at the midlevels (3-9 km AGL) and at the ends of the convective line of QLCSs. The southern vortex is

anticyclonic while the northern vortex is cyclonic. When the influence of the Coriolis force increases, the cyclonic vortex becomes dominate and that is when the comma head appearance in bow echoes is observed (Figure 2.4) (Weisman, 1993). There can be subsystem scale (~5-10 km diameter) bookend vortices or system-scale (tens of kilometers) bookend vortices. The subsystem bookend vortices are formed as the "ambient crosswise horizontal vorticity is vertically tilted by the downdrafts associated with embedded bowing segments" (Trapp and Weisman, 2003). Bookend vortices on the system-scale are formed "through the vertical tilting, by the system-scale updraft, of crosswise horizontal vorticity generated in horizontal buoyancy gradients along the gust front" (Figure 2.5) (Trapp and Weisman, 2003). The development of bookend vortices can aid in the development of another feature; the rear inflow jet.

The rear inflow jet (RIJ) is a rear-to-front airflow in the midlevels that can help sustain the life of a QLCS. It can also descend toward the surface and be responsible for damaging surface winds. The RIJ develops at the beginning of the decaying stage; when the cold pool begins to overcome the environmental shear (Figure 2.6). The "horizontal buoyancy gradients along the rear edge of the buoyant plume aloft and cold pool near the surface generate horizontal vorticity, thereby accelerating the flow from rear-to-front at midlevels" (Weisman, 1993). In other words, there is a buoyancy-produced mesolow that extends above and behind the spreading cold pool that enhances the rear-to-front flow. This can occur when there is sufficient CAPE (2000 Jkg^{-1}) and strong environmental shear (20 ms^{-1} over lowest 5 km AGL, with most confined to lowest 2.5 km AGL).

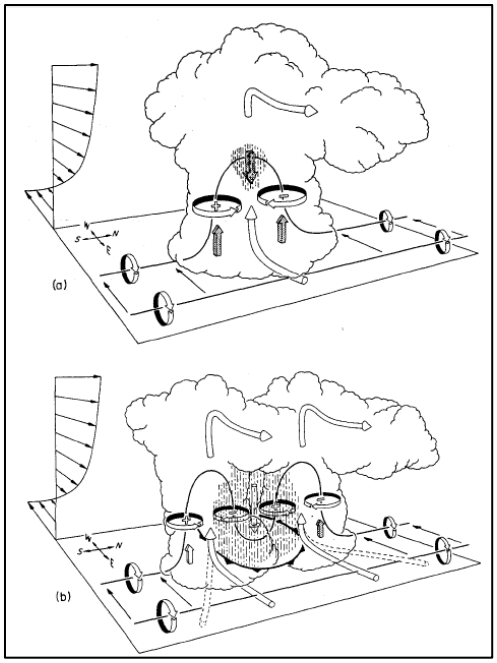

Figure 2.5 Fig. 15 from Weisman (1993) – Schematic depicting how a typical vortex tube contained within (westerly) environmental shear is deformed as it interacts with a convective cell (viewed from the southeast). Cylindrical arrows show the direction of cloud-relative airflow, and heavy solid lines represent vortex lines with the sense of rotation indicated by circular arrows. Shaded arrows represent the forcing influences that promote new updraft and downdraft growth. Vertical dashed lines denote regions of precipitation, (a) Initial stage: vortex tube loops into the vertical as it is swept into the updraft. (b) Splitting stage: downdraft forming between the splitting updraft cell tilts vortex tubes downward, producing two vortex pairs. The barbed line at the surface marks the boundary of the cold air spreading out beneath the storm (from Klemp 1987).

Once the RIJ develops it can accelerate from 5 ms^{-1} to 20 ms^{-1} and extend the life of a QLCS. The horizontal vorticity beneath the jet level is opposite of the horizontal vorticity produced by the cold pool and thereby counteracts the negative influence of the cold pool circulation. Deep lifting at the leading edge of the gust front begins again and there is continual regeneration of strong erect updrafts at that location (Weisman, 1993). At higher levels, updrafts are weaker because the air transported above the RIJ gets taken back to the rear above the cold pool. This occurs because the air is under the influence of the horizontal vorticity associated with the upper portion of the jet. If influence of the

cold pool overwhelms the contribution from the warm plume aloft, the RIJ begins to descend and spread along the surface behind the leading edge gust front, resulting in a shallower, weaker system-scale circulation (Weisman, 1993). Again, the descent of the RIJ is when damaging surface winds are observed. The generation of the RIJ is also aided by the bookend vortices. Their circulations help initiate and focus the RIJ into the core of the system (Weisman, 1993). In fact, bookend vortices can contribute as much as 30%-50% of the resultant inflow strength (Weisman, 1993). Additionally, RIJs have been found to enhance the development of tornadic mesovortices. In conclusion, the RIJ is seems to be an important factor for the strength and longevity of bowing QLCSs.

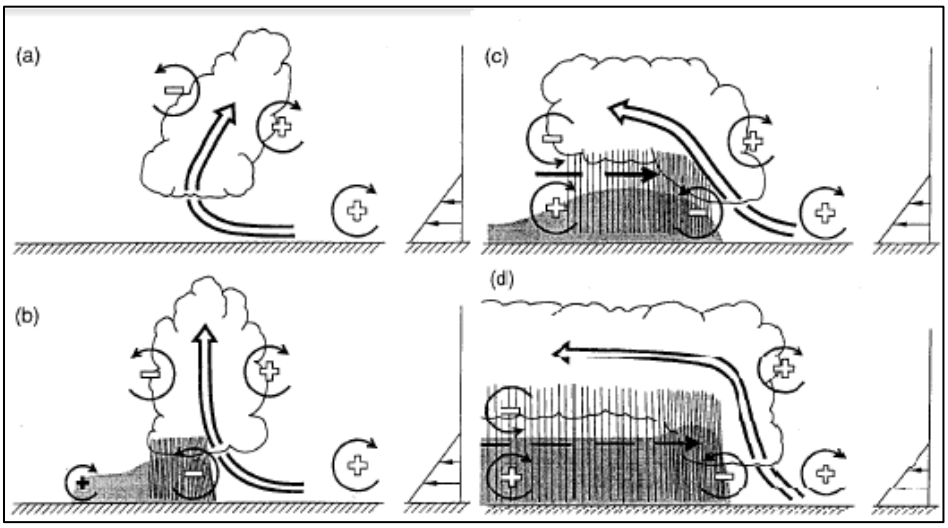

Figure 2.6 Fig. 14 from Weisman (1993) – Four stages in the evolution of an idealized bow echo, (a) An initial updraft leans downshear in response to the ambient vertical wind shear, which is shown on the right, (b) The circulation generated by the storm-induced cold pool balances the ambient shear, and the system becomes upright, (c) The cold pool circulation overwhelms the ambient shear, and the system tilts upshear, producing a rear-inflow jet. (d) A new steady state is achieved whereby the circulation of the cold pool is balanced by both the ambient vertical wind shear and the elevated rear-inflow jet. The updraft current is denoted by the thick double-lined flow vector, with the rear-inflow current in (c) and (d) denoted by the thick dashed vector. The shading denotes the surface cold pool. The thin, circular arrows depict the most significant sources of horizontal vorticity, which are either associated with the ambient shear or are generated within the convective system, as described in the text. Regions of lighter or heavier rainfall are indicated by the more sparsely or densely packed vertical lines, respectively. The scalloped line denotes the outline of the cloud (adapted from Weisman 1992).

2.3 QLCS Organizational Modes

Knowledge about the organizational mode of a QLCS can be helpful for forecasting hazardous weather and issuing warnings. Organizational mode can also allow insight about the latent heating profiles of the convective and stratiform regions, the vertical wind profile, and general environment the QLCS is in. Many studies have been executed to investigate the different organizational modes of QLCSs. Five dominant modes have been identified: trailing stratiform (TS), leading stratiform (LS), parallel stratiform (PS), non-stratiform (NS), and bow echo (BE) (Gallus et al., 2008). A TS QLCS has the convective line ahead of the stratiform region. The LS QLCS case is just the opposite: the stratiform region is ahead of the convective region. For the PS QLCS, the stratiform region is located parallel (north) to the convective region. The non-stratiform case consists of only a convective line with no stratiform precipitation present. Lastly, a bow echo is very similar to a TS QLCS but a portion of the convective line gets pushed out slightly ahead of the rest of the line, creating a bow shaped look. Parker and Johnson (2000) focus on the first three types: TS, LS, and PS.

Fovell and Dailey (1995) established "various modes of modeled multicell thunderstorms, regardless of regeneration periodicity, exhibited new convection near the leading edge of storm outflow, with subsequent upward and rearward motion within a canted updraft flow." This results in the advection of hydrometeors back behind the convective line creating the stratiform region also known as the trailing stratiform QLCS. Houze et al. (1990) noted that most of the linear precipitation systems they assessed during the spring of 1977-82 converted to the TS mode. The second type of organizational mode, LS, was first mentioned by Schiesser et al. (1995). Parker (1999)

exposed that multiple cases in his research exhibited a leading stratiform region. That very little attention given to this particular mode was due to the complicated nature of the LS QLCSs in numerical simulations. Lastly, PS was found as an organizational mode for QLCSs but has received the least amount of attention of all. However, knowledge of the last two modes goes back to Newton and Fankhauser (1964) who discussed characteristics of both LS and PS.

Parker and Johnson (2000) used these past experiments as their ground work "to document the existence and frequency of these convective modes and to outline a conceptual model for the LS and PS archetypes that is consistent with the observations" from their study. They describe an MCS as "a convective phenomenon for which the Coriolis acceleration is of the same order as other terms in the Navier-Stokes equations." As a result, the MCS timescale is f^{-1} which is the same time scale for an MCS as seen in Houze (2004). This is sufficient for the study because a midlatitude value for f gives an MCS timescale (τ) of about three hours, which matches the mesoscale circulations identified by Emanuel (1986). The length scale was defined as $L = U\tau$. With an average wind speed, U = 10 ms^{-1}, the length scale becomes 100 km, which is the same as Houze (1993). In conclusion, Parker and Johnson (2000) define their events as "convective echoes with extents greater than 100 km and durations greater than 3 hours." From this definition, they assigned each case as either linear or nonlinear. A system was categorized as a linear MCS if they contained a contiguous or nearly contiguous line of convective echoes. Nonlinear MCSs are the cases in which there were eccentric precipitation patterns without convective lines. Only linear MCSs were considered for this study.

The domain evaluated in Parker and Johnson (2000) was the Great Plains due to the frequency of convective weather. Radar composites were used to evaluate each linear case; 20-40 dBZ were the stratiform echoes and greater than 40 dBZ were convective echoes. Also, one radiosonde was used for each event to determine the pre-convective environment, the NOAA Profiler Network was employed to create a wind profile for each archetype, and lastly, surface data and NCEP gridded reanalysis data was utilized for identifying synoptic features in the warm sector of the synoptic set up.

During the linear MCS study, the synoptic environment was noted. Active periods were associated with an approaching short wave trough and/or wave cyclone. The average mean sea level pressures were typically lower across the central plains. The strongest indication was the tendency for a low pressure center to be located in southwestern Kansas. Strong upper-tropospheric cyclonic vorticity advection was also present, which implied quasi-geostrophic ascent. In addition, on average, the linear MCSs were located near the right entrance region of the upper level jet streak, which indicates upper level divergence and upward motion. A southerly low-level jet was also found during active periods which contributed to the warm air advected into the desired area. Finally, linear triggers were found to be of the utmost importance, especially for those cases that were located in the warm sector of the synoptic set up. These warm sector cases were usually associated with warm fronts quickly followed by surface pressure troughs and cold fronts. This confirmed the importance of low level convergence to organized convection (Parker and Johnson, 2000).

Eighty-eight linear MCSs within the central United States in May 1996-97 were categorized as TS, LS, or PS (Figure 2.7). If an event displayed multiple archetypes, the

dominant one was assigned to that case. Cases were deemed unclassifiable if they were a non-stratiform case, or a dominant mode could not be established. Three of the 88 were unclassifiable. In general, majority of the cases were oriented NE-SW and moved from the W/NW. In addition, well over half of the LS and PS cases evolved toward a TS structure at some point in their lifetime (Figure 2.8). Also, a maximum occurrence existed around 0300Z in the warm sector of the synoptic arrangement (Parker and Johnson, 2000).

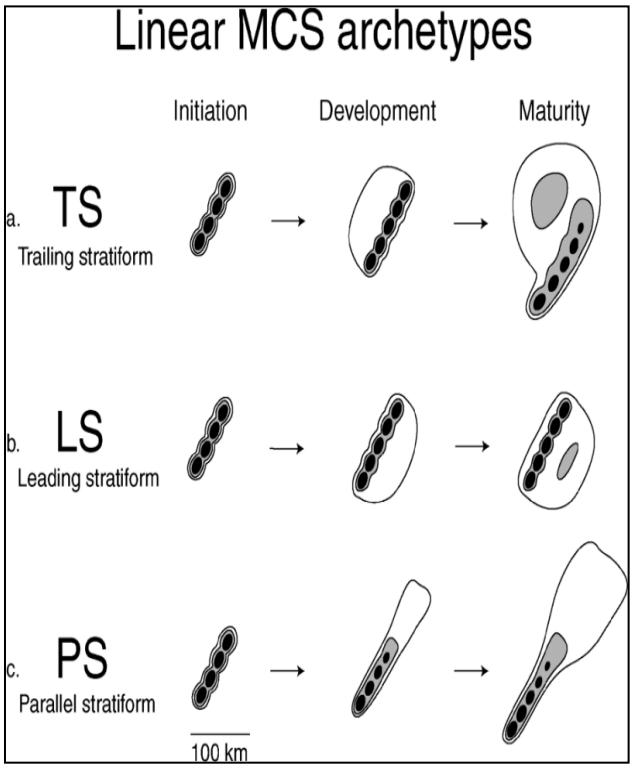

Figure 2.7 Fig. 4 from Parker and Johnson (2000) – Schematic reflectivity drawing of idealized life cycles for three linear MCS archetypes: (a) TS, (b) LS, and (c) PS. Approximate time intervals between phases: for TS 3–4 h; for LS 2–3 h; for PS 2–3 h. Levels of shading roughly correspond to 20, 40, and 50 dBZ.

2.3.1 Trailing stratiform

Trailing stratiform QLCSs have "a very strong reflectivity gradient at the leading edge and a large trailing stratiform precipitation region, often exhibiting a secondary maximum of reflectivity separated from the convective line by a narrow channel of lower reflectivity" (Parker and Johnson, 2000). The TS archetype has been found to be the most common type of QLCS. In the Parker and Johnson (2000) study, TS consisted of about 60% of the total cases. This type also moved a lot quicker than the other two and lasted about twice as long (12.2 hours). The duration of TS cases appears to be correlated with the stability of the air masses associated with them and strength of the cold pool. Different environmental parameters suggest that TS QLCSs occur in air masses with a lot of conditional instability. In addition, TS QLCSs occurred in environments with stronger cold pools than the other two categories. A vertical wind profile was generated for the TS category (Figure 2.9). The results show there are negative line-perpendicular storm relative winds are every level. Above 2 km these winds are much stronger than in the other two types. This result helps explain the rearward advection of hydrometeors; the mean flow creates the trailing stratiform region (Parker and Johnson, 2000).

2.3.2 Parallel stratiform

Parallel Stratiform QLCSs "have a convective line with parallel stratiform precipitation if most or all of the stratiform precipitation region associated with the convective line moves parallel to the line itself and to the left of the line's motion vector throughout its life cycle" (Parker and Johnson, 2000). The PS archetype consisted of

about 20% of the total cases. Of the three categories the PS QLCS lifetime was the shortest, 6.3 hours. A wind profile was also created for this category (Figure 2.9). The PS type contains a much stronger negative line-perpendicular flow than the TS in the 0-1 km layer. However, there are weaker mid-tropospheric storm-relative winds and modest rear-to-front storm relative winds at the upper levels. The winds that set this type apart from the rest are the deep line-parallel storm-relative flow above 2 km. This flow is considerably larger than in the other two archetypes and flows to the north direction. This shows why the stratiform region is positioned parallel to the convective region (Parker and Johnson, 2000).

2.3.3 Leading stratiform

Leading stratiform QLCSs are lines "whose stratiform precipitation is predominately located in advance of the convective line" (Parker and Johnson, 2000). Typically, LS QLCSs contain moderate leading stratiform regions without transition zones and secondary bands. The LS archetype consists of the remaining 20% of the total cases. Of the three categories this type lasted on average about 6.5 hours but moved the slowest. The reason LS QLCSs move slower is because the air flowing into the system moves through the stratiform region first. Also, the strength of the cold pool associated with LS QLCSs is typically less than the other two categories. However, it is thought that LS QLCSs do last because there is inflow into the rear of their convective lines. LS cases are very similar to PS cases in regards to the line-perpendicular fields, the weak mid-tropospheric storm-relative winds, and the modest rear-to-front storm-relative winds at

the upper levels (Figure 2.9). The main difference for the LS category is that there is a much greater average rear-to-front component of the storm relative winds aloft. This result can help explain the forward advection of hydrometeors that produces the stratiform region to be ahead of the convective region (Parker and Johnson, 2000).

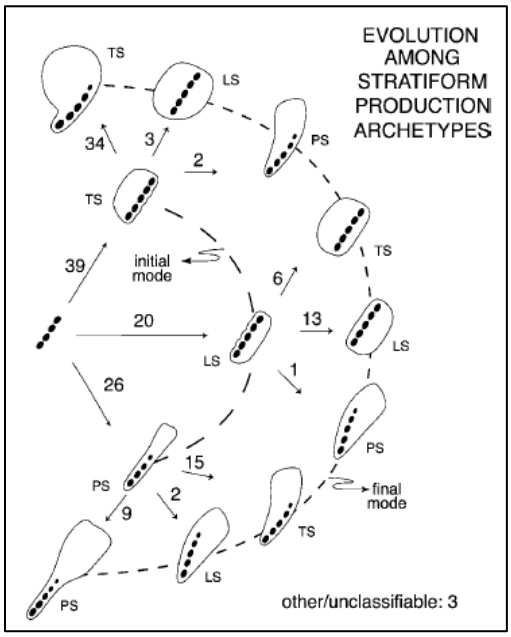

Figure 2.8 Fig. 9 from Parker and Johnson (2000) – Illustration of evolutionary pathways for MCSs in this study. Labels along each pathway denote the initial and final modes of stratiform precipitation production. The total number of cases following each step is indicated. Idealized composite positions of convective elements and stratiform precipitation are depicted schematically along each pathway. Note: some pairs of evolutionary pathways (e.g., TS→PS and PS→TS) resulted in generally similar reflectivity patterns. As discussed in the text, MCSs were classified based upon their predominant organizational mode, which could be either their initial or final organization.

In conclusion, TS QLCSs are the most common out of the three archetypes. Also, half the time, a QLCS of a different mode will transform into a TS QLCS. Linear triggers were found to be very important for the existence of QLCSs and during active periods, "convective systems were located in a region of lower-level warm air advection in

advance of an approaching upper-level short-wave trough" (Parker and Johnson, 2000). In addition, knowing the vertical storm-relative wind profile could be very useful in determining which type of QLCS will form. TS cases have strong negative line-perpendicular storm relative winds at every level. PS cases have deep line-parallel storm-relative flow above 2km. Finally, LS cases have a greater average rear-to-front component of the storm-relative winds aloft. Therefore, the primary indicator of organizational mode is the middle- and upper-tropospheric storm-relative flow (Parker and Johnson, 2000).

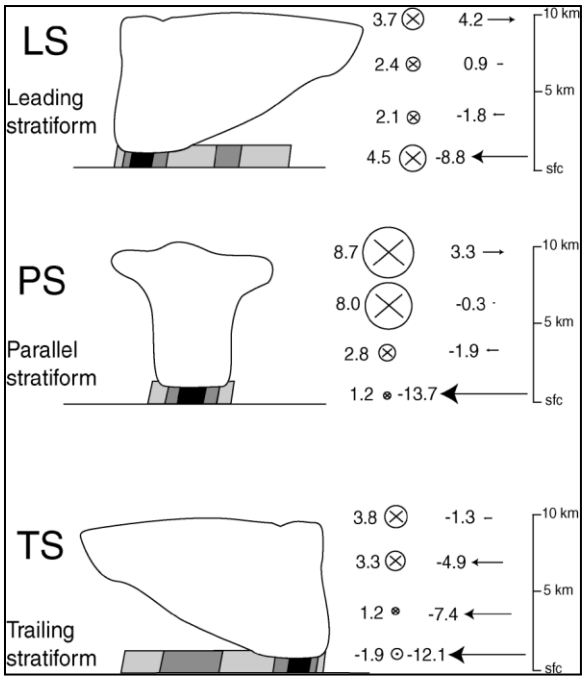

Figure 2.9 Fig. 12 from Parker and Johnson (2000) – Vertical profiles of layer-mean storm-relative pre-MCS winds for linear MCS classes. Wind vectors depicted as line-parallel (Ⓧ) and line-perpendicular (→) components in m s^{-1}. Layers depicted are 0–1, 2–4, 5–8, and 9–10 km. Typical base scan radar reflectivity patterns (shading) and hypothetical cloud outlines are drawn schematically for reference. MCSs' leading edges are to the right.

2.4 Structure and Dynamics of Quasi-2D MCSs

Following Parker and Johnson (2000), Parker and Johnson (2004) built on their previous research to explore the kinematics and dynamics of the TS case and the LS case. The PS case was not evaluated because of the complex three dimensionality of the archetype. The previous study found that most LS cases have air inflow from the front but some cases exhibited air inflow from the rear. The LS cases with the rear inflow appeared to be very similar to TS cases. Therefore, Parker and Johnson (2004) broke the LS cases into two types: front-fed leading stratiform (FFLS) and rear-fed leading stratiform (RFLS). The TS cases were known as front-fed trailing stratiform (FFTS) QLCSs. The goal was to find similarities and differences of each type kinematically then dynamically by generating numerical simulations.

2.4.1 Kinematic features of front-fed trailing stratiform systems

The FFTS systems are fed by front-to-rear storm-relative flow in the lower troposphere which ascends and weakly overturns (Figure 2.10). Activated hydrometeors move rearward to where there is continued condensational and depositional growth. This creates the trailing stratiform region. Leftover buoyancy, which generates small upward accelerations from the convective region, and in situ latent heating render modest ascent in the front-to-rear flow stream. Below the ascending front-to-rear flow a pressure minimum develops which helps accelerate air behind the system inward to form a rear inflow jet (Parker and Johnson, 2004). Due to precipitation falling in this area and hydrometeor loading, a descending slope occurs. Finally, the jump draft was found to be

predominant with this type of system.

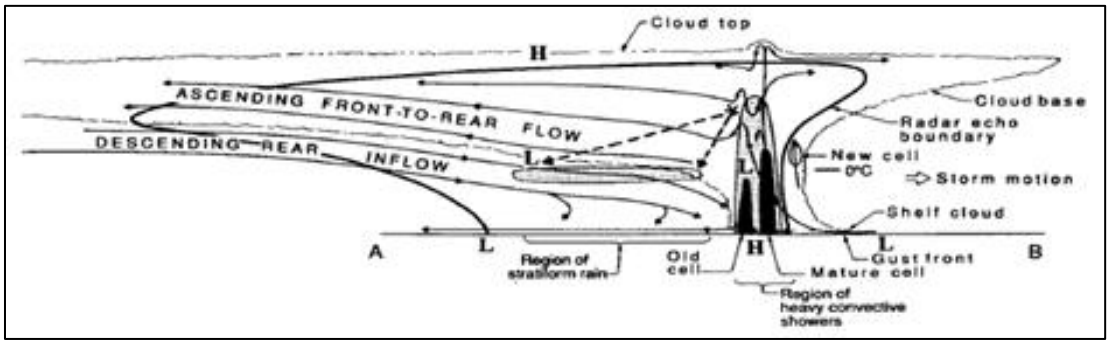

Figure 2.10 Fig. 4 from Parker and Johnson (2004) – Conceptual model from Houze et al. (1989) of front-fed convective line with trailing (stratiform) precipitation, viewed in a vertical cross section oriented perpendicular to the convective line and parallel to its motion.

2.4.2 Kinematic features of rear-fed leading stratiform systems

Observations of RFLS are notably less common than those of FFTS but it has been found they are similar to FFTS (Figure 2.11). For example, the jump draft of the RFLS is also predominant. The airflow throughout the system is just the opposite of FFTS QLCSs. There is a rear-to-front component that feeds the convective line and then ascends upward and forward generating the leading precipitation region. In addition, there is a descending jet of front-to-rear flow which is analogous to the rear inflow jet. According to Parker and Johnson (2004), this work and the work of Pettet and Johnson (2003) suggest that, kinematically, a RFLS system is a reversed FFTS system. However, later in the study, Parker and Johnson (2004) find evidence that depict the two are different dynamically.

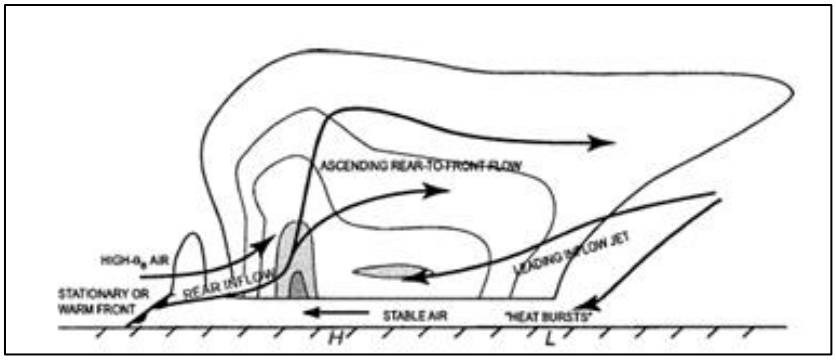

Figure 2.11 Fig. 5 from Parker and Johnson (2004) – Conceptual model, from Pettet and Johnson (2003), of a rear-fed convective line with leading precipitation, viewed in a vertical cross section oriented perpendicular to the convective line and parallel to its motion.

2.4.3 Kinematic features of front-fed leading stratiform systems

Kinematically the FFLS is notably different from the other two categories (Figure 2.12). For example, the overturning updraft is predominant instead of the jump updraft. However, there is front-to-rear flow in the lower levels much like the FFTS system. Previous cases suggest "some air in the front-to-rear stream ascended near the surface gust front and then descended and joined the surface cold pool" (Parker and Johnson, 2004). In the middle and upper troposphere, there is strong, horizontal rear-to-front flow. This rear-to-front inflow appears to be the dominant source of humidity and hydrometeors for the leading line of stratiform precipitation, much like the ascending front-to-rear flow in the FFTS system and the ascending rear-to-front flow in the RFLS system.

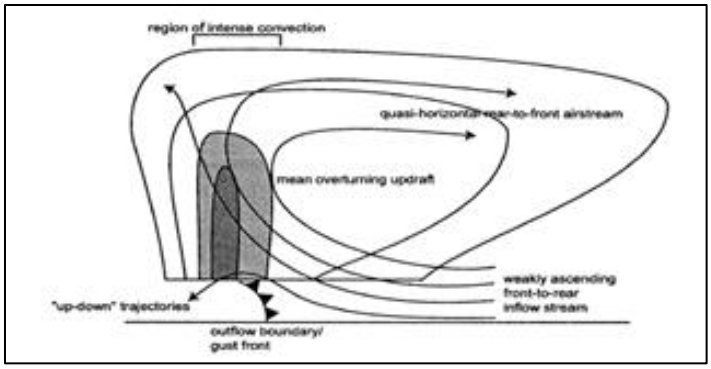

Figure 2.12 Fig. 8 from Parker and Johnson (2004) – Conceptual model, based on compiled radar observations, of a front-fed convective line with leading precipitation, viewed in a vertical cross section oriented perpendicular to the convective line and parallel to its motion.

2.4.4 Results of numerical simulations of quasi-2D MCSs

The next step of the study by Parker and Johnson (2004) was to use idealized numerical simulations to determine the dynamic structure of the FFTS, RFLS, and FFLS systems. They assessed the basic dynamics of the three flow regimes by incorporating five simulations using simple wind profiles. The 2D simulations consisted of a 2 km deep surface cold box that had minimal strength to initiate long-lived convective systems in all idealized wind profiles, base-state wind profiles, and base-state soundings. All in all, the results suggest that the organizational mode can be predicted by considering the preferred direction of the acceleration owing to the combined effects of local buoyancy and the gradient in the buoyant pressure field (ACCB) and the acceleration owing to the gradient in the linear dynamic pressure field (ACCDL) (Parker and Johnson, 2004).

The buoyant pressure field slows the inflowing air and accelerates it upward for a period of time near the boundary of the surface cold pool. It then accelerates the inflowing air quickly rearward over the cold pool and then downward. For the FFTS case,

the linear dynamic pressure field associated with an updraft within mean environmental shear generates a downshear-directed ACCDL that opposes the rearward ACCB. This creates a more upright and stronger updraft. An important note is this all occurs on the downshear side of the cold pool for the FFTS case. Alternatively, for the RFLS case, the action takes place on the upshear side of the cold pool which means the ACCDL contributes additional downshear, forward acceleration. This forward acceleration renders trajectories that have very shallow slopes which then hinders the development of deep convection in the basic RFLS setting. As a result, the RFLS systems are not dynamically equivalent of a "reversed FFTS system." However, when a low-level jet is present in the RFLS setting, there is reverse shear that exists above it. This creates a stronger and more upright updraft due to the rearward ACCDL in the middle troposphere. The updraft is even stronger when the system is also associated with an elevated high ϑ_e inflow source. When these conditions are present, the RFLS system is more similar, dynamically, to the FFTS system than a RFLS system without these conditions (Parker and Johnson, 2004).

When deep-layer shear (3-10 km layer) is added to the common set up of development on the downshear side of the surface cold pool, an overturning updraft structure is created. This occurs as a result of the downshear-directed ACCDL in the mid- and upper-troposphere. The addition of deep-layer shear can lead to a FFLS system "in which air leaves the convective region with rear-to-fore momentum and carries hydrometeors into the leading precipitation region" (Parker and Johnson, 2004). Although the deep-layer shear is important, the idealized simulations propose the lower-tropospheric shear has a greater effect.

The idealized simulation results imply predictability of QLCS modes. For a certain arrangement, awareness of where convection is forming; upshear or downshear side of a cold pool or baroclinic boundary, along with knowledge of the strength and depth of that shear can allow one to forecast which organizational mode, FFTS, RFLS, FFLS, is most likely. Additionally, from an acceleration perspective, the differences in vertical wind shear must account for the different structures. This transpires as a result of the "direct impact of the magnitude of the environmental shear upon the linear part of the dynamic pressure perturbation" (Parker and Johnson, 2004).

2.5 QLCS Climatology

The exploration of the climatology of severe weather hazards associated with QLCSs has reached a peak of interest in the last ten years. Many have found that knowledge of the convective mode present is important because it can inform a forecaster of the likelihood and type of severe weather approaching. Trapp et al. (2005) pioneered the research by estimating the percentage of U.S. tornadoes that are produced annually by QLCSs. The database incorporated 3828 tornadoes over a three year period (1998-2000) and radar was employed to classify the convective storms. Three basic categories were utilized: cell, QLCS, and other. A convective storm was classified as one of the three based on radar criteria. A convective system was labeled a cell if it "was a relatively isolated, circular or elliptically shaped region of reflectivity with maximum values typically greater than or equal to 50 dBZ; a QLCS was a quasi-linear region of radar reflectivity greater than or equal to 40 dBZ, continuously distributed over a horizontal

distance greater than 100 km; and the other category was populated primarily by tornadic outer rainbands of land fallen tropical cyclones" (Trapp et al., 2005). Although classifying this way can be subjective at times and difficult due to transitions, the authors were confident that their classification was consistent with other studies, such as Parker and Johnson (2000).

In order to discern whether a convective storm produced a tornado, the National Climatic Data Center (NCDC) publication *Storm Data* was utilized. However, there are biases and limitations with this publication. For example, the number of reports has increased, population density and time of day affect report frequencies, wind speeds tend to be overestimated by human observers, and lastly, wind and hail reports are treated as point events but should be assigned pathlengths like tornadoes (Weiss et al., 2002, Trapp et al., 2005, Doswell et al., 2005, Trapp et al., 2006, Gallus et al., 2008, Duda and Gallus, 2010, Smith et al., 2012). These shortcomings were acknowledged but no attempt was made to adjust the reported event magnitudes.

Trapp et al. (2005) concluded that QLCSs produced 18% of the total tornadoes that occurred in the three year period. Cells were responsible for 79% and the other storm type category was only credited with 3% of the total tornadoes. These are very promising results since there was good year-to-year consistency and the classification process was done sporadically over the time frame. For QLCS tornadoes, the percentage is higher when looking at the distribution of total tornado days by parent storm type (25%) (Table 2.1). Assessing the data this way prevents large outbreaks over a single day from affecting the tornado distribution. Also, there is "less temporal variability owing to lower sensitivity to the nonmeteorological factors that have inflated the tornado record over the

past 50 yr" (Trapp et al., 2005). The geographical distribution was also accounted for in this study. Although most tornado days (and tornadoes) were associated with cells, the percentage of tornado days (and tornadoes) linked to QLCSs exceeded 25% in the Mississippi and Ohio River Valleys (Figure 2.13). The highest was in Indiana with 50% of the tornado days being associated with QLCSs.

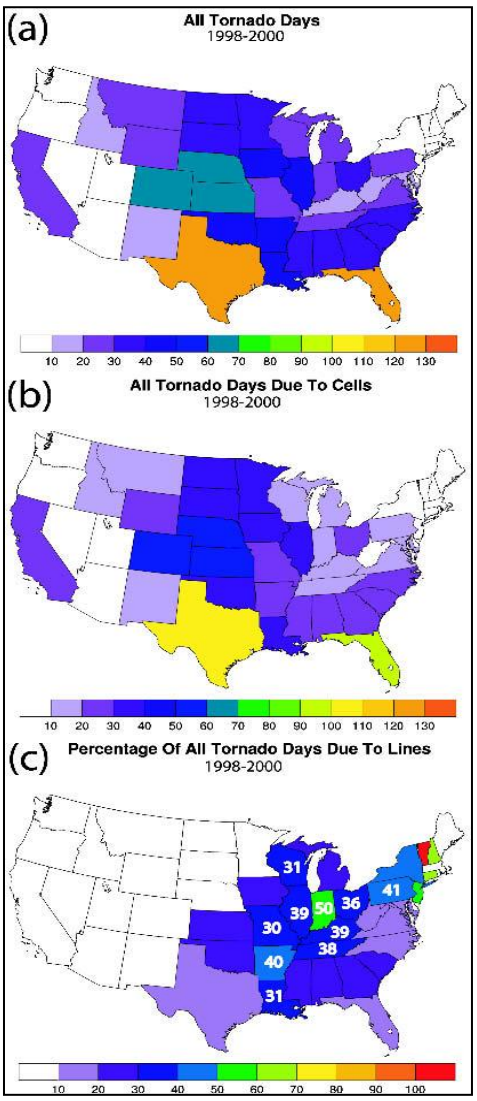

Figure 2.13 Fig. 2 from Trapp et al. (2005) – Geographical distribution of (a) all tornado days, (b) all tornado days due to cells, and (c) the percentage of all tornado days due to QLCSs, for 1998–2000.

Next, the data was distributed by F-scale. Using the Monte Carlo method, the authors were able to conclude that the distribution of QLCS tornadoes was significantly different than that of cell tornadoes. When compared to cells, QLCSs produced a great proportion of F1 tornadoes, but many fewer F2-F3 tornadoes. F4 and F5 tornadoes are particularly rare, even in cells; therefore, no noteworthy conclusions could be drawn. Subsequently, a distribution by monthly occurrence was created. Both cells and QLCS tornadoes tended to be most frequent during April through June. However, that data shows that "32% (29%) of the QLCS tornadoes (tornado days) occurred within the first three months of the year, compared to only 14% (16%) of cell tornadoes (tornado days)" (Trapp et al., 2005). Thus, QLCS tornadoes are more probable to occur during the cool season, especially January through March, than cell tornadoes. Interestingly, stronger QLCS tornadoes (F2-F3) also occurred with a slightly higher frequency during January through March than in May and June.

	Cumulative	1998	1999	2000
Cell	540 (72%)	185 (71%)	162 (70%)	193 (75%)
QLCS	185 (25%)	64 (24%)	60 (26%)	61 (24%)
Other	25 (3%)	13 (5%)	8 (3%)	4 (1%)
Total	**750** *587*	**262** *198*	**230** *181*	**258** *208*

Table 2.1 Table 2 from Trapp et al. (2005) – The distribution of total U.S. tornado days by parent storm type during 1998–2000. Percentages are computed using the boldfaced value in "total" row, which is sum of cell, QLCS, and other values ($\Sigma\, d_C + d_L + d_O$). This need not be equal to the total number of tornado days ($\Sigma\, d_T$), indicated in italics.

Finally, a distribution of hourly occurrence (3-hour running means) was generated. Cell and QLCS tornadoes both had a clear peak in the afternoon (1800 LST), but QLCSs had a secondary peak in the late night/early morning hours. The secondary peak reinforces how, in general, QLCSs tend to form in the late afternoon/early evening and continue until morning. Cumulative probabilities of the 3-hour running means of tornado occurrence depict 37% of QLCS tornadoes occurred between 2000 and 1000 LST, while 88% of cell tornadoes took place between 1000 and 2000 LST. After performing a statistical significant test, the authors found significantly more QLCS tornadoes form during the nighttime and morning hours of 2100-0900 LST than cell tornadoes. However, significantly fewer QLCS tornadoes occur between 1600 and 2000 LST than cell tornadoes. In addition, during the overnight hours (2300-0300 LST) the percentage of strong QLCS tornadoes is 21% which is noticeably higher than the percentage of weak QLCS tornadoes (9%). This could be due to the fact that weak QLCS tornadoes are underreported or that the intensity-limiting processes of weak versus strong QLCS tornadoes is different throughout the day (Trapp et al., 2005). Knupp (2000) suggested that weaker QLCS tornadoes also can be mistakenly reported as straight-line wind damage. In addition, it is more difficult to visually confirm tornadoes at night. Overall, it was proven that tornadoes produced by QLCSs deserve more attention. QLCSs are responsible for as much as 35%-50% of all tornadoes in the Midwest, especially in Indiana and surrounding states. They may not account for a majority of the tornadoes spawned annually in the U.S. but they do pose a threat.

Grams et al. (2012) did a very similar study but instead of an “other” category they had “clusters” and only EF2+ damage was included over the nine year period, so

their sample size was not quite as large (448). Either way their results were very similar to Trapp et al. (2005). They found QLCSs accounted for 27% of their events (20% of total tornadoes). In addition, Grams et al. (2012) broke down hourly occurrence based on the warm and cool seasons. However, while the warm season results were very similar to that of Trapp et al. (2005), the cool season results were different. Significant tornado events were more evenly distributed but there was a minimum near the peak of the diurnal heating cycle with a maximum near 0600 and 1500Z. The minimum suggests cool season QLCS significant tornado events are more synoptically driven.

Gallus et al. (2008) also did similar studies but included subclassifications of the three basic types (QLCS, cell, and other) and assessed not only tornadoes but severe wind and hail, and flooding. The year 2002 was evaluated from April to August. QLCSs were broken down into non-stratiform (NS), bow echo (BE), trailing stratiform (TS), leading stratiform (LS), and parallel stratiform (PS). Cells were divided into isolated cells (IC), clusters of cells (CC), broken line (BL), and the other category was called nonlinear (NL) (Figure 2.14). It was concluded that all morphologies (not necessarily all events) have a severe threat. For the QLCS subclassifications, "all types of severe weather were a threat but the frequencies depended greatly on the specific type of linear system" (Gallus et al., 2008). The most common threat with QLCSs is severe wind. This was mostly associated with bow echoes and the TS QLCSs. Severe hail reports were not uncommon for any type of QLCS but were especially linked to bow echoes. TS and PS QLCSs were the types to be most likely associated with flooding. Finally, LS and PS QLCSs pose a greater threat for tornadoes because the environments leading up to these structures may contain higher wind shear which would increase the chances of embedded supercells

(Gallus et al., 2008). During this study PS QLCSs were found to have one of the highest numbers of tornado reports per case. On the other hand, TS QLCSs had the smallest frequency of tornadoes.

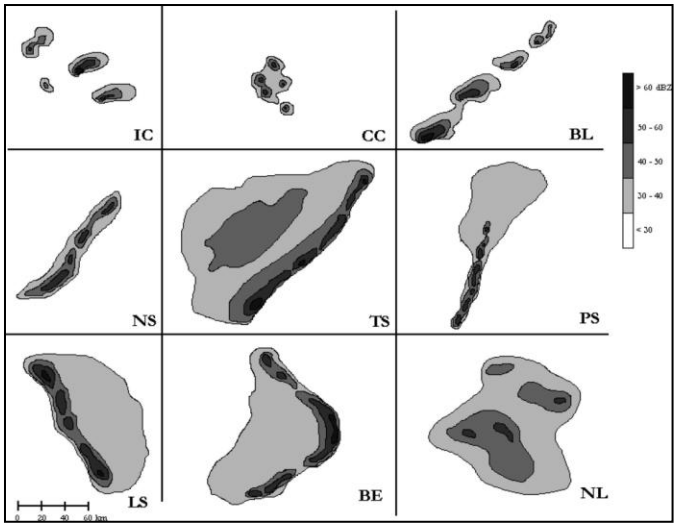

Figure 2.14 Fig. 2 from Gallus et al. (2008) – Schematic demonstrating each of the nine storm morphologies used in the classification system. Morphologies are abbreviated as follows: IC, isolated cells; CC, clusters of cells; BL, broken line; NS, squall line with no stratiform rain; TS, squall line with trailing stratiform rain; PS, squall line with parallel stratiform rain; LS, squall line with leading stratiform rain; BE, bow echo; and NL, nonlinear system.

Duda and Gallus (2010) expanded on Gallus et al. (2008) by assessing a different year (2007) and adding supercells as a morphology. For the most part similar results were established. QLCS systems composed about the same percentage of all systems for both the years of 2002 and 2007 (24% and 22%). QLCS systems again were associated with the second most severe reports. In fact, about 75% of all QLCS systems in 2007 (85% in 2002) produced severe weather in contrast to the 55% (66% in 2002) for cellular and nonlinear systems. In addition, "the contribution of storm reports from linear systems in

both years is noticeably larger than the fraction of systems identified as linear" (Duda and Gallus, 2010). This is most likely due to the increased organization of QLCS systems and their relatively large size. LS QLCSs, however, had the least number of severe reports and were relatively rare in occurrence along with PS QLCSs. This was the case for both Duda and Gallus (2010) and Gallus et al. (2008). Bow echo systems produced the largest average reports per system and had the greatest average number of reports of severe wind along with TS QLCSs. This is consistent with Gallus et al. (2008). Also consistent with the previous study is that PS and TS QLCSs are responsible for the most reports of flooding.

Finally, Smith et al. (2012) conducted an experiment similar to the previous research discussed. Their study "complements and enhances results from past convective mode investigations by increasing the number of radar-recognizable storm classifications" for a large sample (Smith et al., 2012). The period used was 2003-11 with 22,901 severe thunderstorm events evaluated. Events were broken into major convective modes following Trapp et al. (2005): QLCS, supercell, and disorganized. Then they were broken into subclassifications similar to Duda and Gallus (2010): QLCSs comprised of bow echo and line; right-moving (RM) and left-moving (LM) supercells included discrete cell, cell in cluster, and cell in line; and the disorganized category consisted of discrete cell, cell in cluster and cluster. Two additional minor classifications were also added: linear hybrids which are a mix of QLCS and line RM cells; and marginal supercell (Figure 2.15). The linear hybrid category was generated to depict a level of uncertainty in classification due to many cases exhibiting a mix of RM and QLCS structures. The

definition of each general classification and subclassification are again similar to the preceding studies.

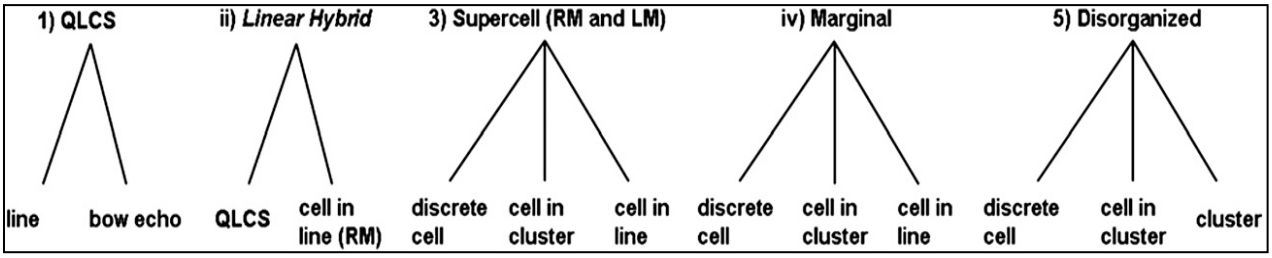

Figure 2.15 Fig. 2 from Smith et al. (2012) – Convective mode decision tree.

Results proved to follow similar patterns as the previous experiments. QLCS systems are associated with more EF1 + tornadoes compared to the total sample of tornado events. In addition, QLCS EF0 tornadoes are most likely to be underreported. For this experiment QLCSs were also most common in the Mississippi and Ohio River Valleys, as well as, QLCSs that produced tornadoes (Figure 2.16). When looking at the data seasonally, tornado events with QLCSs peak in the spring but this peak is less than those associated with discrete and cluster RMs. During the fall and winter, however, "tornadoes with linear convective modes were nearly as frequent" as discrete or cluster RMs (Smith et al., 2012). In fact, QLCS systems have a relative frequency near 50% from November to February which coincides with Trapp et al. (2005).

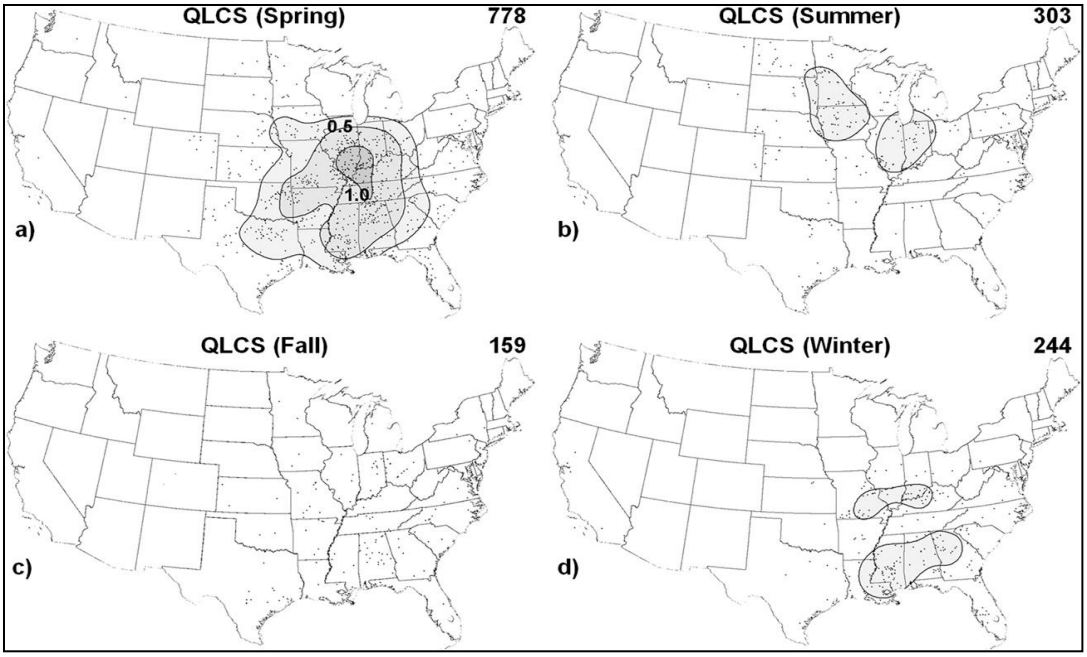

Figure 2.16 Fig. 15 from Smith et al. (2012) – All QLCS tornado events by season (a) March–May (spring), (b) June–August (summer), (c) September–November (fall), and (d) December–February (winter). The minimum contour is 0.25 events per 10-yr estimate based on 2003–11 data. Labeled contours begin at 0.5 events per 10 yr. Other conventions are the same as in Fig. 6.

All of this research, with the slightly varying convective mode classes, demonstrates the need for a universal convective mode classification method. "This is necessary to uniformly describe the full spectrum of storm types, such that classification differences do not dominate the interpretation of atmospheric variables related to the various convective modes" (Smith et al., 2012). All in all, these papers depict the same important information regarding QLCS systems. They are not the most common system linked to tornadoes but still pose a threat not only in spring and summer but also in the winter. In addition, they usually generate weaker (EF0-EF1) tornadoes but can produce stronger tornadoes (EF2-EF3). Next, QLCS systems are most frequent in the Mississippi and Ohio River Valleys. Finally, QLCS tornado events tend to have two hourly peaks, one in the afternoon and a secondary peak in the overnight to early morning hours.

2.6 Mesovortices

2.6.1 General

The low-level circulations associated with QLCSs are known as mesovortices and they are capable of producing severe straight-line winds and tornadoes. They are included in the meso-γ scale, which has a horizontal scale of 2-20 km and a time-scale of about one hour (Orlanski, 1975). Typically, mesovortices have couplet diameters that range from 0.5 km to 9 km with an average lifetime of about an hour (Atkins et al., 2004). In addition, mesovortices form in the lowest 2.5 km AGL and tend to build quickly upward. Sometimes they can build upward to about 6-8 km AGL and become a new midlevel line-end vortex. It is important to note, however, that "the low-level mesovortices need not be preceded by and form beneath a midlevel mesovortex. Conversely, the midlevel mesovortices need not precede and otherwise be associated with a low-level mesovortex" (Trapp and Weisman, 2003). This independence confirms that mesovortices are "nondescending" (Trapp et al., 1999, Atkins et al., 2004). Mesovortices can form along any part of the QLCS line initially, but once a QLCS becomes bow shaped (sub-system scale or system scale), the mesovortices are primarily located north of the apex (Weisman and Trapp, 2003, Trapp and Weisman, 2003). They have also been observed at the intersection point of the convective system and a preexisting boundary, such as, a stationary or warm front, or an outflow boundary oriented nearly perpendicular to the convective line (Atkins et al., 2004). Also, multiple circulations can exist simultaneously at different stages of QLCS development and they can merge together which tends to make them stronger (Funk et al., 1999, Weisman and Trapp, 2003).

Initiation of the low-level mesovortices is a result of the "tilting, in downdrafts, of initially crosswise baroclinic horizontal vorticity; such horizontal vorticity may be associated with a rear inflow jet (RIJ) (mature QLCS) or the cool outflow of a rainy downdraft (developing QLCS)" (Figure 2.17) (Trapp and Weisman, 2003). A majority of these vortices become cyclonic due to the vertical stretching of the planetary vorticity; thus the Coriolis force directly influences low-level mesovortexgenesis. Atkins and St. Laurent (2009b) identified two genesis mechanisms; one that was observed to occur at all stages of QLCS evolution and one that occurred predominately during the early bow echo stage. The first is very similar to what Trapp and Weisman (2003) found. Mesovortices were generated when parcels descended in the downdraft and attained horizontal vorticity that was generated by the baroclinic zone across the gust front. The parcels were then tilted by the updraft along the gust front. The second mechanism created couplets with the cyclonic vortex north of the anticyclonic vortex. Just behind and along the gust front, vortex lines were oriented south. "Localized updrafts tilted the initially horizontal cold-pool vortex lines upward, creating arches of vortex lines centered on the updraft. Thus, cyclonic (anticyclonic) vertical vorticity was produced on the northern (southern) side of the updraft" (Atkins and St. Laurent, 2009a). The convective-scale downdraft that produced outflow, which locally accelerated the gust front outward, generated the localized updraft maximum. They concluded that the preferred mesovortex genesis mechanism appeared to depend on the environmental shear, Coriolis forcing, and cold pool strength. Specifically, as the shear strength increased, the first mechanism dominated (mature stage). All in all, more than one process can be responsible for producing mesovortices.

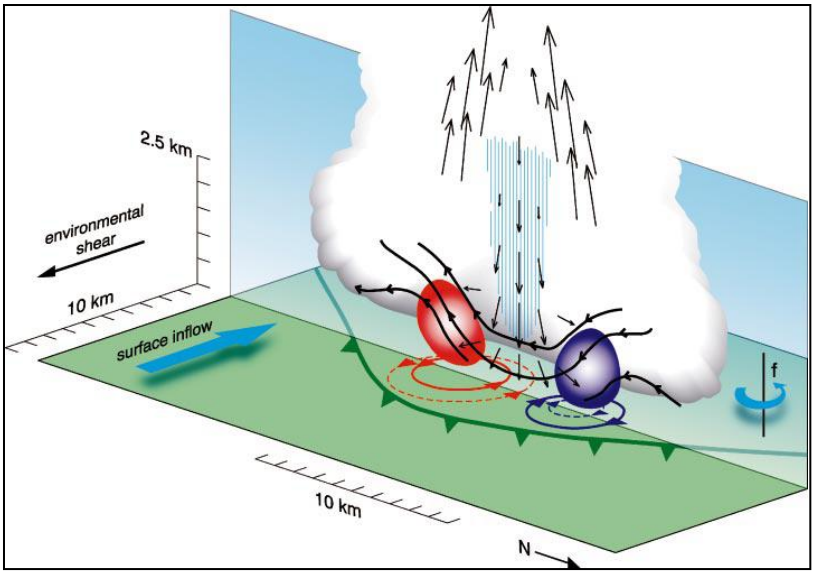

Figure 2.17 Fig 23 from Trapp and Weisman (2003) – Schematic showing a proposed mechanism for low-level mesovortexgenesis within a QLCS. The green barbed line indicates the gust front, vectors are of air motion in the vertical plane, blue hatching depicts rain core, bold black lines are vortex lines in the vertical plane, and red (purple) areas indicate positive (negative) vertical vorticity in the vertical plane. Vortex lines are tilted vertically by the downdraft, resulting in a surface vortex couplet (red is cyclonic vortex; purple is anticyclonic vortex). The future state of the vortex couplet, which results in part from the stretching of planetary vorticity (*f*), is shown by the dashed red and purple circles. Schematic represents early-QLCS-stage vortexgenesis. During the mature QLCS stage, relevant vortex lines would have opposite orientation; hence, resultant vortex couplet orientation would be reversed.

Atkins and St. Laurent (2009a) also investigated mesovortex strength. Through a series of simulated experiments, they concluded the same parameters (shear, Coriolis forcing, and cold pool strength) that influence the preferred mesovortex genesis mechanism, influence the strength of a mesovortex. When low-level shear was nearly balanced by the cold pool, stronger, more potentially damaging mesovortices formed. Weaker and fewer mesovortices, as well as, a delay in formation resulted when the shear was weaker. Weisman and Trapp (2003) found stronger vortices occurred when environmental shear values were 20 ms^{-1} or greater over the lowest 2.5-5 km AGL, while weaker, shallower vortices were produced when shear magnitudes of 15 ms^{-1} or less were

present. This was the same case for the deeper shear (up to 5 km) simulations. As the deeper shear decreased, mesovortex production was delayed and the vortices tended to be weaker. When the Coriolis forcing increased, more low-level circulation was created. "The increased low-level circulation was attributed to more intense and a larger number of mesovortices" (Atkins and St. Laurent, 2009a). All of these results are consistent with previous literature. Finally, the relationship between cold pool strength and mesovortices was assessed. There was less low-level circulation produced as the cold pool decreased in strength because a weaker cold pool is spatially smaller. This provides fewer areas for vortex generation along the gust front as well as a weaker system as a whole.

2.6.2 Tornadic mesovortices vs. nontornadic mesovortices

Mesovortices have been found to produce not only damaging straight-line winds but also tornadoes. Typically these tornadoes produce EF0-EF2 damage with occasional EF3 and even EF4 damage (Atkins et al., 2004, Trapp et al., 2005). Tornadogenesis has been found to occur "as transient low-level shear zones along and north of the apexes of bowing segments spun-up rapidly into well-defined, deep layered cyclonic circulations" (DeWald and Funk, 2000, Weisman and Trapp, 2003). However, tornadoes have been seen south of the apexes as well. The amount of shear over the lowest 2.5-5 km AGL found in tornado producing environments has been established to be greater than 15 ms^{-1}, which was noted early as the amount of wind shear necessary for the production of mesovortices (Weisman and Trapp, 2003). Atkins et al. (2005) established, based on their experiment, that the mean tornado lifetime was about 5.5 minutes. This is relatively short

compared to the parent mesovortex, but damage to life and property can still be accomplished. The small scale and short lifetimes of these tornadoes and their parent circulations make it very hard to detect them on radar. This makes issuing warnings for QLCS tornadoes also difficult.

Not all mesovortices, however, produce tornadoes. Atkins et al. (2004) were among the first to do an in depth study about what makes tornadic mesovortices different from nontornadic mesovortices. Sizes for tornadic and nontornadic mesovortices range from 0.5-9 km. Sometimes mesovortices become larger with time but typically remain smaller than midlevel vortices. Again, mesovortices can form anywhere on the linear system at any time but generation is favorable once there is embedded bowing or system-scale bowing. The average lifetime of a mesovortex is 56 minutes while, more specifically, tornadic mesovortices live on average for 76 minutes and nontornadic mesovortices exist on average for 32 minutes (Atkins et al., 2004). Strength also tends to vary between tornadic and nontornadic mesovortices. Tornadic cases were connected to larger V_r (defined in Figure 2.18) values, typically greater than 25 ms^{-1}, while nontornadic values were generally less than 20 ms^{-1} (Figure 2.18). This implies tornadic mesovortices have larger rotational velocities than nontornadic mesovortices. The difference in strength becomes more apparent when evaluating the mean radial velocity vertical profiles for both cases (Figure 2.19). Results show that a big difference can be seen below 2 km, but it is below 0.5 km that tornadic and nontornadic radial velocities differ as much as 8 ms^{-1} (Atkins et al., 2004).

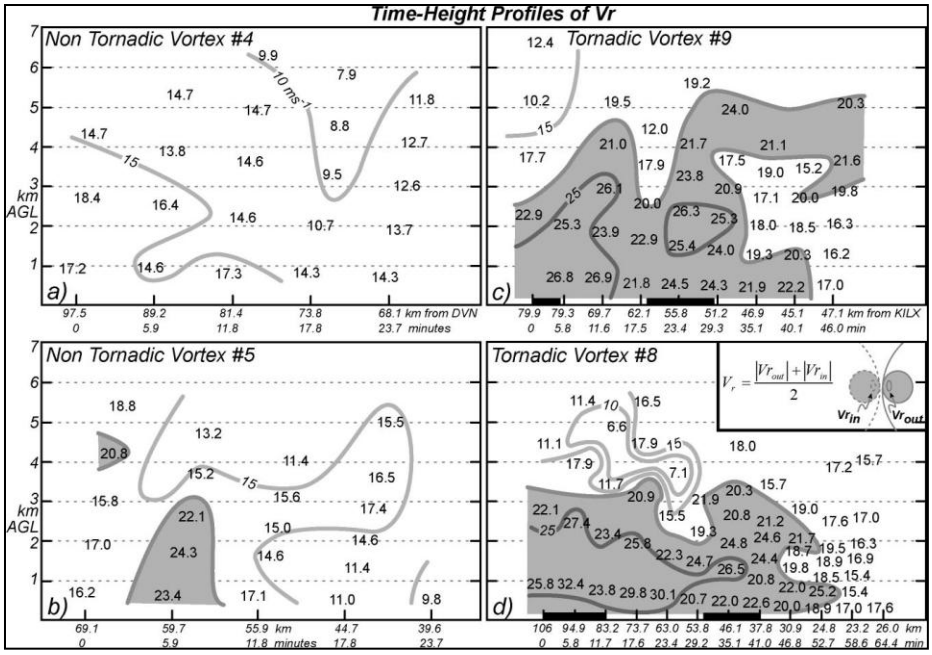

Figure 2.18 Fig. 11 from Atkins et al. (2004) – Time –height profiles of average radial velocity, *Vr* for nontornadic vortices 4 and 5 and tornadic vortices 9 and 8. As shown in the inset diagram, *Vr* is defined as the average of the absolute values of the inbound and outbound radial velocity values associated with the rotational couplet; *Vr* values are contoured every 5 m s^{-1}, with values greater than 20 m s^{-1} shaded gray. The black bars in (c) and (d) represent the time periods of tornadic damage.

Atkins et al. (2005) expanded upon Atkins et al. (2004) and found very similar results as well as new compelling results. For example, "on average, only 12 minutes elapse from the genesis of the parent mesovortex until it produces a tornado, suggesting that forecasters have little time to determine which mesovortices will become tornadic" (Atkins et al., 2005). This is consistent with what is known about the short timescale of mesovortices, however, more cases need to be evaluated before this can become a general conclusion. Furthermore, when assessing the time prior to tornadogenesis, tornadic vortices are stronger than nontornadic vortices in the lowest 2.5 km AGL. Also in agreement with Atkins et al. (2004) is the result that when all time steps are incorporated, the strength difference between tornadic and nontornadic mesovortices is slightly larger

below 3 km AGL. This suggests that tornadic mesovortices strengthen only in the lowest 3 km during and after tornadogenesis (Atkins et al., 2005). Finally, results propose that tornadic mesovortices evolve differently than nontornadic mesovortices. Evidence can be seen when evaluating V_r, $\Delta V_r/\Delta t$, mesovortex couplet diameter, and azimuthal shear (Figure 2.20). "Examination of the V_r and $\Delta V_r/\Delta t$ fields prior to tornadogenesis revealed a mesovortex that was deepening and intensifying rapidly," especially in the lowest 2 km (Atkins et al., 2005). Couplet size tended to slightly decrease as the circulation intensified and then it grew modestly until the mesovortex dissipated. Finally, in response to the strengthening mesovortex and, to a smaller degree, the decreasing couplet diameter, the azimuthal shear increased as well. In contrast, V_r and azimuthal shear proved that nontornadic circulations were much weaker and shallower. In addition, couplet diameter evolution was inconsistent from case to case.

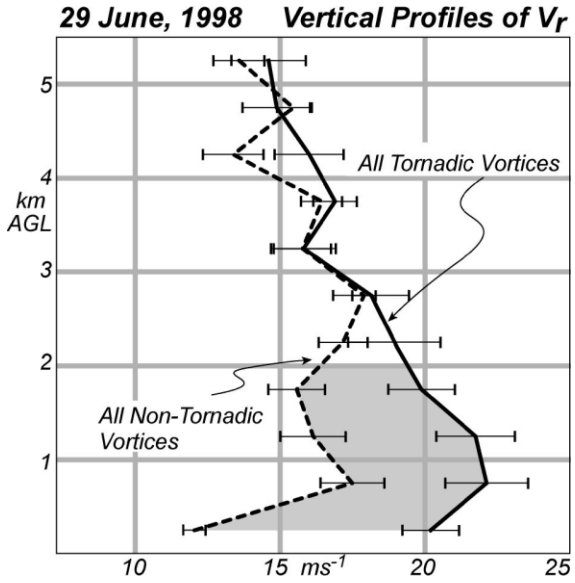

Figure 2.19 Fig. 12 from Atkins et al. (2004) – Composite vertical profiles of *Vr* for all tornadic (solid line) and nontornadic (dashed line) mesovortices shown in Fig. 7. Error bars represent 1 std dev for all data points at the respective level.

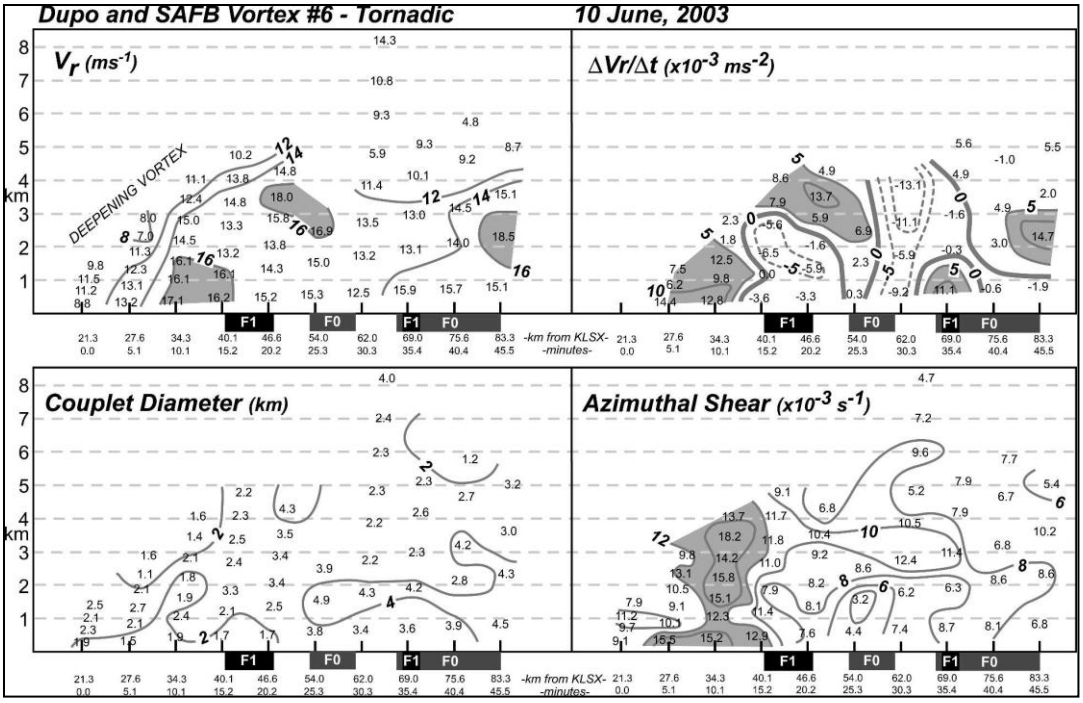

Figure 2.20 Fig. 11 from Atkins et al. (2005) – Time-height profiles of *Vr*, *_Vr* /*_t*, mesovortex couplet diameter, and azimuthal shear for tornadic mesovortex 6. Here *Vr* is contoured every 4 m s^{-1} with values greater than 16 m s^{-1} shaded gray, and *_Vr* /*_t* (x 10^{-3} m s^{-2}) is contoured every 5 x 10^{-3} m s^{-2} with values greater than 5 x 10^{-3} m s^{-2} shaded gray. Couplet diameter is contoured every 2 km while azimuthal shear (x 10^{-3} s^{-1}) is contoured every 2 x 10^{-3} s^{-1} with values greater than 12 x 10^{-3} s^{-1} shaded gray. A distance scale relative to KLSX along with a time scale relative to vortexgenesis are indicated along the horizontal axis. The intensity and times of tornado and straight-line wind damage produced by the mesovortex are shown as black and gray bars, respectively, along the horizontal axis.

A new result from Atkins et al. (2005) depicted that tornadic mesovortices can be associated with the rear inflow jet (RIJ). In this case study, all but one tornadic mesovortex formed once the system began to bow. This suggests that these tornadic mesovortices were generated concurrently or at a time just after the RIJ formed and "at a location along the gust front where convergence was locally enhanced by descending rear-to-front flow" (Atkins et al., 2005). Therefore, Atkins et al. (2005) hypothesized that QLCSs are more likely to become tornadic if mesovortices form at a location along the gust front that has been strengthened by the RIJ.

2.6.3 Mesovortices vs. mesocyclones

Mesovortices in QLCSs are the counterpart to mesocyclones in supercells. They have a few similarities but overall are very different circulations. Mesocyclones typically have a diameter of 7-10 km, while mesovortices are generally between 2 and 9 km (Atkins et al., 2004). Therefore, sometimes, mesovortices can become just as large as or larger than some mesocyclones. However, mesovortices do not usually get that large until later stages in their lifetime (Weisman and Trapp, 2003). Moreover, mesovortices are occasionally associated with a hook structure in the reflectivity field similar to mesocyclones. Finally, some mesovortices can have strengths comparable to mesocyclones; such mesovortices met the mesocyclone rotational velocity criteria (DeWald and Funk, 2000, Weisman and Trapp, 2003).

Despite the similarities, mesovortices and mesocyclones are very different. For example, the way these circulations form. In the midlevels, mesocyclones typically develop when there is vertical tilting and stretching by the updraft of ambient horizontal vorticity. At low levels, mesocyclogenesis "occurs as streamwise horizontal vorticity, generated primarily in buoyancy gradients along the forward- (rear) flank gust front, and is vertically tilted in the storm's main updraft (rear-flank downdraft)" (Rotunno and Klemp, 1985, Trapp and Weisman, 2003). Mesovortices can also been seen at midlevels as well as low-levels. Both form similarly in that they are initiated "by the tilting, in downdrafts, of initially crosswise baroclinic horizontal vorticity" (Trapp and Weisman, 2003). Furthermore, planetary vorticity plays an important role in the initiation of mesovortices unlike mesocyclones.

Additionally, mesovortices form within the lowest 2.5 km AGL and build upward, whereas, mesocyclones begin in the midlevels and descend toward the ground. Mesovortices can build up into the midlevels but are independent of midlevel circulations. On the other hand, midlevel mesocyclones develop prior to the development of low-level mesocyclones, making the low-level mesocyclone dependent on the midlevel circulation (Weisman and Trapp, 2003). These distinctions demonstrate it is much easier to identify mesocyclones on radar than mesovortices, especially at far distances. However, it has been proven that differentiating between tornadic and nontornadic low-level mesocyclones is not yet possible, while it may be possible to determine whether a mesovortex is tornadic or nontornadic (Wakimoto and Cai, 2000; Trapp, 1999; Atkins et al., 2004).

Mesovortices also are not associated with a preexisting steady rotating updraft at the mid- and upper-levels. Conversely, steady and vertically erect updrafts are a key structural feature of supercells and are important for mesocyclone development (Figure 2.21). Subsequently, the average lifetimes of the two circulations differ. Mesovortices tend to exist for about 56 minutes, whereas, mesocyclones typically live for about 90 minutes (Atkins et al., 2004). Finally, mesovortices tend to propagate with the mean wind but mesocyclones have been proven to propagate significantly to the right of the mean wind (Weisman and Trapp, 2003). All in all, mesovortices and mesocyclones do not display similar characteristics.

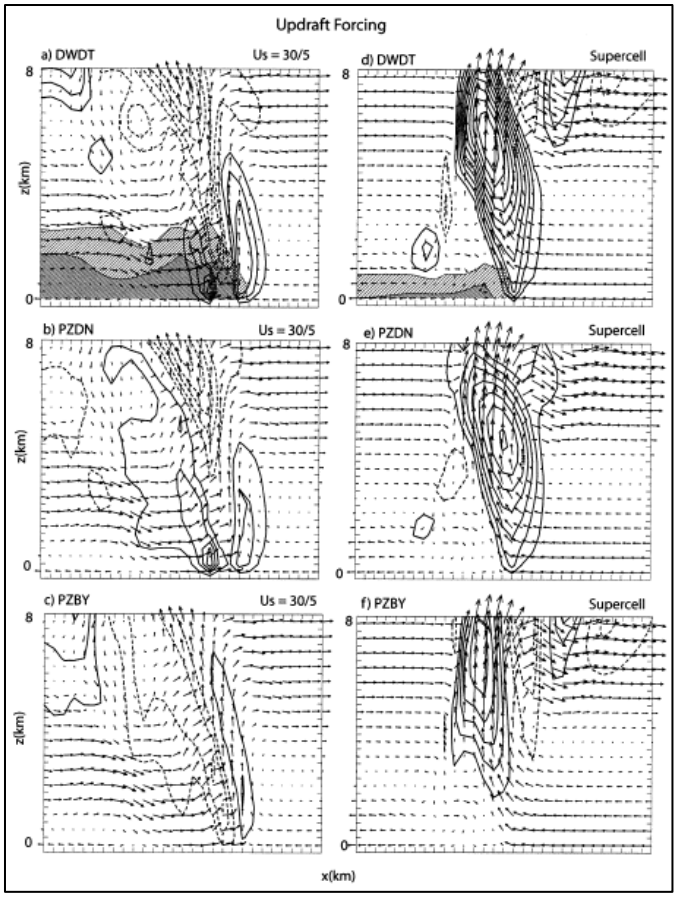

Figure 2.21 Fig. 20 from Weisman and Trapp (2003) – Total vertical velocity forcing (DWDT), dynamic forcing (PZDN), and buoyant forcing (PZBY) for (a), (b), (c) vortex Vi for the U_s = 30 m s^{-1} over 5 km QLCS simulation and (d), (e), (f) the isolated supercell simulation, respectively, as described in the text. Forcing terms are contoured using a 0.002 m s^{-2} interval, with the zero contour omitted. Vectors and shading are the same as in Fig. 11.

In conclusion, the knowledge of mesovortices is important to forecasters, especially those forecasting in the Mississippi and Ohio River Valleys. Being familiar with the size, lifetime, strength, and propagation of mesovortices can alleviate some of the difficulty of forecasting and issuance of warnings for mesovortices. Also, it may be possible to successfully distinguish between tornadic and nontornadic mesovortices. However, the results also emphasize the need for higher spatial and temporal resolution data specifically at low levels so forecasters can effectively monitor mesovortex

development. Either way, tornadic vortices tend to be stronger and longer-lived than nontornadic vortices with the greatest differences just before tornadogenesis in the lowest 2 km. Therefore, examining the time history of the strength and longevity of each mesovortex may prove to be valuable for issuing advanced tornado warnings. Finally, most forecasters are very familiar with mesocyclones but not mesovortices. Knowledge of the distinctions between the two allows a forecaster to adjust to the specific situation at hand and gives them a better chance to issue warnings with greater lead times.

2.7 Summary

Research on QLCSs has come to the forefront the past 30 years. From extensive work on MCS structure and dynamics (Houze, 2004) to more specific work on linear MCSs or QLCSs and their maintenance (Rotunno et al., 1988), organizational modes (Parker and Johnson, 2000; Parker and Johnson, 2004), and climatology (Trapp et al., 2005; Gallus et al., 2008; Grams et al., 2012; Smith et al., 2012), the topic continues to receive much deserved attention. In addition, the work of Weisman and Trapp (2003), Atkins et al. (2004, 2005), and Atkins and St. Laurent (2009a, 2009b) provided insight into mesovortices and how to differentiate them between tornadic and non-tornadic mesovortices. It is the expectation of this study to determine the differences between radar parameters of tornadic and non-tornadic QLCSs in the central United States, and to provide aid to forecasters in regards to accurately identifying tornado circulations within QLCS systems.

Chapter 3 Methodology

3.1 Event Selection

The project focused on 57 QLCS events between 2005 and 2012 that encompassed the following NWS County Warning Areas (CWA): St. Louis, Springfield, Kansas City (Pleasant Hill), Tulsa, Paducah, Little Rock, Louisville, Indianapolis, Chicago, Omaha, Bismark, Sioux Falls, and Minneapolis. A map highlighting the region of the area studied can be found in Figure 1.1. This area was chosen to limit geographical and climatological variations, and these NWS CWAs are located where QLCSs are most commonly observed (Trapp et al., 2005, Smith et al., 2012).

In order for a case to be included, the system had to be linear (based off NCDC's Historical Mosaic Radar) and a tornado or tornado warning had to be associated with the convective line. From there the cases were divided into tornadic and non-tornadic based upon whether tornadoes were actually produced. This approach was taken due to the difficultly a forecaster has in discriminating between tornadic QLCSs and non-tornadic QLCSs and issuing timely accurate warnings. Non-tornadic cases that did not have a tornado warning associated with them were not included because it was clear the forecaster knew the system did not pose a tornado threat. A system was labeled tornadic if the QLCS produced one or more verified tornadoes regardless of EF rating or non-tornadic as long as one tornado warning was issued by the NWS but no tornadoes were verified. An event day was broken into two events if the tornadoes (warnings) occurred at

least two hours apart. The Iowa State University Iowa Environmental Mesonet Cow (IEM Cow) Storm Based Warning Verification web page was utilized to determine whether a tornado warning was issued or not and the Storm Events Database was employed to verify whether there was a tornado and the time and location of that tornado. It is important to note, however, that numerous studies have indicated there are biases and limitations with using the Storm Events Database. For instance, population density and time of day affect report frequencies, the number of reports has increased, wind speeds tend to be overestimated by human observers, QLCS EF0 tornadoes are underreported, and wind and hail reports are treated as point events when they should be assigned pathlengths like tornadoes (Weiss et al., 2002; Trapp et al., 2005; Doswell et al., 2005; Trapp et al., 2006; Gallus et al., 2008; Duda and Gallus, 2010; Smith et al., 2012). With that said, the limitations are acknowledged but use of these resources continued as they are the best available.

Once the events were classified as tornadic and non-tornadic, they were sub-divided into warm season and cold season. This was done to account for seasonal differences; the warm season severe weather events typically possess lower wind shear and higher instability, while the opposite is generally seen for cold season events. The warm season was defined as the end of March through October and the cold season was defined as November through the beginning of March (Grams et al., 2012). Therefore, the 57 events were divided in the following way: 19 warm season tornadic, 18 warm season non-tornadic, 10 cold season tornadic, and 10 cold season non-tornadic. A complete list of the events is found in Tables 3.1-3.4.

Table 3.1. List of all warm-season tornadic events with date, times, CWA(s) affected, total number of tornadoes, number of EF0s, EF1s, EF2s, and EF3s.

Date	Pre-event	Event	Post-event	CWA(s)	# Torns	EF0	EF1	EF2	EF3
03/31/2006	0212z	0222z	0243z	EAX	3	2	1	0	0
04/02/2006	2148z	2158z	2309z	LSX	11	7	2	2	0
07/21/2006	1623z	1633z	1713z	LSX	6	5	1	0	0
08/23/2007	1953z	2003z	2014z	LOT	1	0	1	0	0
05/02/2008	0649z	0659z	0709z	EAX	2	0	0	1	1
06/06/2008	2314z 0026z	2325z 0036z	2345z 0057z	OAX	4	1	2	1	0
06/08/2008	0659z	0709z	0729z	OAX	3	0	1	2	0
04/10/2009	0114z	0124z	0134z	SGF	1	1	0	0	0
05/08/2009	1241z	1251z	1505z	SGF	23	3	13	6	1
05/08/2009	1620z	1630z	1641z	PAH	2	1	1	0	0
04/30/2010	2312z	2323z	0013z	SGF	2	0	2	0	0
05/13/2010	0933z	0944z	1024z	INX	9	1	4	4	0
06/27/2010	0057z 0204z	0108z 0215z	0128z 0256z	FSD/MPX	8	8	0	0	0
10/26/2010	1341z	1351z	1432z	IND	2	2	0	0	0
04/20/2011	0408z	0418z	0549z	LVX	19	10	7	2	0
05/26/2011	0107z 0140z	0117z 0150z	0239z 0242z	IND/LVX	11	0	9	2	0
06/19/2011	0424z	0434z	0515z	SGF	6	2	4	0	0
07/10/2011	2023z	2034z	2146z	BIS	4	3	1	0	0
08/10/2011	0825z	0836z	0847z	INX	3	0	2	1	0

Table 3.2. List of all cold-season tornadic events with date, times, CWA(s) affected, total number of tornadoes, number of EF0s, EF1s, EF2s, EF3s and EF4s.

Date	Pre-event	Event	Post-event	CWA(s)	# Torns	EF0	EF1	EF2	EF3	EF4
11/06/2005	0722z	0732z	0833z	PAH	8	1	0	1	6	0
11/15/2005	2310z	2320z	0012z	LVX	3	0	2	1	0	0
11/27/2005	2129z 2220z 0234z	2139z 2230z 0244z	2200z 0214z 0254z	LZK	38	3	21	11	3	0
01/08/2008	0248z 0435z	0258z 0445z	0411z 0456z	SGF	6	3	2	1	0	0
01/29/2008	2254z	2304z	2324z	PAH	2	0	0	2	0	0
11/06/2008	0733z	0743z	0753z	SGF	1	0	1	0	0	0
12/27/2008	1657z	1707z	1717z	LSX	1	0	1	0	0	0
12/31/2010	1704z	1714z	1835z	LSX	13	6	5	1	1	0
02/29/2012	0441z	0451z	0734z	SGF	13	1	9	3	0	0
02/29/2012	0907z	0917z	1141z	PAH	14	0	3	8	1	2

Table 3.3. List of all warm-season non-tornadic events with date, times, CWA(s) affected, and total number of tornado warnings issued.

Date	Pre-event	Event	Post-event	CWA (s)	# of Warnings
06/08/2005	1834z	1844z	1935z	LSX	2
07/20/2006	0007z 0128z	0018z 0139z	0118z 0159z	LSX	3
09/23/2006	1613z	1624z	1825z	PAH	5
09/06/2007	2230z	2240z	2321z	LSX	2
07/08/2008	2013z 2145	2024z 2155z	2115z 2236z	LSX	2
08/06/2008	0032z	0042z	0102z	LSX	1
05/15/2009	2153z	2204z	2345z	LSX	3
06/16/2009	0333z	0343z	0414z	EAX	2
06/15/2010	1923z	1934z	2026z	LSX	2
07/11/2010	2113z	2123z	2244z	LSX	2
07/18/2010	1532z	1542z	1613z	LSX	1
07/25/2010	0012z	0022z	0032z	LSX	1
06/18/2011	1022z	1032z	1205z	LSX	2
06/19/2011	0721z	0732z	0833z	LSX	2
06/21/2011	2131z	2141z	2212z	LSX	1
06/27/2011	0634z	0645z	0716z	LSX	1
07/08/2011	0010z	0020z	0030z	LSX	1
10/17/2012	2212z	2222z	2232z	LSX	1

Table 3.4. List of all cold-season non-tornadic events with date, times, CWA(s) affected, and total number of tornado warnings issued.

Date	Pre-event	Event	Post-event	CWA(s)	# of Warnings
11/06/2005	0142z	0152z	0232z	LSX	1
11/13/2005	0014z 0146z	0024z 0156z	0115z 0216z	SGF	2
11/15/2005	1735z 1847z	1746z 1857z	1827z 1918z	LSX	2
11/28/2005	0218z 0500z	0228z 0510z	0419z 0541z	LSX	5
01/13/2006	0302z	0312z	0343z	SGF	1
11/30/2006	0134z	0144z	0225z	SGF	1
01/07/2008	2013z	2023z	2044z	EAX	1
02/05/2008	2307z	2317z	0130z	SGF	3
03/08/2009	1210z 1321z	1221z 1331z	1301z 1443z	SGF	3
11/25/2010	0412z	0422z	0633z	LSX	4

3.2 Data Downloading and Processing

For this research, NEXRAD Level II radar data was obtained through the National Climatic Data Center's (NCDC) Hierarchical Data Storage System (HDSS). Once the requested raw data was delivered, it was processed through the National Severe Storms Laboratory's Warning Decision Support System – Integrated Information (WDSS-II), using the algorithm "ldm2netcdf," to be converted into a "netCDF" file. A

second algorithm, "llsd," was then used to process circulation data to obtain azimuthal shear, divergence, and rotation tracks (2h and 6h). Lastly, the "w2merger" algorithm was employed to convert the radar data from a multi-elevation polar grid to a Cartesian grid. The field was a 256 km × 256 km gridded data at a 1 km × 1 km resolution centered on the radar location. This made the data easier to handle for the duration of the experiment.

There were 10 parameters used for this study from the "w2merger" algorithm: merged reflectivity at 2 km, merged spectrum width at 2 km, merged divergence at 2 km, merged azimuthal shear at 2 km, spectrum width maximum below 3 km, spectrum width maximum 3-7 km, divergence maximum below 3 km, divergence maximum 3-7 km, azimuthal shear maximum below 3 km, and azimuthal shear maximum 3-7 km. Divergence and azimuthal shear were assessed to evaluate wind speed/direction, which is information available to forecasters at warning time. Spectrum width is also readily available during warning time so the parameter was assessed to determine if there are any distinctions between tornadic and nontornadic cases that would aid a forecaster.

3.3 Analysis of Data from Chosen QLCS Events

For the analysis of the 57 QLCS events chosen, NEXRAD Level-II radar was examined. Time and location for each tornado (tornado warning for non-tornadic cases) associated with each case was found using the ICOW Mesonet data and the Storm Events Database. It was established that most of the tornadoes (tornado warnings) were so close in time, a representative pre-event, event, and post-event time was chosen for the entire event. An event had multiple representative pre-event, event, and post-event times if

tornadoes (tornado warnings) were at least 20 minutes apart. From there the radar time steps that corresponded closest to the representative pre-event, event, and post-event times were selected. A representative pre-event time is included in this study to assess the values of the different parameters before a system becomes, or is thought to become (non-tornadic cases) tornadic so probability of detection can increase and false alarm rate can decrease.

3.4 MATLAB and ProStat

To begin the process of evaluating the ten radar parameters, the radar time steps that corresponded to the representative pre-event, event, and post-event times for each event were processed through MATLAB. The MATLAB code identifies storm cells as areas of adjacent pixels that exceed the reflectivity threshold selected. To determine how linear each event really was, three reflectivity thresholds were used: 35 dBZ, 40 dBZ, and 45 dBZ (Figure 3.1). These thresholds were chosen based on previous literature (Trapp et al., 2005; Gallus et al., 2008). Two of the reflectivity thresholds (35 dBZ and 40 dBZ) at the event time were also used to determine how many events fulfilled the definition set by Trapp et al. (2005). Each time step chosen was processed with each reflectivity threshold used. A final array table was then created which contained the following 21 parameters:

- cell ID
- cell size
- axial ratio

- orientation
- maximum and mean merged azimuthal shear at 2 km
- maximum and mean merged divergence at 2 km
- maximum and mean merged spectrum width at 2 km
- maximum and mean azimuthal shear below 3 km
- maximum and mean divergence below 3 km
- maximum and mean spectrum width below 3 km
- maximum and mean azimuthal shear 3-7 km
- maximum and mean divergence 3-7 km
- maximum and mean spectrum width 3-7 km.

These parameters were then extracted for the areas of all cells greater than 200 km^2. For some cases there were multiple cells (cell IDs) in the grid box analyzed. In the interest of time, each cell was not evaluated to determine if it was tornadic (thought to be tornadic) or not. Therefore, the values for each parameter, for every cell ID, were used for this study. It is noted that this could skew the data, but future studies could do this to better the results.

Next, the data were organized into excel files for the warm season tornadic, warm season non-tornadic, cold season tornadic, and cold season non-tornadic so it would be easier to input the information into ProStat. ProStat was utilized to create box and whisker plots and to run the non-parametric one-tail Mann-Whitney Test. Box and whisker plots were generated because they give a good look at the mean, median, and spread of the data. A box and whisker plot was created for each season (tornadic and non-

tornadic), for each parameter from the final array table, for all three reflectivity thresholds, and for all three representative time steps for each event. The Mann-Whitney Test was used because it performs well with normal and non-normal distributions. All of the data from the warm (cold) season tornadic events and warm (cold) season non-tornadic events was included for the test to determine if the parameters at each time step for each reflectivity threshold were statistically significantly different from one another. To be statistically significantly different, the z-value calculated from the test had to be less than -1.65. If it was, the two data sets were statistically significantly different at the 95% probability level or higher. The data provided by both the box and whisker plots and the Mann-Whitney Test were then used to analyze the differences between tornadic and non-tornadic events for both the warm and cold seasons.

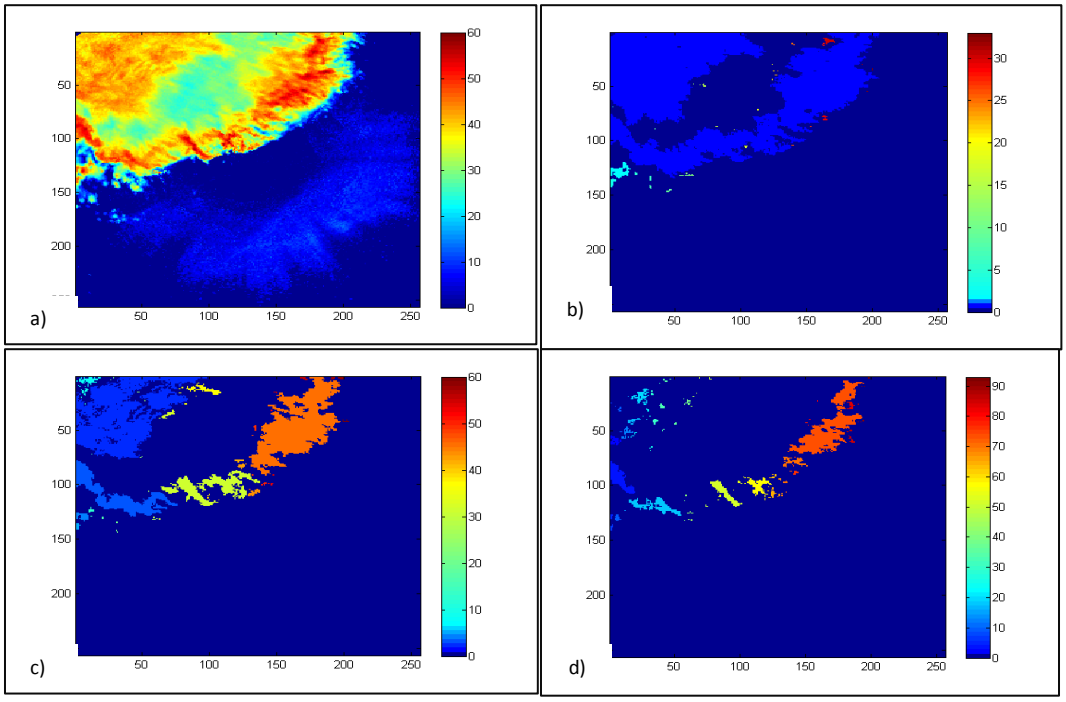

Figure 3.1 An event example of the MATLAB program identifying cells with a specific reflectivity threshold. a) composite reflectivity, b) 35 dBZ and greater reflectivity, c) 40 dBZ and greater reflectivity, and d) 45 dBZ and greater reflectivity.

Chapter 4 Statistical Results and Discussion for Event Comparison

Before revealing the results for this study it must be understood why the data were divided into the categories chosen. Tornadic cases produced at least one verified tornado, while non-tornadic cases did not produce any verified tornadoes but did have at least one tornado warning issued on them. Some tornadic cases had multiple tornadoes form along the entire line, while some only had one or two. All scenarios were included because even one weaker tornado can result in damage to life and property; therefore, those cases should be examined as well. From here the data were sub-classified as warm season and cold season. This distinction was made due to the differences in the environment from season to season. For that reason the main comparison of this thesis is warm season tornadic versus warm season non-tornadic and cold season tornadic versus cold season non-tornadic. Again, the warm season is from late March to October and the cold season is from November to early March. The reflectivity images for each case at the event time can be seen in Figures B.1-B.10. Box and whisker plots were created to show a comparison of all four subclassifications, but the main focus is the tornadic cases versus the non-tornadic cases. The expectation is to find statistically significant differences in the parameters assessed for this study.

An interesting note regarding the data sets is that the cold season produced higher rated tornadoes than the warm season. There were more EF2-EF4 tornadoes for the cold season than the warm season. On the other hand, the warm season produced more EF0-EF1 tornadoes than the cold season. This is consistent with the results from Trapp et al.

(2005). This could be due to the fact that, typically, the cold season troposphere has more wind shear.

In addition, the major axis of each event was analyzed for the event time for the 35 dBZ and the 40 dBZ reflectivity thresholds to determine how many events fulfilled the definition set by Trapp et al. (2005). For both the warm season tornadic and warm season non-tornadic cases, nine events from each category did not meet the required 100 km length for the 40 dBZ threshold. For the cold season tornadic and cold season non-tornadic cases, seven events from each category did not meet the required 100 km length for the 40 dBZ threshold. In conclusion, the 40 dBZ threshold is not a desirable reflectivity threshold for the QLCS definition. There were eleven cases total that did not meet the required 100 km length for the 35 dBZ threshold. However, this research proposes that 35 dBZ is a better reflectivity threshold for Trapp et al.'s (2005) definition than the 40 dBZ threshold.

Next, the mean, median, and standard deviation for all 21 radar parameters for each reflectivity threshold (35 dBZ, 40 dBZ, and 45 dBZ) and each time step (pre-event, event, and post-event) were analyzed for warm season tornadic cases and were compared to those for warm season non-tornadic cases in Tables C.1-C.9 in the Appendix C. The same was done for the cold season tornadic and non-tornadic cases in Tables C.10-C.18 in the Appendix C.

In addition, box and whisker plots were generated for all of the radar parameters for each reflectivity threshold and each time step for a straightforward graphical display. For each radar parameter, at each time step, there are four box plots: warm season

tornadic, warm season non-tornadic, cold season tornadic, and cold season non-tornadic. Each box and whisker plot contains the minimum and maximum value, 1st and 3rd quartile, median, and mean. This provides a good look at the mean, median, and spread of the data at hand (Figures A.1-A.36 in Appendix A).

First, the statistically significantly different parameters for the pre-event, event, and post-event times for all reflectivity thresholds for the warm season tornadic and non-tornadic cases will be discussed, followed by a discussion about the statistically significantly different parameters for the pre-event, event, and post-event times for all reflectivity thresholds for the cold season tornadic and non-tornadic events. Again to be considered statistically significantly different, the z-value for the parameters had to be less than -1.65. This means there is a 95% probability level or higher that the parameter values are greater than or less than the tornadic cases from the non-tornadic cases.

4.1 Warm Season Tornadic and Non-tornadic Results and Discussion

4.1.1 Pre-event time

For the time step before the start time of each event (pre-event time), the 35 dBZ threshold had six parameters that were shown to be statistically significantly different when the tornadic data set was compared to the non-tornadic data set. The z-value, direction of significance, and probability level of these parameters can be found in Table 4.1. The tornadic cases displayed greater maximum spectrum width values at 2 km,

below 3 km, and between 3 km and 7 km, as well as, greater mean spectrum width values between 3 km and 7 km than non-tornadic cases. Spectrum width shows a range of wind velocities in the volume. This can be due to turbulence or rotation (or both). Therefore, in the tornadic cases there is more turbulent air, as shown by the greater spectrum width values. For the non-tornadic cases, it appears the airflow is "smoother." They also had greater maximum and mean azimuthal shear values between 3 km and 7 km than non-tornadic cases. The positive azimuthal shear values also correlate with the fact that positive values indicate cyclonic rotation, which is the direction most tornadoes rotate. The greater, positive azimuthal shear values for the tornadic cases means greater cyclonic rotation, so an environment more conducive to tornadoes exists in the tornadic cases than the non-tornadic cases. The probability level for spectrum width at the various heights is very high, which allows confidence that this parameter can be used under the assumption that the parameter's values will be greater for the tornadic cases than the non-tornadic cases.

Parameter	z-value	Direction of Significance	Probability Level
Max SW at 2 km	-2.335	Tornadic > Non-tornadic	99.02%
Max SW Below 3 km	-2.105	Tornadic > Non-tornadic	98.24%
Max Az Shear 3-7 km	-1.731	Tornadic > Non-tornadic	95.84%
Mean Az Shear 3-7 km	-1.731	Tornadic > Non-tornadic	95.84%
Max SW 3-7 km	-2.926	Tornadic > Non-tornadic	99.83%
Mean SW 3-7 km	-2.375	Tornadic > Non-tornadic	99.12%

Table 4.1. The Mann-Whitney test comparing warm season tornadic events to warm season non-tornadic events for the 35 dBZ threshold at the pre-event time for the events.

For the pre-event time, the 40 dBZ threshold had two parameters that were statistically significantly different. These parameters are: mean divergence below 3 km, and mean divergence between 3 km and 7 km (Table 4.2). For both parameters, tornadic cases exhibited greater values than the non-tornadic cases. This can imply more convergence is also present and increased convergence can aid in stretching a vertically rotation column, which then leads to tornadogenesis. The reason divergence was calculated instead of convergence will be discussed further in section 4.1.4.

Parameter	z-value	Direction of Significance	Probability Level
Mean Div below 3 km	-2.303	Tornadic > Non-tornadic	98.94%
Mean Div 3-7 km	-2.414	Tornadic > Non-tornadic	99.21%

Table 4.2. The Mann-Whitney test comparing warm season tornadic events to warm season non-tornadic events for the 40 dBZ threshold at the pre-event time for the events.

Lastly, for the pre-event time, the 45 dBZ threshold had ten parameters that were proven to be statistically significantly different when the tornadic data was compared to the non-tornadic data (Table 4.3). The ten parameters are: maximum azimuthal shear at 2 km, mean azimuthal shear at 2 km, maximum azimuthal shear below 3 km, maximum azimuthal shear between 3 km and 7 km, mean azimuthal shear between 3 km and 7 km, mean divergence between 3 km and 7 km, maximum and mean spectrum width between 3 km and 7 km, orientation, and axial ratio. The maximum azimuthal shear parameters at the various heights are expected to be greater and positive for the tornadic cases than the non-tornadic cases. This suggests there is more cyclonic rotation present in the tornadic cases. An interesting result is the mean azimuthal shear at 2 km. The non-tornadic values

are greater than the tornadic values. Also, the values are negative. This will be discussed further in section 4.1.4. The mean divergence displaying greater values for tornadic events than non-tornadic events implies more convergence is present which can aid in stretching a rotating vertical column of air. The maximum and mean spectrum width between 3 km and 7 km having greater values for the tornadic cases than the non-tornadic cases is to be expected due to the airflow being more turbulent than smooth when rotation is present. The results regarding the axial ratio and orientation suggest that the 45 dBZ and greater area at the pre-event time is more linear and orientated more east to west for tornadic cases than non-tornadic cases. This is very interesting as it is generally thought that in a lot of tornadic QLCSs there are embedded supercells. Embedded supercells would be apparent in the 45 dBZ and greater area, but would have more of a cellular shape or smaller ratio, indicating the ratio for tornadic cases would be smaller than for non-tornadic cases. This study shows the opposite; QLCSs do not have to have embedded supercells to produce tornadoes.

Parameter	z-value	Direction of Significance	Probability Level
Max Az Shear at 2 km	-1.939	Tornadic > Non-tornadic	97.38%
Mean Az Shear at 2 km	-1.851	Tornadic < Non-tornadic	96.79%
Max Az Shear Below 3 km	-1.779	Tornadic > Non-tornadic	96.24%
Max Az Shear 3-7 km	-2.658	Tornadic > Non-tornadic	99.61%
Mean Az Shear 3-7 km	-2.178	Tornadic > Non-tornadic	98.53%
Mean Div 3-7 km	-2.904	Tornadic > Non-tornadic	99.82%
Max SW 3-7 km	-2.106	Tornadic > Non-tornadic	98.24%
Mean SW 3-7 km	-2.922	Tornadic > Non-tornadic	99.83%
Orientation	-2.126	Tornadic > Non-tornadic	98.33%
Axial Ratio	-1.859	Tornadic > Non-tornadic	96.85%

Table 4.3. The Mann-Whitney test comparing warm season tornadic events to warm season non-tornadic events for the 45 dBZ threshold at the pre-event time for the events.

4.1.2 Event time

For the time step closest to the start time of each event (event time) the 35 dBZ threshold had eleven statistically significant parameters for tornadic events when compared to non-tornadic events: maximum and mean azimuthal shear at 2 km, maximum azimuthal shear below 3 km, maximum divergence below 3 km, maximum and mean spectrum width below 3 km, maximum and mean azimuthal shear between 3 km and 7 km, mean divergence between 3 km and 7 km, and maximum and mean spectrum width between 3 km and 7 km (Table 4.4).

Parameter	z-value	Direction of Significance	Probability Level
Max Az Shear at 2 km	-2.378	Tornadic > Non-tornadic	99.13%
Mean Az Shear at 2 km	-2.179	Tornadic < Non-tornadic	98.53%
Max Az Shear below 3 km	-2.491	Tornadic > Non-tornadic	99.36%
Max Div below 3 km	-1.791	Tornadic > Non-tornadic	96.34%
Max SW below 3 km	-1.848	Tornadic > Non-tornadic	96.78%
Mean SW below 3 km	-2.143	Tornadic > Non-tornadic	98.40%
Max Az Shear 3-7 km	-2.481	Tornadic > Non-tornadic	99.35%
Mean Az Shear 3-7 km	-2.332	Tornadic > Non-tornadic	99.02%
Mean Div 3-7 km	-2.456	Tornadic > Non-tornadic	99.30%
Max SW 3-7 km	-2.255	Tornadic > Non-tornadic	98.80%
Mean SW 3-7 km	-1.748	Tornadic > Non-tornadic	95.98%

Table 4.4. The Mann-Whitney test comparing warm season tornadic events to warm season non-tornadic events for the 35 dBZ threshold at the event time for the events.

The maximum azimuthal shear values at the various heights were positive and greater for tornadic cases than non-tornadic cases. This implies more cyclonic rotation in tornadic QLCSs than non-tornadic QLCSs. The maximum and mean divergence below 3 km and between 3 km and 7 km implies a greater potential for the vertical stretching of a

rotating column in tornadic cases than non-tornadic cases. Maximum and mean spectrum width values below 3 km and between 3 km and 7 km also suggest more rotation or turbulent airflow in tornadic cases than non-tornadic cases. The mean azimuthal shear values between 3 km and 7 km also depicts more cyclonic rotation in tornadic events than non-tornadic events.

The 40 dBZ threshold for the event time resulted in eight parameters being statistically significantly different for tornadic events when compared to non-tornadic events: maximum and mean azimuthal shear at 2 km, maximum azimuthal shear below 3 km, mean divergence below 3 km, maximum and mean azimuthal shear between 3 km and 7 km, mean divergence between 3 km and 7 km, and maximum spectrum width between 3 km and 7 km (Table 4.5). The result that the mean azimuthal shear at 2 km is less for tornadic cases than for non-tornadic cases is intriguing and will be discussed in section 4.1.4. The maximum azimuthal shear results at the various levels propose that there is more cyclonic rotation in tornadic cases than the non-tornadic cases. Specifically, for the maximum and mean azimuthal shear between 3 km and 7 km, one can conclude that these parameters can be used to distinguish between a tornadic signature and a non-tornadic signature, due to their high probability level. Next, the mean divergence below 3 km and between 3 km and 7 km suggests throughout these layers tornadic cases are more likely to contain a divergence/convergence couplet that will aid in stretching a rotating vertical column of air which can lead to tornadogenesis. Finally, the maximum spectrum width between 3 km and 7 km outcome depicts one will see higher values for cases that produce tornadoes than for those that do not.

Parameter	z-value	Direction of Significance	Probability Level
Max Az Shear at 2 km	-1.775	Tornadic > Non-tornadic	96.21%
Mean Az Shear at 2 km	-1.775	Tornadic < Non-tornadic	96.21%
Max Az Shear below 3 km	-2.272	Tornadic > Non-tornadic	98.85%
Mean Div below 3 km	-2.518	Tornadic > Non-tornadic	99.41%
Max Az Shear 3-7 km	-2.670	Tornadic > Non-tornadic	99.62%
Mean Az Shear 3-7 km	-2.699	Tornadic > Non-tornadic	99.65%
Mean Div 3-7 km	-2.707	Tornadic > Non-tornadic	99.66%
Max SW 3-7 km	-1.801	Tornadic > Non-tornadic	96.42%

Table 4.5. The Mann-Whitney test comparing warm season tornadic events to warm season non-tornadic events for the 40 dBZ threshold at the event time for the events.

Parameter	z-value	Direction of Significance	Probability Level
Mean Div at 2 km	-1.928	Tornadic > Non-tornadic	97.31%
Max Az Shear 3-7km	-2.629	Tornadic > Non-tornadic	99.57%
Mean Az Shear 3-7 km	-2.106	Tornadic > Non-tornadic	98.24%
Mean Div 3-7 km	-2.530	Tornadic > Non-tornadic	99.43%
Max SW 3-7 km	-1.809	Tornadic > Non-tornadic	96.48%
Mean SW 3-7 km	-2.926	Tornadic > Non-tornadic	99.83%

Table 4.6. The Mann-Whitney test comparing warm season tornadic events to warm season non-tornadic events for the 45 dBZ threshold at the event time for the events.

Lastly, the 45 dBZ threshold, for the event time, was found to have six statistically significantly different parameters for tornadic events when compared to non-tornadic events: mean divergence at 2 km, maximum and mean azimuthal shear between 3 km and 7 km, mean divergence between 3 km and 7 km, and the maximum and mean spectrum width between 3 km and 7 km (Table 4.6). Again, higher maximum and mean azimuthal shear values above the boundary layer can be a good indicator of cyclonic rotation that can produce a tornado. Also, higher divergence values for tornadic cases imply higher convergence values which create an environment more suitable for

tornadogenesis. Furthermore, the maximum and mean spectrum width in the 3-7 km layer supports that result because these values are also higher for tornadic cases than non-tornadic cases. Finally, the inconsistent results from the mean divergence at 2 km will be discussed further in section 4.1.4.

4.1.3 Post-event time

There were seven parameters there were statistically significant for the 35 dBZ threshold at the post-event time for tornadic events when compared to non-tornadic events: maximum divergence at 2 km, maximum azimuthal shear below 3 km, maximum divergence below 3 km, maximum spectrum width below 3 km, maximum and mean azimuthal shear between 3 km and 7 km, and maximum spectrum width between 3 km and 7 km (Table 4.7). The maximum azimuthal shear values for both layers are greater for the tornadic cases than the non-tornadic cases which is an indication of more cyclonic rotation appearing in the tornadic cases. The mean azimuthal shear from 3 km to7 km also supports this conclusion. Furthermore, at 2 km, the maximum divergence implies that tornadic cases have more convergence. This would create more vertical motion which would aid in stretching a vertical column of rotating air. However, the maximum divergence below 3 km, proposes non-tornadic cases display greater divergence values. This will be discussed further in section 4.1.4. In addition, the greater maximum spectrum width values for the tornadic cases support the idea that there is more turbulent air or more rotational air. The non-tornadic cases display less turbulent or "smoother" flow.

Parameter	z-value	Direction of Significance	Probability Level
Max Div at 2 km	-1.735	Tornadic > Non-tornadic	95.86%
Max Az Shear below 3 km	-2.034	Tornadic > Non-tornadic	97.90%
Max Div below 3 km	-1.674	Tornadic < Non-tornadic	95.29%
Max SW below 3 km	-2.063	Tornadic > Non-tornadic	98.05%
Max Az Shear 3-7 km	-2.911	Tornadic > Non-tornadic	99.82%
Mean Az Shear 3-7 km	-2.363	Tornadic > Non-tornadic	99.10%
Max SW 3-7 km	-2.577	Tornadic > Non-tornadic	99.50%

Table 4.7. The Mann-Whitney test comparing warm season tornadic events to warm season non-tornadic events for the 35 dBZ threshold at the post-event time for the events.

Parameter	z-value	Direction of Significance	Probability Level
Mean SW at 2 km	-2.009	Tornadic < Non-tornadic	97.78%
Mean SW below 3 km	-1.811	Tornadic < Non-tornadic	96.50%
Mean Div 3-7 km	-1.984	Tornadic > Non-tornadic	97.64%

Table 4.8. The Mann-Whitney test comparing warm season tornadic events to warm season non-tornadic events for the 40 dBZ threshold at the post-event time for the events.

Only three parameters were established to be statistically significantly different for the 40 dBZ threshold at the post-event time for tornadic events when compared to non-tornadic events: mean spectrum width at 2 km, mean spectrum width below 3 km, and mean divergence between 3 km and 7 km (Table 4.8). Interestingly, the values for the spectrum width parameters were lower for tornadic events than non-tornadic events. This would suggest that more turbulent air would exist for non-tornadic events, but this is the opposite of the results already discussed. The mean divergence between 3 km and 7 km, however, is consistent with what has been observed so far. The tornadic cases have higher values than the non-tornadic cases. This proposes more convergence in tornadic cases which would results in more vertical motion that can lead to tornadogenesis.

Finally, there were five parameters that were statistically significantly different for the 45 dBZ threshold for the post-event time for tornadic events when compared to non-tornadic events: mean divergence at 2 km, maximum azimuthal shear below 3 km and between 3 km and 7 km, and maximum and mean divergence between 3 km and 7 km (Table 4.9). These results, again, show that tornadic cases tend to have more cyclonic rotation associated with them than non-tornadic cases. This cyclonic rotation would allow for tornadoes to form. In addition, the divergence parameters agree. The greater values imply that the cyclonic rotation is more likely to be stretched vertically leading to tornadogenesis. However, the mean divergence at 2 km appears to have the same conclusion as the mean azimuthal shear at 2 km parameter, and this will be discussed further in section 4.1.4.

Parameter	z-value	Direction of Significance	Probability Level
Mean Div at 2 km	-2.122	Tornadic < Non-tornadic	98.31%
Max Az Shear below 3 km	-1.726	Tornadic > Non-tornadic	95.80%
Max Az Shear 3-7 km	-3.026	Tornadic > Non-tornadic	99.88%
Max Div 3-7 km	-2.893	Tornadic > Non-tornadic	99.81%
Mean Div 3-7 km	-3.112	Tornadic > Non-tornadic	99.91%

Table 4.9. The Mann-Whitney test comparing warm season tornadic events to warm season non-tornadic events for the 45 dBZ threshold at the post-event time for the events.

4.1.4 Discussion

Overall, it would appear the maximum azimuthal shear parameter from 3 km to 7 km and the mean divergence parameter from 3 km to 7 km have the greatest significance during the warm season. Higher azimuthal shear and divergence values were seen for

tornadic cases than non-tornadic cases (similar to Atkins et al. 2005). When comparing warm season tornadic and non-tornadic events, both parameters were statistically significantly different for all reflectivity thresholds at all time steps; except for two reflectivity thresholds and time steps. The azimuthal shear implies tornadic cases contain more cyclonic rotation than non-tornadic cases which would aid in tornadogenesis. The divergence in this layer suggests mid-level support for convection or is indicative of column stretching. Not only were maximum azimuthal shear between 3 km and 7 km and mean divergence between 3 km and 7 km statistically significant, the probability level was always 99% or greater with only one exception for each parameter. Despite this, the results show that azimuthal shear and divergence in this layer can be used with confidence to help determine if a system will become tornadic. The maximum spectrum width from 3 km to 7 km was the second most statistically significant parameter. Spectrum width contained higher values for cases that produced tornadoes than for those that did not because the circulation creates a variety in velocities within the system causing the spectrum width to increase. This coincides with the azimuthal shear and divergence, and proposes that spectrum width is also a useful parameter when determining whether a system will become tornadic or not.

In addition, the layer these parameters encompass is desirable. No matter how far the storm is from the radar this layer can be observed making 3 km to 7 km more reliable. This is where issues can be found for the below 3 km parameters and the 2 km parameters. They are good for cases close to the radar, but will not be much help for those at farther distances. This could be a reason why they were not as commonly significant as the 3 km to 7 km parameters. Also, during the warm season the height of

the boundary layer and vertical extent of the convection is greater so the boundary layer is less compact. However, the below 3 km parameters and the 2 km parameter were expected to be useful because this is where mesovortices form. Mesovortices can be seen between 3 km and 7 km but, as Atkins et al. (2004) found, the greatest difference between tornadic mesovortices and non-tornadic mesovortices is in the lowest 2.5 km. One solution to this issue would be the installation of more radars, at least in the Mississippi and Ohio River Valleys, where QLCSs pose the greatest threat.

Parameters that presented interesting results were the mean azimuthal shear at 2 km and the mean divergence at 2 km. They were not significant for all reflectivity thresholds at every time step, but when they were statistically significant, they indicated inconsistent results. The azimuthal shear implied more anti-cyclonic rotation in tornadic events and more cyclonic rotation in non-tornadic events. In addition, the divergence at 2 km suggested more divergence in non-tornadic cases than tornadic cases. Also, the mean at this height was negative for both parameters whereas the mean below 3 km and between 3 km and 7 km was positive. The reason for this is the way they were all processed. The values for the azimuthal shear and divergence below 3 km and between 3 km and 7 km goes through a series of stages where the maximum of the mean in the layer is always being picked out, which filters out the negative values. For the mean azimuthal shear and mean divergence at 2 km, raw data is being used only at one level. Therefore, a maximum of the mean is not being chosen, just the value at that level, so the negative values are a part of the data set. Negative values are not unexpected in tornadic cases because wherever you have cyclonic motion or divergence you have anti-cyclonic motion

or convergence nearby, however, for this study, only cyclonic motion is of interest. For the divergence parameters, what they imply is of interest.

Convergence is more desirable than divergence but the "w2merger" algorithm would not allow the minimum divergence, or maximum convergence, to be found. However, typically there is a divergence/convergence couplet present within convective systems. Therefore, a strong presence of divergence can imply a strong presence of convergence. The strong presence of convergence then steers to the conclusion that there is more vertical motion which can aid in stretching a rotating vertical column of air that can lead to tornadogenesis. With that said, caution must be taken when interpreting these divergence results. There were some outliers within the divergence data that could have skewed the results. Nonetheless, the results were presented as they still convey some confidence that there are differences between divergence values in tornadic cases when compared to non-tornadic cases.

Another observation was that the significant parameters differed among the reflectivity thresholds during a specified time step. This would be because all identified cells were included. Since all of the cells were included not every 35 dBZ area contained areas of 40 dBZ and greater or 45 dBZ and greater, and not all 40 dBZ areas contained 45 dBZ and greater. Therefore, the significant parameters differed among the three reflectivity thresholds. If only certain identified cells were chosen, then they would most likely all have contained areas of 40 dBZ and greater, and areas of 45 dBZ and greater which probably would have made the significant parameters more consistent for each threshold.

4.2 Cold Season Tornadic and Non-tornadic Results and Discussion

4.2.1 Pre-event time

The Mann-Whitney test for the 35 dBZ threshold at the pre-event time established twelve parameters that were statistically significantly different when comparing cold season tornadic and non-tornadic cases. Those twelve parameters are: maximum and mean azimuthal shear at 2 km, maximum and mean divergence at 2 km, maximum spectrum width at 2 km, maximum and mean azimuthal shear below 3 km, maximum spectrum width below 3 km, maximum and mean azimuthal shear between 3 km and 7 km, maximum divergence between 3 km and 7 km, and maximum spectrum width between 3 km and 7 km (Table 4.10). The maximum azimuthal shear values at the various layers suggest that there is more cyclonic rotation in tornadic events than non-tornadic events. The maximum spectrum width values at the various layers agree. The tornadic cases exhibit more turbulent flow, which suggests circulations are present in the tornadic events, whereas, there is "smoother" flow in the non-tornadic events. The maximum divergence at 2 km and between 3 km and 7 km imply that there is more convergence in tornadic cases which creates an environment more conducive to tornadogenesis. The mean azimuthal shear below 3 km and between 3 km and 7 km also proposes more cyclonic rotation, making the environment more conducive to tornadogenesis. However, the mean azimuthal shear and mean divergence at 2 km indicates that there is more cyclonic rotation and more divergence in non-tornadic cases

than tornadic cases. This will be discussed further in section 4.2.4.

Parameter	z-value	Direction of Significance	Probability Level
Max Az Shear at 2 km	-3.275	Tornadic > Non-tornadic	99.95%
Mean Az Shear at 2 km	-1.878	Tornadic < Non-tornadic	96.99%
Max Div at 2 km	-2.561	Tornadic > Non-tornadic	99.48%
Mean Div at 2 km	-2.582	Tornadic < Non-tornadic	99.51%
Max SW at 2 km	-2.909	Tornadic > Non-tornadic	99.82%
Max Az Shear below 3 km	-2.853	Tornadic > Non-tornadic	99.78%
Mean Az Shear below 3 km	-2.441	Tornadic > Non-tornadic	99.27%
Max SW Below 3 km	-2.126	Tornadic > Non-tornadic	98.33%
Max Az Shear 3-7 km	-1.838	Tornadic > Non-tornadic	96.70%
Mean Az Shear 3-7 km	-2.380	Tornadic > Non-tornadic	99.14%
Max Div 3-7 km	-2.381	Tornadic > Non-tornadic	99.14%
Max SW 3-7 km	-2.044	Tornadic > Non-tornadic	97.96%

Table 4.10. The Mann-Whitney test comparing cold season tornadic events to cold season non-tornadic events for the 35 dBZ threshold at the pre-event time for the events.

Parameter	z-value	Direction of Significance	Probability Level
Max Az Shear at 2 km	-2.028	Tornadic > Non-tornadic	97.87%
Max Div at 2 km	-2.183	Tornadic > Non-tornadic	98.55%
Max Az Shear below 3 km	-1.937	Tornadic > Non-tornadic	97.37%
Mean Az Shear below 3 km	-1.744	Tornadic > Non-tornadic	95.94%
Max Div below 3 km	-2.143	Tornadic > Non-tornadic	98.39%
Mean Az Shear 3-7 km	-1.976	Tornadic > Non-tornadic	97.59%

Table 4.11. The Mann-Whitney test comparing cold season tornadic events to cold season non-tornadic events for the 40 dBZ threshold at the pre-event time for the events.

The 40 dBZ threshold, at the pre-event time, depicted six parameters to be statistically significantly different for tornadic events when compared to non-tornadic events: maximum azimuthal shear at 2 km, maximum divergence at 2 km, maximum and mean azimuthal shear below 3 km, maximum divergence below 3 km, and mean

azimuthal shear between 3 km and 7 km (Table 4.11). The values for all of these parameters are greater for tornadic events than non-tornadic events. This implies in a tornadic system contains more cyclonic rotation, which is favorable for tornadogenesis. In addition, tornadic events have stronger divergence, implying stronger convergence which is also favorable for tornadogenesis.

When comparing the tornadic cases to the non-tornadic cases for the 45 dBZ threshold at the pre-event time, five parameters were established to be statistically significantly different: maximum and mean azimuthal shear at 2 km, maximum divergence at 2 km, maximum azimuthal shear below 3 km, mean divergence below 3 km (Table 4.12). The maximum azimuthal shear at 2 km and below 3 km indicates more cyclonic rotation for the tornadic cases than the non-tornadic cases. The maximum divergence at 2 km and the mean divergence below 3 km are also greater for tornadic cases suggesting stronger convergence is present. The increased cyclonic rotation and convergence creates a system more likely to produce a tornado.

Parameter	z-value	Direction of Significance	Probability Level
Max Az Shear at 2 km	-1.883	Tornadic > Non-tornadic	97.02%
Mean Az Shear at 2 km	-2.516	Tornadic < Non-tornadic	99.41%
Max Div at 2 km	-1.791	Tornadic > Non-tornadic	96.33%
Max Az Shear below 3 km	-2.150	Tornadic > Non-tornadic	98.42%
Mean Div below 3 km	-2.278	Tornadic > Non-tornadic	98.86%

Table 4.12. The Mann-Whitney test comparing cold season tornadic events to cold season non-tornadic events for the 45 dBZ threshold at the pre-event time for the events.

4.2.2 Event time

The event time displayed eleven parameters that were statistically significantly different for the 35 dBZ threshold for tornadic cases when compared to non-tornadic cases in this study. The eleven parameters are: maximum and mean azimuthal shear at 2 km, maximum and mean divergence at 2 km, maximum spectrum width at 2 km, maximum azimuthal shear below 3 km, maximum divergence below 3 km, maximum and mean azimuthal shear between 3 km and 7 km, maximum divergence between 3 km and 7 km, maximum spectrum width between 3 km and 7 km (Table 4.13).

Parameter	z-value	Direction of Significance	Probability Level
Max Az Shear at 2 km	-2.703	Tornadic > Non-tornadic	99.66%
Mean Az Shear at 2 km	-2.461	Tornadic < Non-tornadic	99.31%
Max Div at 2 km	-3.456	Tornadic > Non-tornadic	99.97%
Mean Div at 2 km	-2.085	Tornadic < Non-tornadic	98.14%
Max SW at 2 km	-2.421	Tornadic > Non-tornadic	99.23%
Max Az Shear below 3 km	-2.795	Tornadic > Non-tornadic	99.74%
Max Div below 3 km	-3.412	Tornadic > Non-tornadic	99.97%
Max Az Shear 3-7 km	-2.807	Tornadic > Non-tornadic	99.75%
Mean Az Shear 3-7 km	-3.026	Tornadic > Non-tornadic	99.88%
Max Div 3-7 km	-2.273	Tornadic > Non-tornadic	98.85%
Max SW 3-7 km	-2.530	Tornadic > Non-tornadic	99.43%

Table 4.13. The Mann-Whitney test comparing cold season tornadic events to cold season non-tornadic events for the 35 dBZ threshold at the event time for the events.

The maximum azimuthal shear values for the various layers were greater for tornadic events than non-tornadic events. This implies there is more cyclonic rotation in tornadic events. The maximum divergence for the various layers is also greater for tornadic cases. Greater divergence proposes greater convergence and vertical motion. The

increase in vertical motion can help stretch a rotating vertical column of air that can lead to tornadogenesis. The maximum spectrum width between 3 km and 7 km agrees, as it implies there is more turbulent flow in the tornadic events than the non-tornadic events. The mean azimuthal shear between 3 km and 7 km also depicts an increase in cyclonic flow in the tornadic cases. However, the mean azimuthal shear and mean divergence at 2 km results are inconsistent. They suggest that the non-tornadic events contain more cyclonic rotation and divergence than the tornadic events. The reason behind this result will be discussed further in section 4.2.4.

Parameter	z-value	Direction of Significance	Probability Level
Max Az Shear at 2 km	-2.297	Tornadic > Non-tornadic	98.92%
Mean Az Shear at 2 km	-2.235	Tornadic < Non-tornadic	98.73%
Max Div at 2 km	-2.346	Tornadic > Non-tornadic	99.05%
Max Az Shear below 3 km	-2.526	Tornadic > Non-tornadic	99.42%
Max Div below 3 km	-2.811	Tornadic > Non-tornadic	99.75%
Max Az Shear 3-7 km	-2.905	Tornadic > Non-tornadic	99.82%
Mean Az Shear 3-7 km	-2.967	Tornadic > Non-tornadic	99.85%
Max Div 3-7 km	-2.253	Tornadic > Non-tornadic	98.79%
Mean Div 3-7 km	-1.657	Tornadic > Non-tornadic	95.12%

Table 4.14. The Mann-Whitney test comparing cold season tornadic events to cold season non-tornadic events for the 40 dBZ threshold at the event time for the events.

When comparing the tornadic cases to the non-tornadic cases, the 40 dBZ threshold at the event time exhibited nine parameters that were statistically significantly different. These parameters are: maximum and mean azimuthal shear at 2 km, maximum divergence at 2 km, maximum azimuthal shear below 3 km, maximum divergence below 3 km, maximum and mean azimuthal shear between 3 km and 7 km, and maximum and mean divergence between 3 km and 7 km (Table 4.14). All of the azimuthal shear

parameters, except the mean azimuthal shear at 2 km, imply that tornadic cases contain more cyclonic rotation than non-tornadic cases. The same result applies to all of the divergence parameters; tornadic events have higher divergence values than non-tornadic events. This suggests tornadic cases exhibit greater convergence which then leads to an environment more conducive to tornadoes.

The 45 dBZ threshold at the event time depicts ten parameters that were statistically significantly different for tornadic cases when compared to non-tornadic cases. The ten parameters are: maximum azimuthal shear at 2 km, maximum divergence at 2 km, maximum and mean azimuthal shear below 3 km, maximum and mean divergence below 3 km, maximum and mean azimuthal shear between 3 km and 7 km, and maximum and mean divergence between 3 km and 7 km (Table 4.15). All of the azimuthal shear parameters suggest cyclonic rotation is more prevalent in tornadic cases than non-tornadic cases. The divergence parameters at the various layers propose there is stronger convergence in tornadic cases than non-tornadic cases.

Parameter	z-value	Direction of Significance	Probability Level
Max Az Shear at 2 km	-1.804	Tornadic > Non-tornadic	96.44%
Max Div at 2 km	-2.352	Tornadic > Non-tornadic	99.07%
Max Az Shear below 3 km	-2.605	Tornadic > Non-tornadic	99.54%
Mean Az Shear below 3 km	-2.151	Tornadic > Non-tornadic	98.43%
Max Div below 3 km	-3.846	Tornadic > Non-tornadic	99.99%
Mean Div below 3 km	-2.111	Tornadic > Non-tornadic	98.26%
Max Az Shear 3-7 km	-2.498	Tornadic > Non-tornadic	99.38%
Mean Az Shear 3-7 km	-2.632	Tornadic > Non-tornadic	99.58%
Max Div 3-7 km	-3.471	Tornadic > Non-tornadic	99.97%
Mean Div 3-7 km	-1.852	Tornadic > Non-tornadic	96.80%

Table 4.15. The Mann-Whitney test comparing cold season tornadic events to cold season non-tornadic events for the 45 dBZ threshold at the event time for the events.

4.2.3 Post-event time

When comparing the tornadic events to the non-tornadic events, the 35 dBZ threshold at the post-event time had six parameters that were statistically significant. These parameters are: maximum divergence at 2 km, maximum divergence below 3 km, mean azimuthal shear between 3 km and 7 km, maximum divergence between 3 km and 7 km, and maximum and mean spectrum width between 3 km and 7 km (Table 4.16). The mean azimuthal shear parameter suggests there is more cyclonic rotation present in tornadic events than non-tornadic events. The divergence parameters at the various layers imply stronger convergence and therefore stronger vertical motion in tornadic cases than non-tornadic cases. The two spectrum width parameters also indicate more turbulent flow or circulations in the tornadic cases. This is unlike the non-tornadic cases which have lower spectrum width values meaning there is "smoother" flow in those systems.

Parameter	z-value	Direction of Significance	Probability Level
Max Div at 2 km	-2.610	Tornadic > Non-tornadic	99.55%
Max Div below 3 km	-2.423	Tornadic > Non-tornadic	99.23%
Mean Az Shear 3-7 km	-1.818	Tornadic > Non-tornadic	96.55%
Max Div 3-7 km	-2.551	Tornadic > Non-tornadic	99.46%
Max SW 3-7 km	-2.073	Tornadic > Non-tornadic	98.09%
Mean SW 3-7 km	-1.686	Tornadic > Non-tornadic	95.41%

Table 4.16. The Mann-Whitney test comparing cold season tornadic events to cold season non-tornadic events for the 35 dBZ threshold at the post-event time for the events.

For the 40 dBZ threshold at the post-event time, the Mann-Whitney test established eight parameters that were statistically significant different between tornadic

cases and non-tornadic cases. These parameters are: maximum azimuthal shear at 2 km, maximum divergence at 2 km, mean azimuthal shear below 3 km, maximum divergence below 3 km, maximum and mean azimuthal shear between 3 km and 7 km, maximum divergence between 3 km and 7 km, and mean spectrum width between 3 km and 7 km (Table 4.17). This implies at all levels, azimuthal shear is much stronger for tornadic cases than non-tornadic cases. In other words, there is more cyclonic rotation associated with tornadic events than non-tornadic events. In addition, spectrum width suggests more turbulence in tornadic events. All three maximum divergence parameters indicate stronger values in tornadic cases than non-tornadic cases. The outcome means more convergence can be observed in tornadic cases resulting in more vertical motion and greater stretching of a vertical rotating column of air.

Parameter	z-value	Direction of Significance	Probability Level
Max Az Shear at 2 km	-1.953	Tornadic > Non-tornadic	97.46%
Max Div at 2 km	-2.450	Tornadic > Non-tornadic	99.29%
Mean Az Shear below 3 km	-1.665	Tornadic > Non-tornadic	95.20%
Max Div below 3 km	-2.502	Tornadic > Non-tornadic	99.38%
Max Az Shear 3-7 km	-2.082	Tornadic > Non-tornadic	98.14%
Mean Az Shear 3-7 km	-2.460	Tornadic > Non-tornadic	99.31%
Max Div 3-7 km	-3.235	Tornadic > Non-tornadic	99.94%
Mean SW 3-7 km	-1.764	Tornadic > Non-tornadic	96.12%

Table 4.17. The Mann-Whitney test comparing cold season tornadic events to cold season non-tornadic events for the 40 dBZ threshold at the post-event time for the events.

Finally, the 45 dBZ threshold for the post-event time had one parameter that was statistically significantly different when comparing tornadic events to non-tornadic events. The parameter is: maximum divergence between 3 km and 7 km (Table 4.18).

This implies in this layer, tornadic cases exhibit stronger divergence or convergence than non-tornadic cases. A possible explanation for this threshold at this time only having one significant parameter could be because half of the cold season events did not display reflectivity that was 45 dBZ and greater.

Parameter	z-value	Direction of Significance	Probability Level
Max Div 3-7 km	-1.775	Tornadic > Non-tornadic	96.20%

Table 4.18. The Mann-Whitney test comparing cold season tornadic events to cold season non-tornadic events for the 45 dBZ threshold at the post-event time for the events.

4.2.4 Discussion

Overall, azimuthal shear and divergence, no matter the height and whether it is the maximum or mean, dominated the Mann-Whitney test for significance for the cold season. Specifically, the maximum azimuthal shear and maximum divergence at 2 km, closely followed by the maximum azimuthal shear and maximum divergence below 3 km were the most common. Higher azimuthal shear and divergence values were seen for tornadic cases over non-tornadic cases (similar to Atkins et al. 2005). When comparing between the cold season tornadic and non-tornadic events, maximum azimuthal shear and maximum divergence were significant for all time steps and thresholds with a few exceptions. The greater azimuthal shear values for tornadic events indicate more cyclonic rotation is associated with these events than non-tornadic events. In other words, events with higher azimuthal shear values are more likely to produce tornadoes. For divergence, values were greater for tornadic cases than non-tornadic cases. Strong divergence can

imply strong convergence which creates stronger vertical motion. An increase in vertical motion can cause stretching in a vertical rotating column of air. This produces an environment more conducive to tornadogenesis. The probability level of these results depicts that azimuthal shear and divergence are parameters that will be very useful, with confidence, when determining whether a system will become tornadic or not. As stated before, the 45 dBZ threshold at the post-event time only had one significant parameter and this could have been due to the fact that half of the cases did not have reflectivity values greater than or equal to 45 dBZ.

Again, the mean azimuthal shear and mean divergence at 2 km parameters presented similar results to the warm season cases. They were not significant for all reflectivity thresholds at every time step but when they were statistically significant, there were inconsistencies. The mean azimuthal shear indicated there was more anti-cyclonic rotation in tornadic events and more cyclonic rotation in non-tornadic events. The mean divergence proposed there was more divergence or convergence in non-tornadic cases than non-tornadic cases; in other words, greater vertical motion in non-tornadic cases than tornadic cases. Also, the mean at this height was negative whereas the mean for the azimuthal shear and divergence below 3 km and between 3 km and 7 km was positive. The reason for this is the way they were all processed. The values for the azimuthal shear and divergence below 3 km and between 3 km and 7 km goes through a series of stages where the maximum of the mean in the layer is always being picked out, which filters out the negative values. For the mean azimuthal shear and divergence at 2 km, raw data is being used only at one level. Therefore, a maximum of the mean is not being chosen, just the value at that level is, so the negative values are a part of the data set. Negative values

are not unexpected in tornadic cases because wherever you have cyclonic motion or divergence you have anti-cyclonic motion or convergence nearby, however, for this study, only cyclonic motion is of interest. For the divergence parameters, what they imply is of interest.

Convergence would have been better to assess than divergence but the "w2merger" algorithm would not allow the minimum divergence, or maximum convergence, to be found. However, typically there is a divergence/convergence couplet present within convective systems. Therefore, a strong presence of divergence can imply a strong presence of convergence. The strong presence of convergence then steers to the conclusion that there is more vertical motion which can aid in stretching a rotating vertical column of air that can lead to tornadogenesis. With that said, caution must be taken when interpreting the divergence results. There were some outliers within the divergence data that could have skewed the results. Nonetheless, the results were presented as they still convey some confidence that there are differences between divergence values in tornadic cases when compared to non-tornadic cases.

Another observation was that the significant parameters differed among the reflectivity thresholds during a specified time step. This would be because all identified cells were included. Since all of the cells were included not every 35 dBZ area contained areas of 40 dBZ and greater or 45 dBZ and greater, and not all 40 dBZ areas contained 45 dBZ and greater. Therefore, the significant parameters differed among the three reflectivity thresholds. If only certain identified cells were chosen, then most of them would likely have contained areas of 40 dBZ and greater and areas of 45 dBZ and greater which probably would have made the significant parameters more consistent for each

threshold. In addition, for the end time, half of the cases did not exhibit reflectivity greater than or equal to 45 dBZ, which would also cause different parameters to be significant.

Comparing the cold season results to the warm season results, there are a few noticeable differences. First, azimuthal shear and divergence clearly dominate the significant parameters in the cold season with very few spectrum width parameters being significant. This is unlike the warm season where azimuthal shear, divergence, and spectrum width all dominated the results. Second, the significant parameters for the cold season are mostly at 2 km and below 3 km. This could be because the boundary layer height and vertical extent of the convection is lower during the cold season. These parameters lower in the atmosphere are more ideal because that is where the biggest differences between tornadic and non-tornadic mesovortices are seen (Atkins et al., 2004). However, as stated before, the farther an event is from the radar the more difficult it is to see at those lower levels. This is why more radars should be installed.

Chapter 5 Conclusions and Future Work

5.1 Summary and Conclusions

QLCSs are most common in the Mississippi and Ohio River Valleys and have been shown to be a producer of many severe weather threats across the United States year round. One such severe weather threat is tornadoes. Unlike their supercell counterpart, QLCS tornadoes are typically not as strong and develop differently. They form within low-level circulations called mesovortices. Mesovortices tend to build quickly upward typically within the lowest 2.5 km AGL. However, not all mesovortices produce tornadoes making it difficult to determine which ones will. Also, because they are low-level and build upwards, identifying them on radar can be particularly difficult. Therefore it is imperative research be conducted so forecasters can accurately identify tornadic circulations within a QLCS line.

In this research, 21 parameters were compared between the tornadic and non-tornadic QLCSs in the warm and cold season. Tornadic QLCSs were events that produced at least one or more verified tornadoes, while non-tornadic QLCSs were events that did not produce verified tornadoes but did have at least one tornado warning issued for them. The events were then divided up into warm and cold season. This distinction was made because the environments tend to be different during the warm season compared to the cold season. Next, each event was assigned a pre-event, event, and post-event time for the tornadoes (warnings for non-tornadic events). From there three different reflectivity thresholds (35 dBZ, 40 dBZ, and 45 dBZ) were utilized for each time step to see which events met the QLCS criteria at what threshold and to see how the

parameters varied. Also, the reflectivity thresholds were used to determine just how linear the events were and whether embedded supercells were responsible for the tornadic cases. The comparison of the tornadic and non-tornadic cases for each season was demonstrated through the use of the non-parametric Mann-Whitney Test, as well as, displayed simply through box and whisker plots. In addition, the mean, median, and standard deviation for each time step and reflectivity threshold were calculated. After the analysis of the data, some conclusions were made for each comparison.

Overall, for the central United States, multiple parameters were proven to be statistically significantly different when comparing between tornadic and non-tornadic cases no matter what the season. For the warm season, the maximum azimuthal shear and maximum divergence parameters from 3 km to 7 km had the greatest significance. The values were greater for tornadic cases than non-tornadic cases, which is similar to the results from Atkins et al. (2005). The higher azimuthal shear values indicate more cyclonic rotation in tornadic cases than non-tornadic cases. More cyclonic rotation in the atmosphere produces an environment more prone to tornadogenesis. The greater divergence values imply greater convergence and therefore more vertical motion. The increased vertical motion can stretch a vertical rotating column of air creating an environment more conducive to tornadogenesis. In addition, almost every maximum azimuthal shear value and maximum divergence value from 3 km to 7 km had a probability level of 99% or greater. This shows that azimuthal shear and divergence in this layer can be used with confidence when trying to identify a tornadic QLCS from a non-tornadic QLCS. Additionally, the maximum spectrum width between 3 km and 7 km was significantly different for most thresholds and time steps. This parameter had greater

values for tornadic cases than non-tornadic cases, which means not only do tornadic cases display more cyclonic rotation and greater convergence, they also have more turbulent airflow, which is expected. Therefore, utilizing all of these parameters during the warning process could be very helpful for distinguishing between tornadic and non-tornadic QLCSs in the warm season.

For the cold season cases, the maximum and mean azimuthal shear and maximum and mean divergence at all levels dominated the Mann-Whitney significance test. Specifically, the maximum azimuthal shear and maximum divergence at 2 km, followed closely by the maximum azimuthal shear and maximum divergence below 3 km were the most common. Greater azimuthal shear and divergence values were recorded for tornadic cases over non-tornadic cases (similar to Atkins et al. 2005) which means there is more cyclonic rotation and greater convergence present in the tornadic cases. In other words, a system with higher azimuthal shear and divergence values lower in the atmosphere is more likely to produce a tornado. In general, the probability levels of the azimuthal shear and divergence values were 99% and greater, giving confidence that these parameters can help successfully distinguish between systems that will become tornadic and systems that will not.

When comparing the significant parameters of the warm and cold season, some differences can be seen. The first is azimuthal shear and divergence are unmistakably the most common significant parameters in the cold season; while, azimuthal shear, divergence, and spectrum width dominate the results during the warm season. Second, the significant parameters for the cold season are mostly at 2 km and below 3 km, whereas, the majority of the warm season significant parameters are in the 3 km to 7 km

layer. This could be because the height of the boundary is lower during the cold season and the vertical extent of convection is typically lower, whereas, during the warm season the height is higher and weather in the boundary layer is not as compact. Either way, the lower height parameters were expected to be significant because that is where mesovortices can be observed. Atkins et al. (2004) found the greatest difference between tornadic mesovortices and non-tornadic mesovortices is in the lowest 2.5 km. Identifying mesovortices can be difficult at that level though if a system is a certain distance away from the radar. To have the best success at identifying mesovortices, more radars would have to be installed, at least in the Mississippi and Ohio River Valleys. However, mesovortices can be seen within the 3 km and 7 km range, the only issue is a tornado may already be on the ground before a forecaster can spot it. Nevertheless, with the current set up of radar locations, this layer is especially useful because it can be seen at farther distances.

Some interesting and unexpected results were also found during this study. For example, the orientation and axial ratio were only significantly different during the warm season, at the post-event time, for the 45 dBZ threshold. The orientation and axial ratio were greater for tornadic cases than non-tornadic cases. This means QLCS events do not necessarily have to have embedded supercells to produce tornadoes. Also, it was thought tornadic cases would display a more north-south orientation. These results suggest a more east to west orientation, at least at the 45 dBZ threshold. However, these two parameters were not significantly different any other time, therefore, it would appear orientation and axial ratio would not help when trying to differentiate between tornadic and non-tornadic QLCSs as previously thought.

Another interesting result is the comparison of each event to the QLCS definition set by Trapp et al. (2005). All of these cases were first defined as a QLCS just by visual appearance on radar. Then the different reflectivity thresholds were applied to see if the 40 dBZ threshold (Trapp et al. 2005) would be best for a definition. Based on the results, the 35 dBZ threshold seems the best, especially for the cold season. Eighteen of the warm season events (tornadic and non-tornadic) did not meet the 40 dBZ criteria and fourteen of the cold season events (tornadic and non-tornadic) did not meet the 40 dBZ criteria. For some of the cold season cases, there were no 40 or 45 dBZ and greater reflectivity. Eleven cases total did not meet the 100 km length criteria at the 35 dBZ threshold. QLCSs generally do not contain high reflectivity like supercells; therefore it would be better to set a lower threshold for the QLCS definition. Despite a few of the cases not meeting the criteria, this research proposes the 35 dBZ threshold would be a better reflectivity threshold for the QLCS definition than the 40 dBZ threshold.

In conclusion, azimuthal shear, divergence, and spectrum width in the 3 km to 7 km range are the best parameters to assess during the warm season for QLCS tornadoes, while azimuthal shear and divergence at 2 km and below 3 km are the best parameters to evaluate for QLCS tornadoes in the cold season. Values for all of these parameters are statistically significantly higher for tornadic cases than non-tornadic cases. Hopefully the results from this paper can aid forecasters during warning operations when QLCSs are present.

5.2 Future Work

There is a great deal of work yet to be done when it comes to studying QLCSs and tornadogenesis. This study showed that radar parameters at different heights do exist that can distinguish between tornadic and non-tornadic QLCSs. For the warm season, three parameters dominated for all time steps and reflectivity thresholds: maximum azimuthal shear between 3 km and 7 km, maximum divergence between 3 km and 7 km, and maximum spectrum width between 3 km and 7 km. This suggests there is more turbulent airflow, convergence, and cyclonic rotation in tornadic events than non-tornadic events. For the cold season, two azimuthal shear parameters and two divergence parameters dominated for all time steps and reflectivity thresholds: the maximum azimuthal shear and maximum divergence at 2 km and below 3 km. These results propose there is significantly more cyclonic rotation in the lower part of the atmosphere for tornadic cases than non-tornadic cases. They also imply there is more convergence in tornadic cases and therefore more vertical motion. This vertical motion can then aid in stretching a rotating vertical column of air that can lead to tornadogenesis. This study is replicable and the results are sound but continued work on this particular subject could produce improved results.

To further this research and better the outcome, more events could be added to generalize the results. In addition, more parameters could also be assessed, especially at different heights and layers. Specifically a 2 km to 4 km layer might be ideal for identifying tornadic mesovortices. This layer would include the area mesovortices form, as well as, is high enough from the ground that it can be seen at farther distances from the radar. Another solution would be to choose events within a certain range from the radar,

although, those results would only be helpful for future events that would be within that range. A further adjustment would be to eliminate any identified cells (from MATLAB) that were not associated with tornadoes (warnings). This would allow for a more concentrated study on the specified areas of interest. Focusing on the potentially hazardous area, would construct more accurate results.

Additionally, the radar time steps could be processed to be five minutes apart instead of ten minutes. The shorter time steps would make the pre-event, event, and post-event times of each event more accurate and the researcher could then observe how the radar parameters change throughout the course of each event. Finally, thresholds for the parameters were not created. Once additional research is completed, results can be generalized and thresholds can be created which would be very useful for forecasters during severe weather operations.

All in all, given the results of this research, it is reasonable to assume that it is possible to distinguish between tornadic QLCSs from non-tornadic QLCSs using radar. This will aid in better forecasting and warning issuance of tornadogenesis within QLCSs. More accurate warnings on QLCSs will decrease the loss of property and life.

Appendix A

The following are box plots for all 21 parameters. They are organized by time step (pre-event, event, and post-event) and reflectivity threshold (35 dBZ, 40 dBZ, and 45 dBZ).

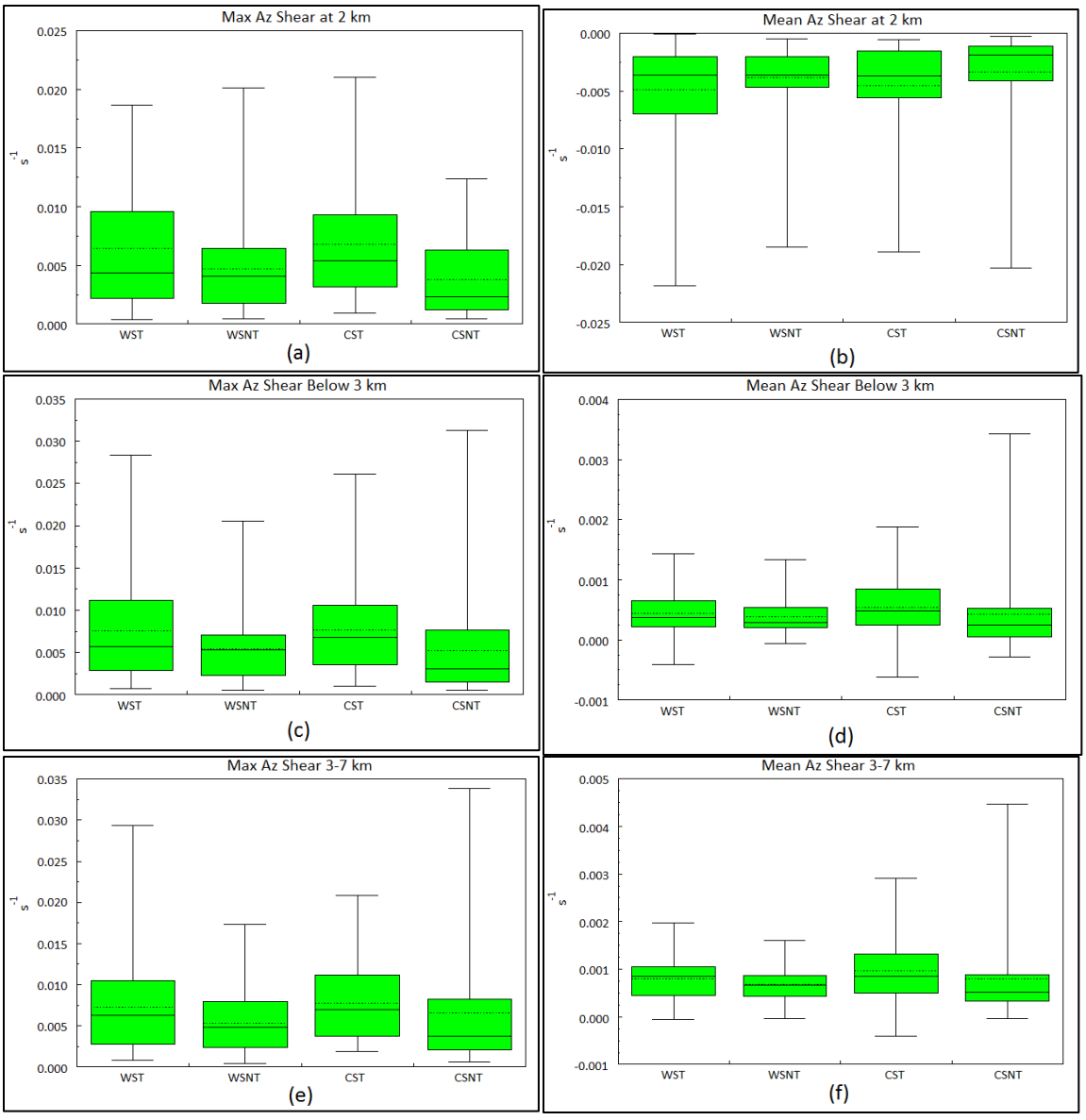

Figure A.1. Box and Whisker plots for the pre-event time step for 35 dBZ. a) max azimuthal shear at 2 km, b) mean azimuthal shear at 2 km, c) max azimuthal shear below 3 km, d) mean azimuthal shear below 3 km, e) max azimuthal shear 3-7 km, f) mean azimuthal shear 3-7 km.

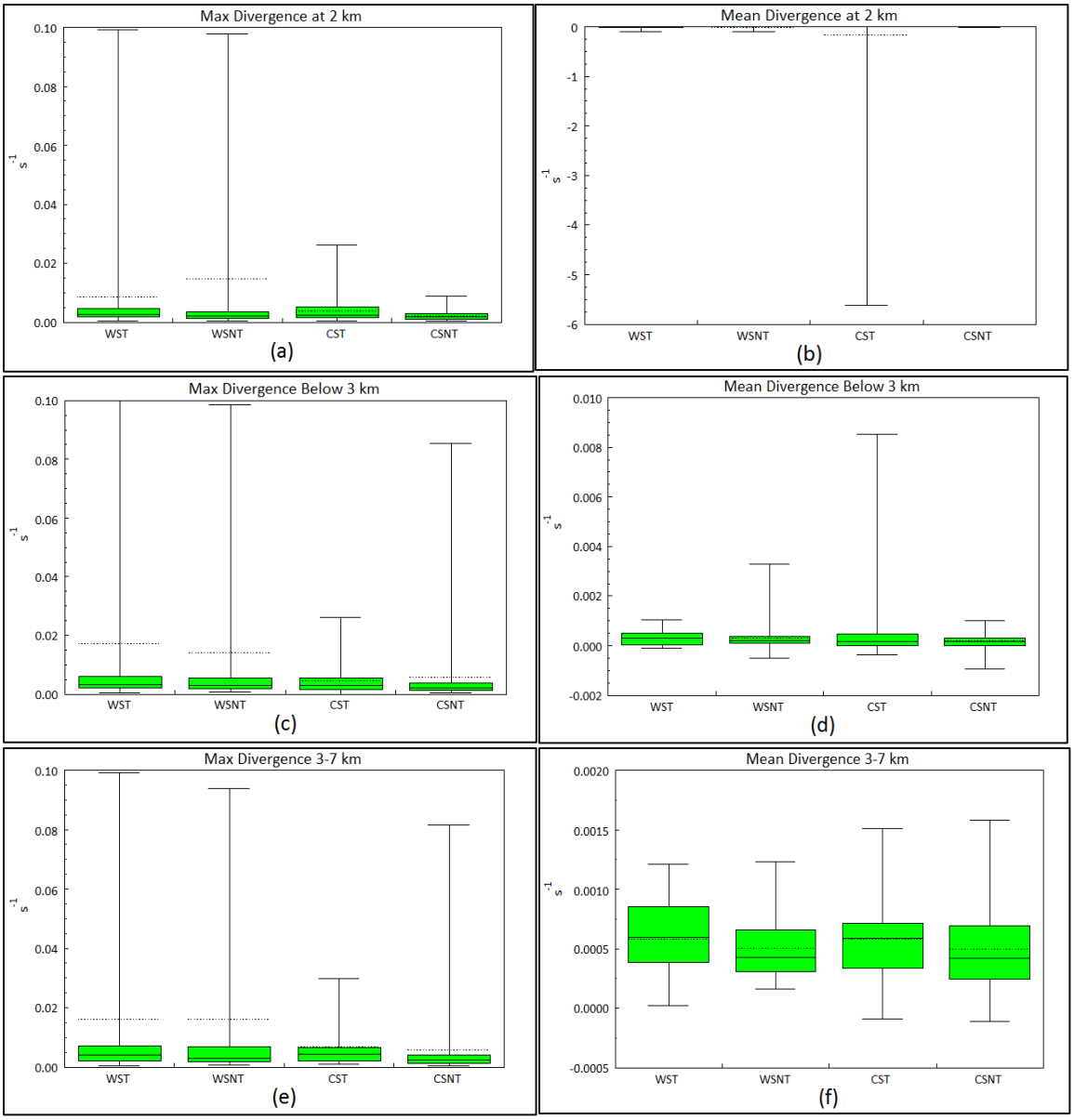

Figure A.2. Box and Whisker plots for the pre-event time step for 35 dBZ. a) max divergence at 2 km, b) mean divergence at 2 km, c) max divergence below 3 km, d) mean divergence below 3 km, e) max divergence 3-7 km, f) mean divergence 3-7 km.

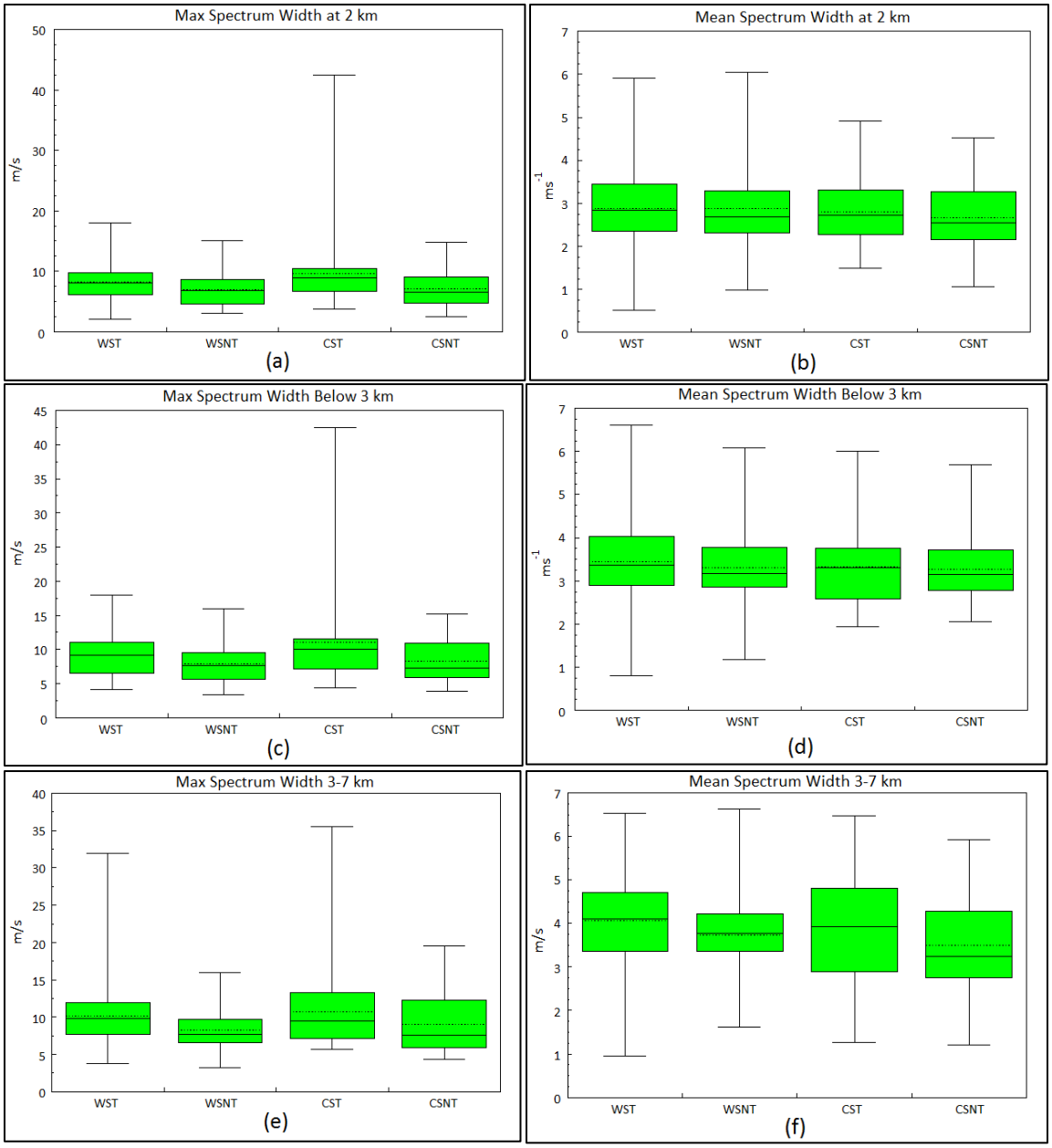

Figure A.3. Box and Whisker plots for the pre-event time step for 35 dBZ. a) max spectrum width at 2 km, b) mean spectrum width at 2 km, c) max spectrum width below 3 km, d) mean spectrum width below 3 km, e) max spectrum width 3-7 km, f) mean spectrum width 3-7 km.

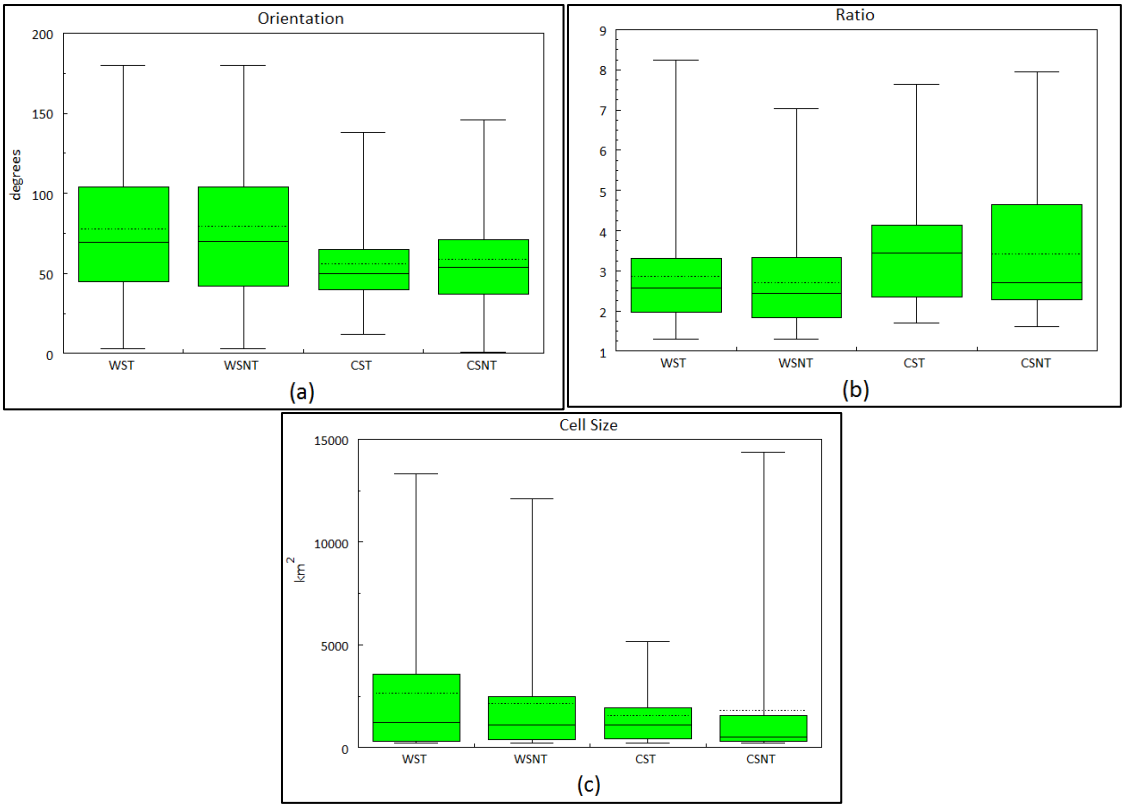

Figure A.4. Box and Whisker plots for the pre-event time step for 35 dBZ. a) orientation, b) ratio, c) cell size.

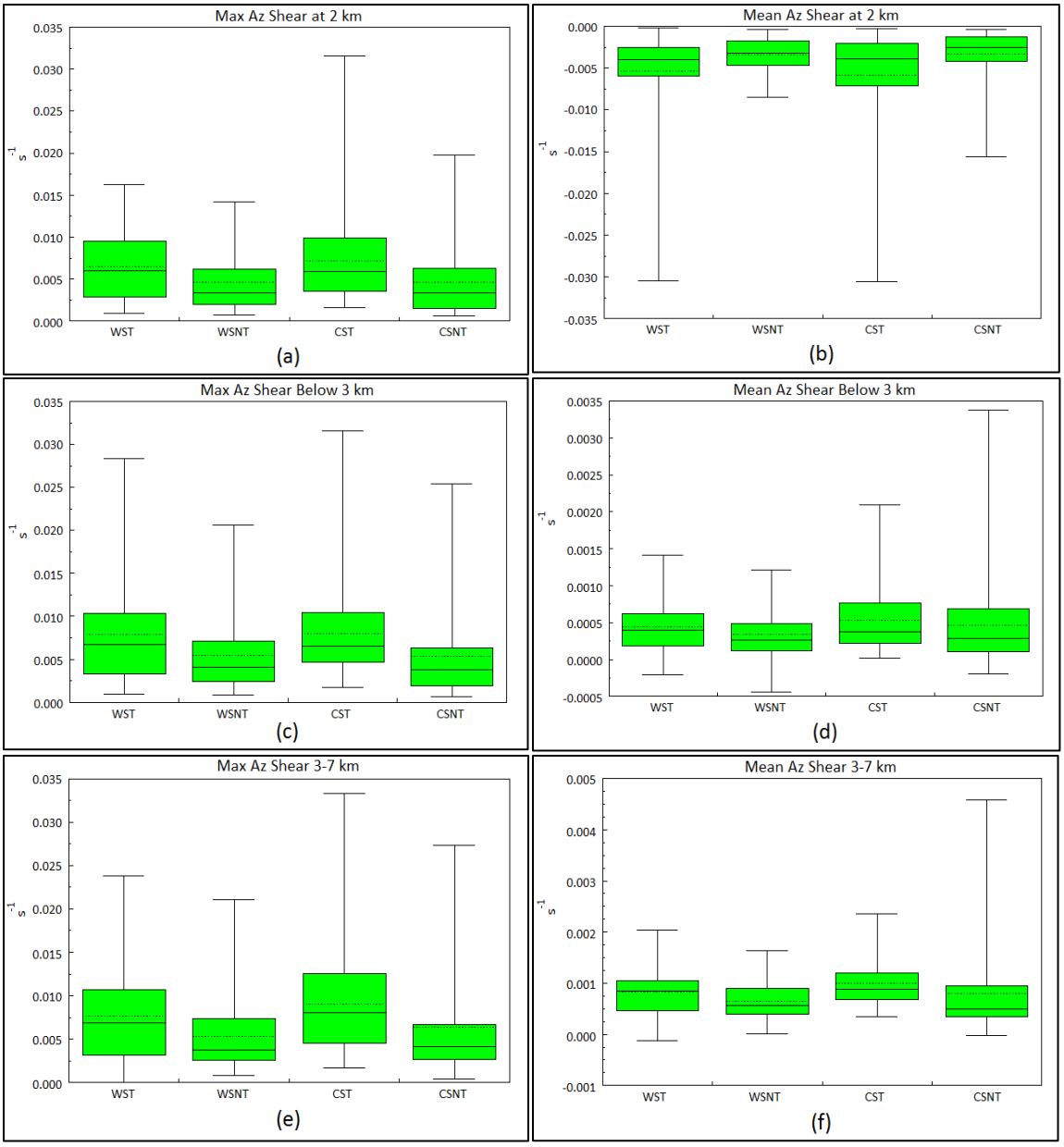

Figure A.5. Box and Whisker plots for the event time step for 35 dBZ. a) max azimuthal shear at 2 km, b) mean azimuthal shear at 2 km, c) max azimuthal shear below 3 km, d) mean azimuthal shear below 3 km, e) max azimuthal shear 3-7 km, f) mean azimuthal shear 3-7 km.

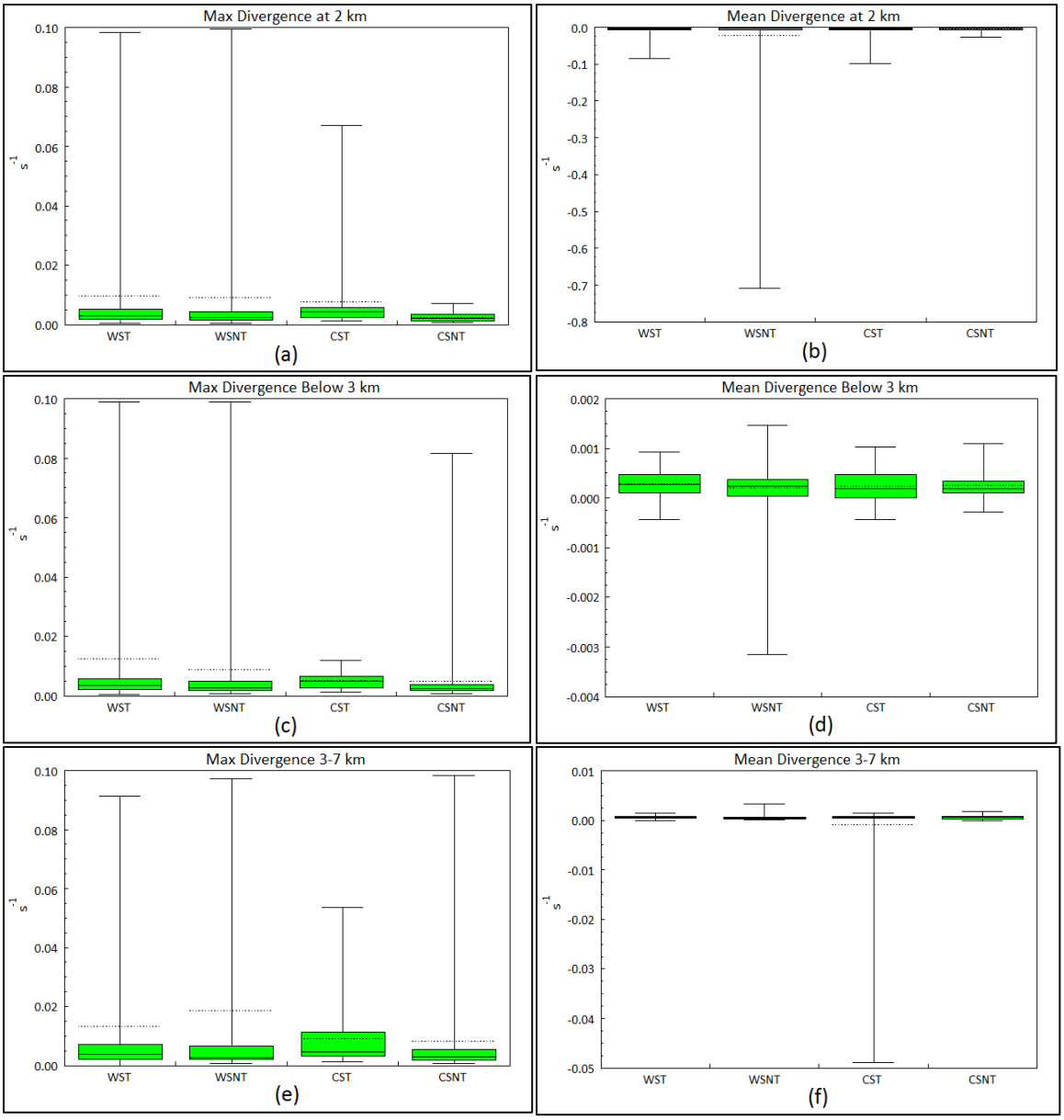

Figure A.6. Box and Whisker plots for the event time step for 35 dBZ. a) max divergence at 2 km, b) mean divergence at 2 km, c) max divergence below 3 km, d) mean divergence below 3 km, e) max divergence 3-7 km, f) mean divergence 3-7 km.

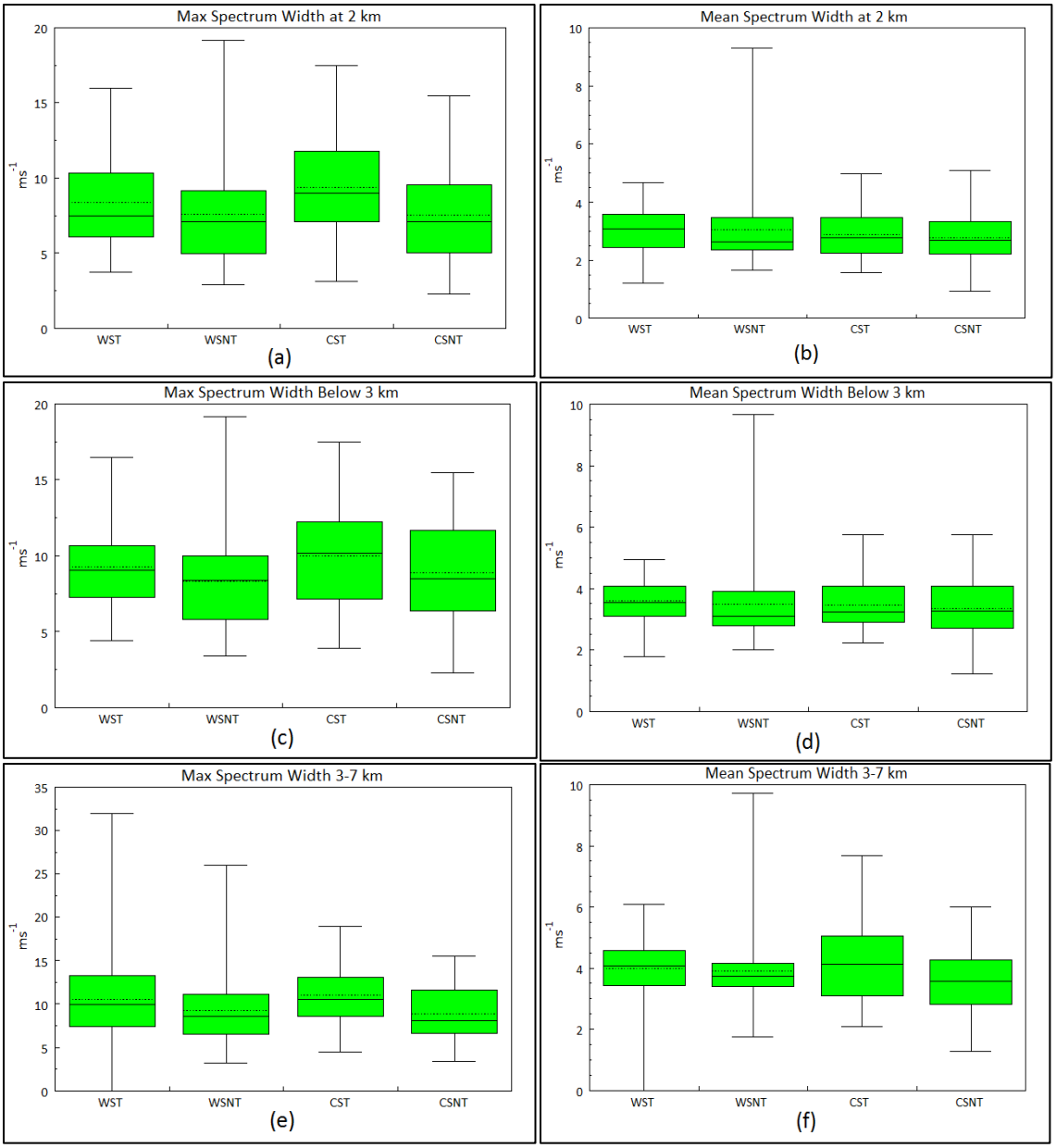

Figure A.7. Box and Whisker plots for the event time step for 35 dBZ. a) max spectrum width at 2 km, b) mean spectrum width at 2 km, c) max spectrum width below 3 km, d) mean spectrum width below 3 km, e) max spectrum width 3-7 km, f) mean spectrum width 3-7 km.

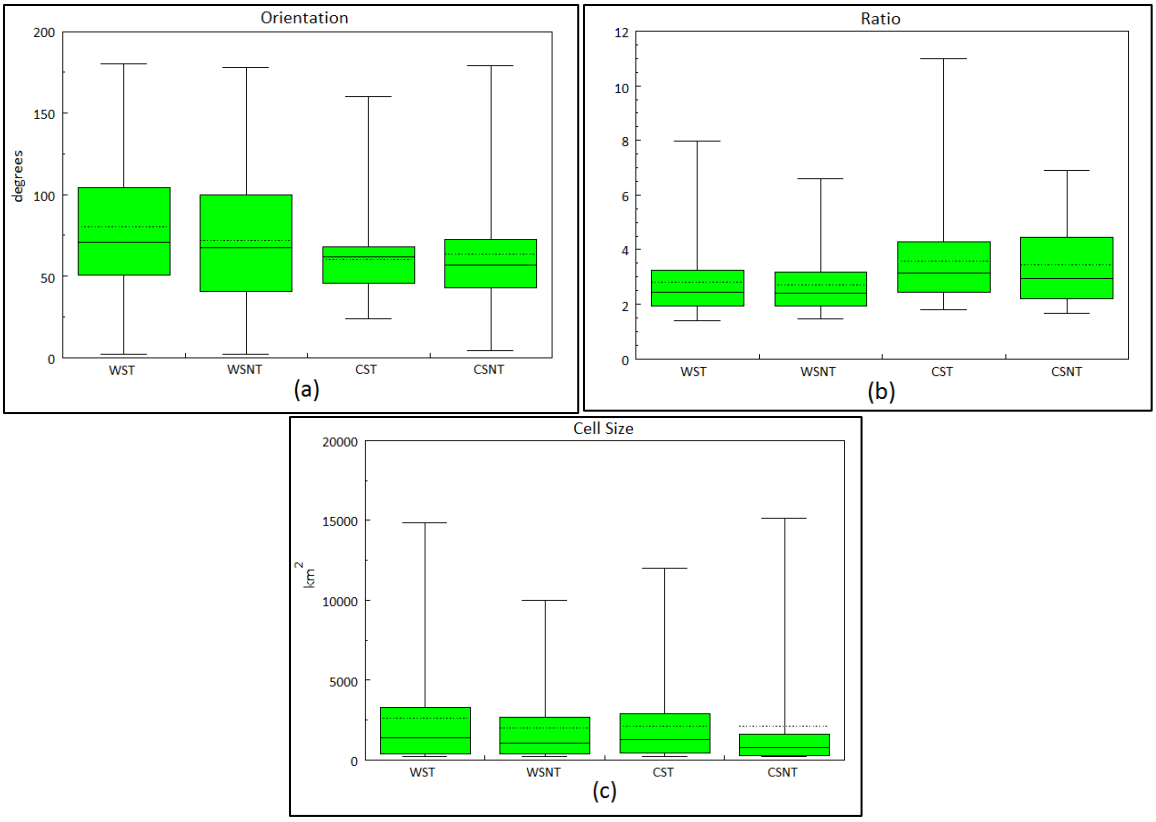

Figure A.8. Box and Whisker plots for the event time step for 35 dBZ. a) orientation, b) ratio, c) cell size.

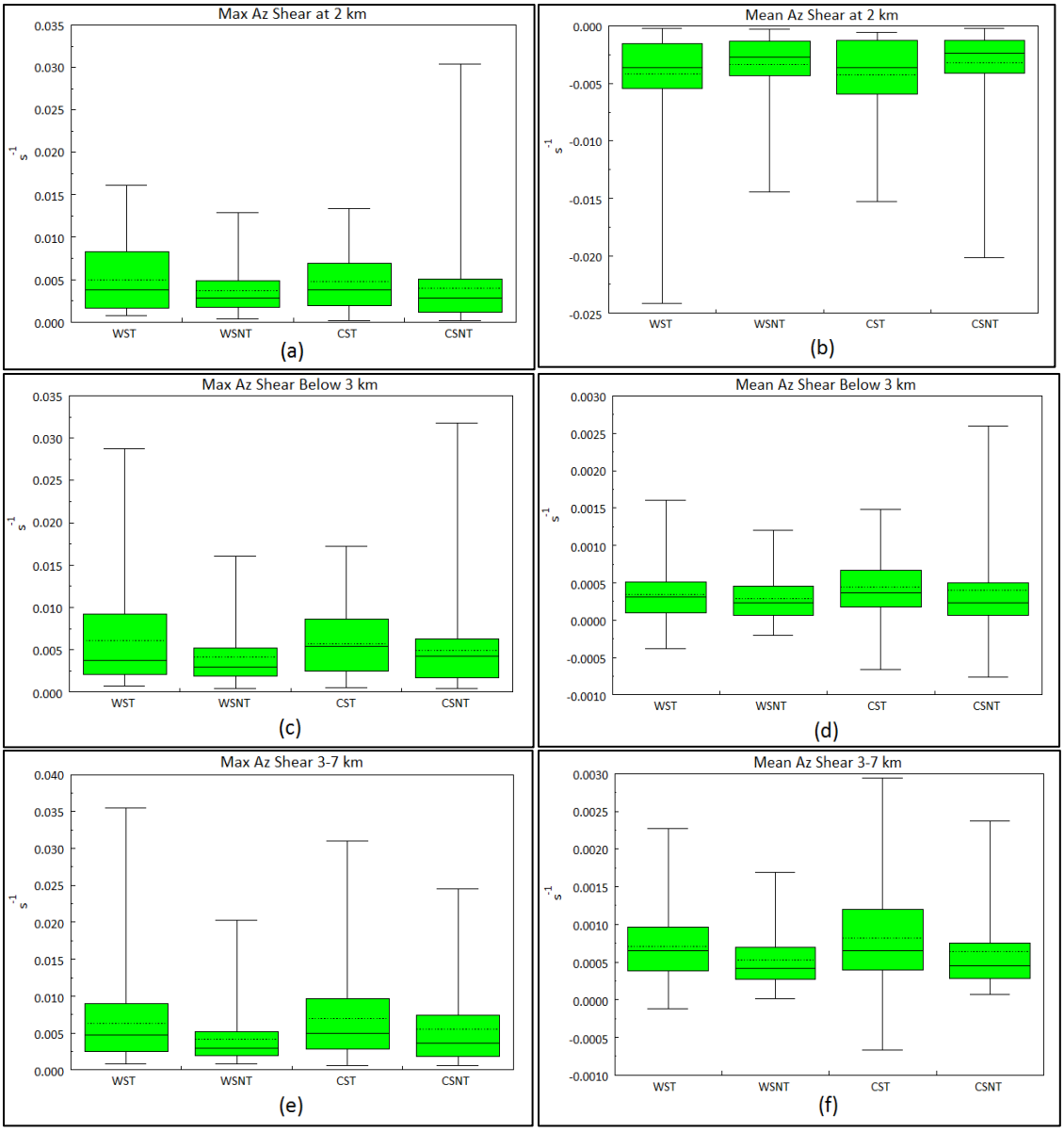

Figure A.9. Box and Whisker plots for the post-event time step for 35 dBZ. a) max azimuthal shear at 2 km, b) mean azimuthal shear at 2 km, c) max azimuthal shear below 3 km, d) mean azimuthal shear below 3 km, e) max azimuthal shear 3-7 km, f) mean azimuthal shear 3-7 km.

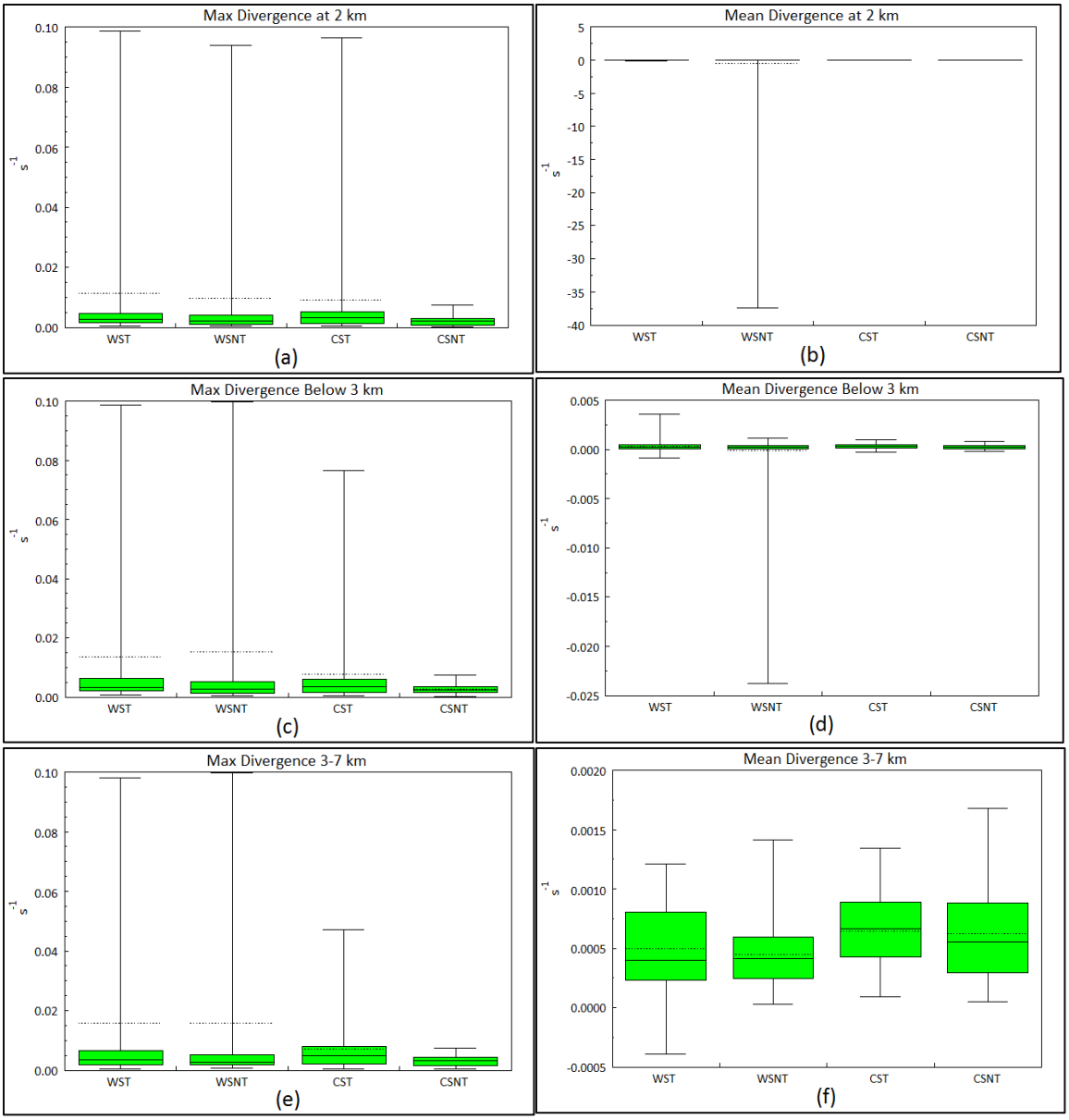

Figure A.10. Box and Whisker plots for the post-event time step for 35 dBZ. a) max divergence at 2 km, b) mean divergence at 2 km, c) max divergence below 3 km, d) mean divergence below 3 km, e) max divergence 3-7 km, f) mean divergence 3-7 km.

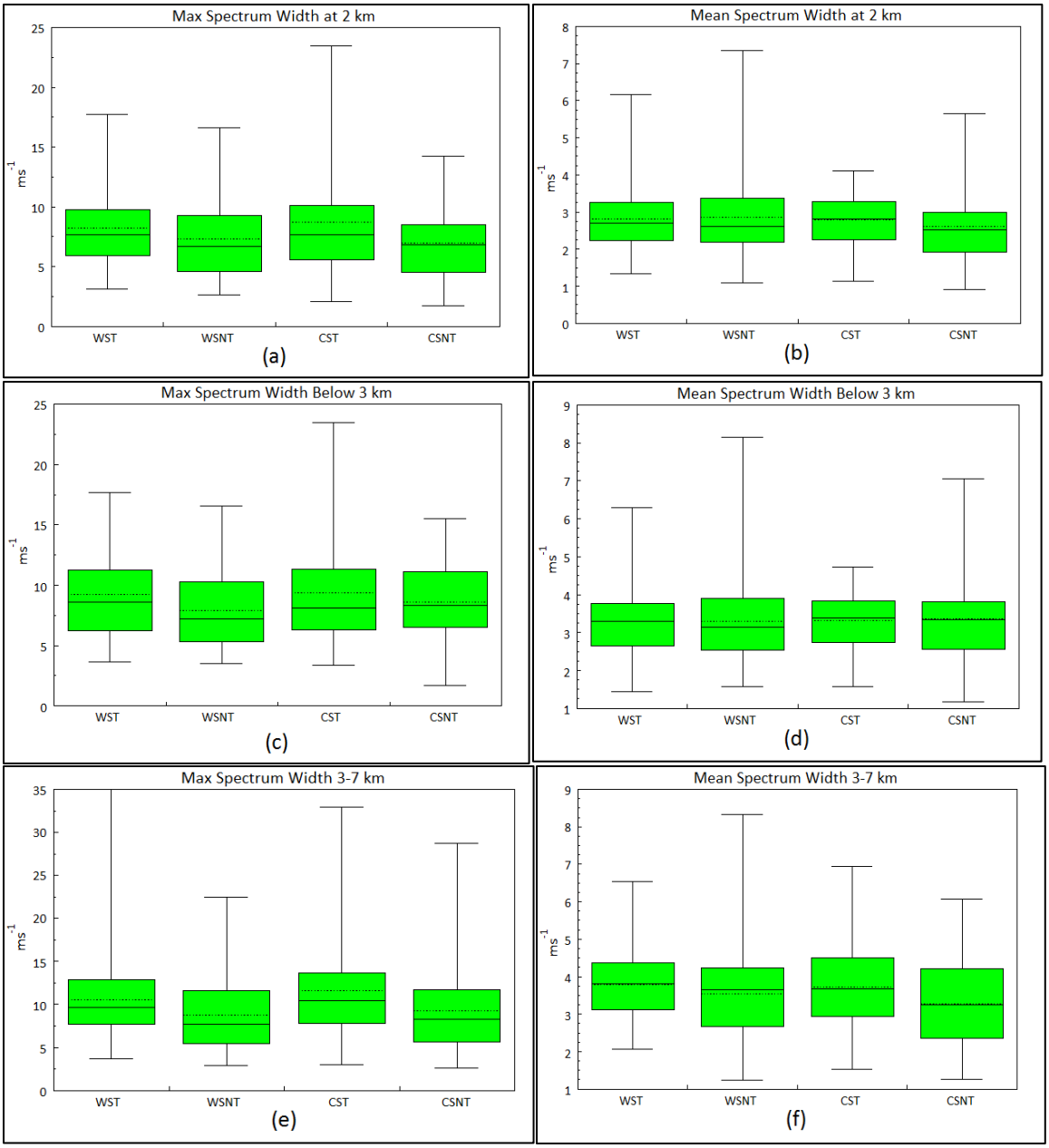

Figure A.11. Box and Whisker plots for the post-event time step for 35 dBZ. a) max spectrum width at 2 km, b) mean spectrum width at 2 km, c) max spectrum width below 3 km, d) mean spectrum width below 3 km, e) max spectrum width 3-7 km, f) mean spectrum width 3-7 km.

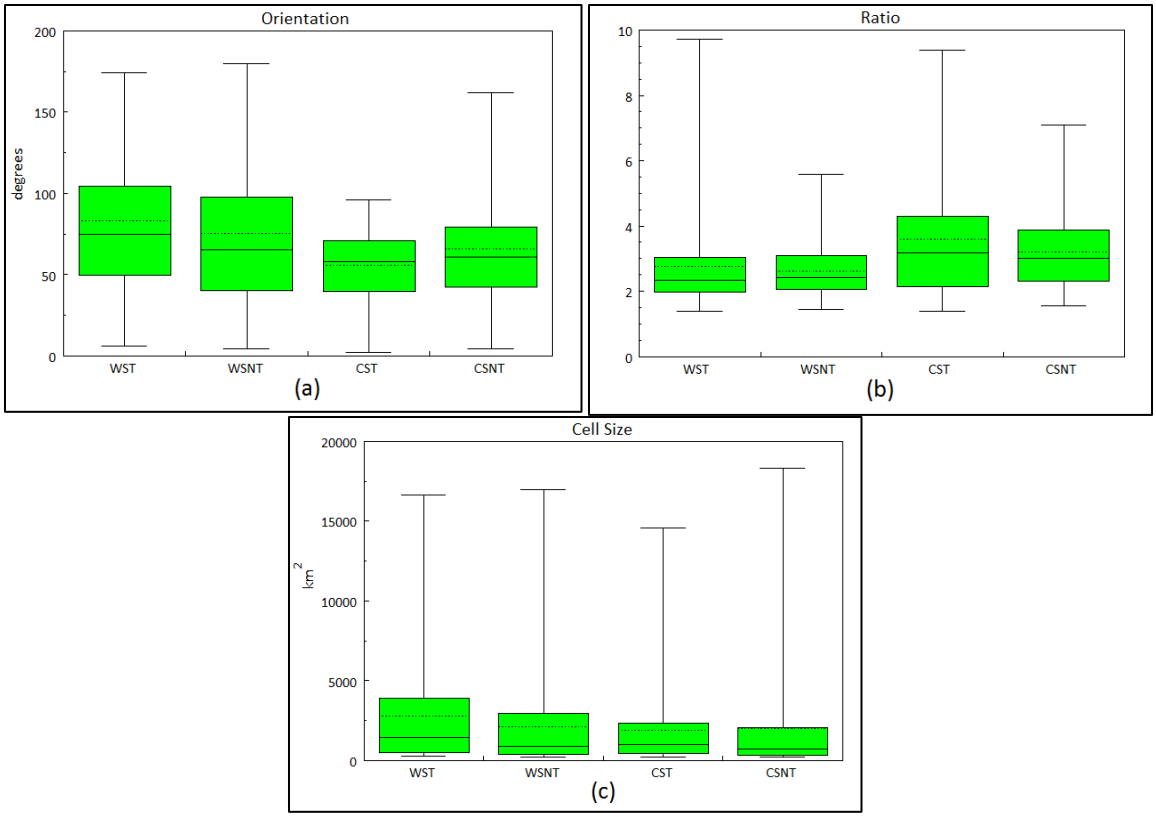

Figure A.12. Box and Whisker plots for the post-event time step for 35 dBZ. a) orientation, b) ratio, c) cell size.

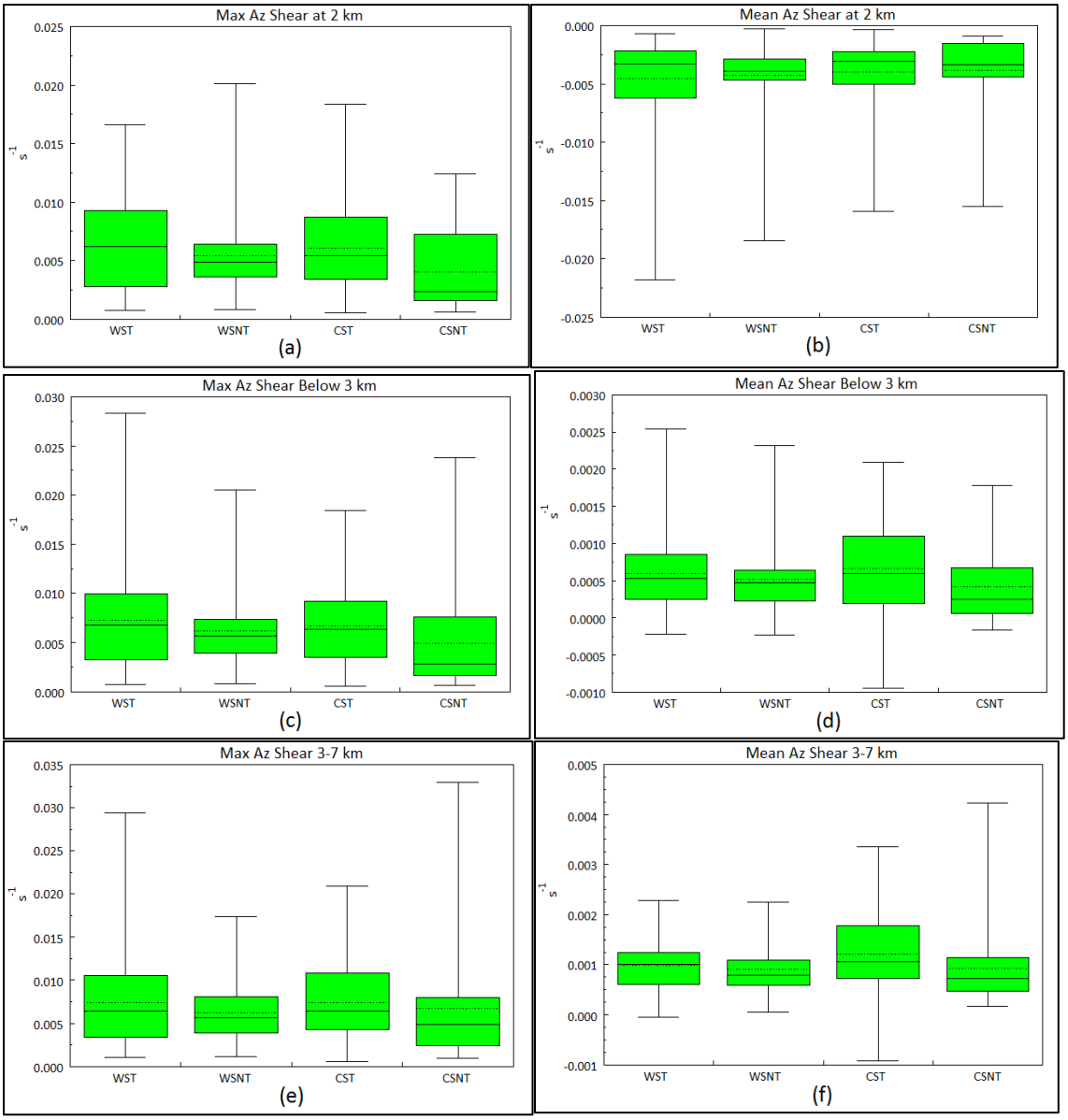

Figure A.13. Box and Whisker plots for the pre-event time step for 40 dBZ. a) max azimuthal shear at 2 km, b) mean azimuthal shear at 2 km, c) max azimuthal shear below 3 km, d) mean azimuthal shear below 3 km, e) max azimuthal shear 3-7 km, f) mean azimuthal shear 3-7 km.

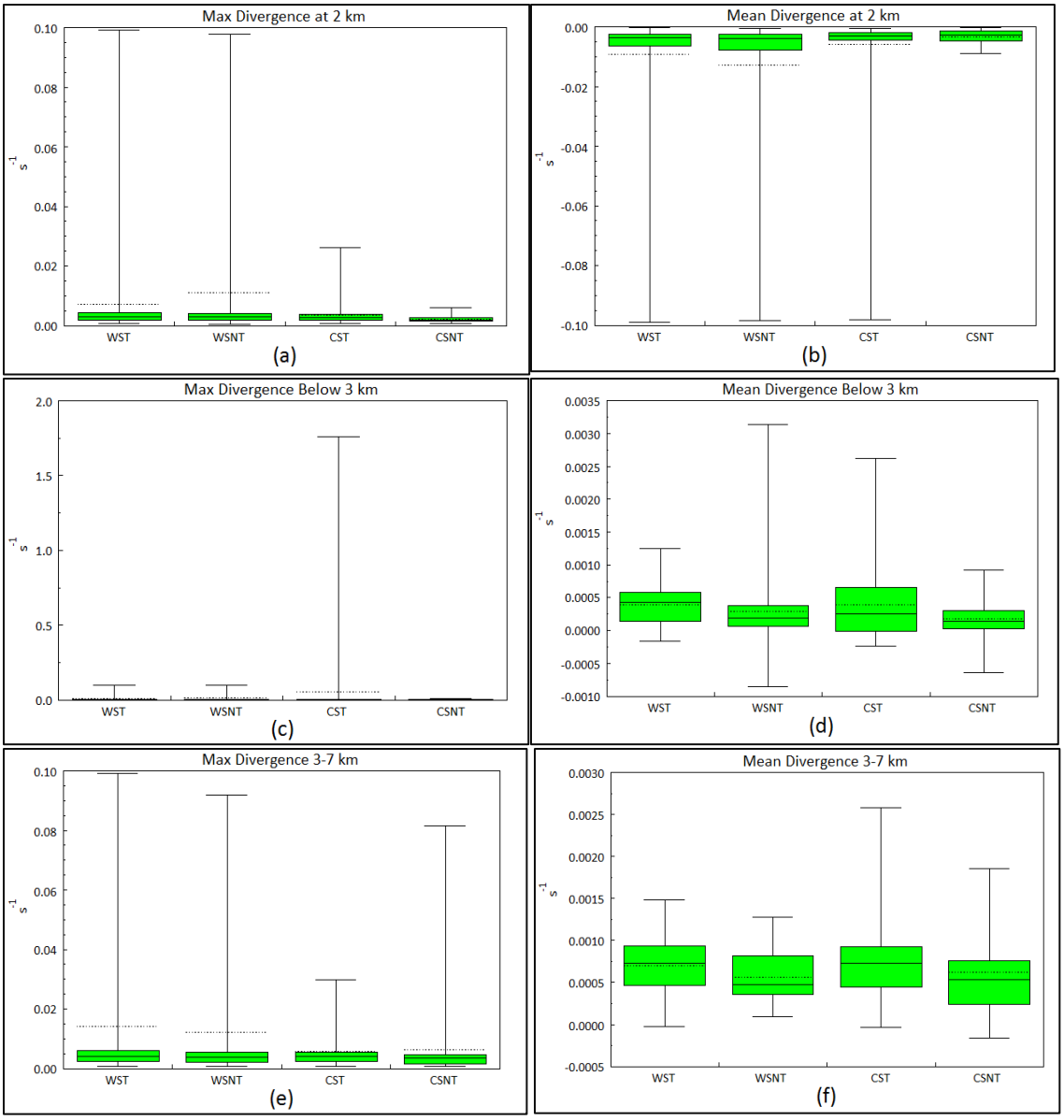

Figure A.14. Box and Whisker plots for the pre-event time step for 40 dBZ. a) max divergence at 2 km, b) mean divergence at 2 km, c) max divergence below 3 km, d) mean divergence below 3 km, e) max divergence 3-7 km, f) mean divergence 3-7 km.

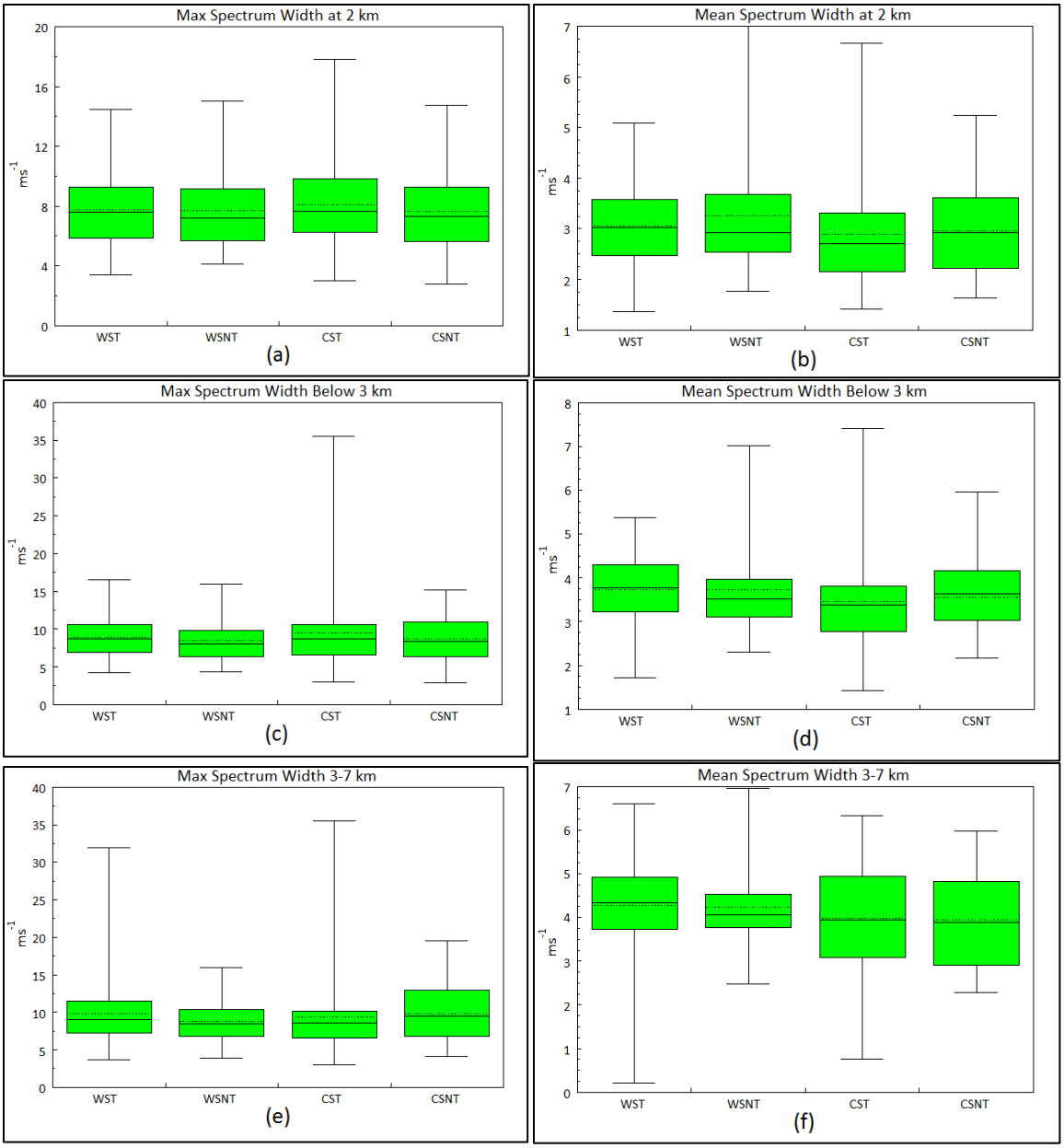

Figure A.15. Box and Whisker plots for the pre-event time step for 40 dBZ. a) max spectrum width at 2 km, b) mean spectrum width at 2 km, c) max spectrum width below 3 km, d) mean spectrum width below 3 km, e) max spectrum width 3-7 km, f) mean spectrum width 3-7 km.

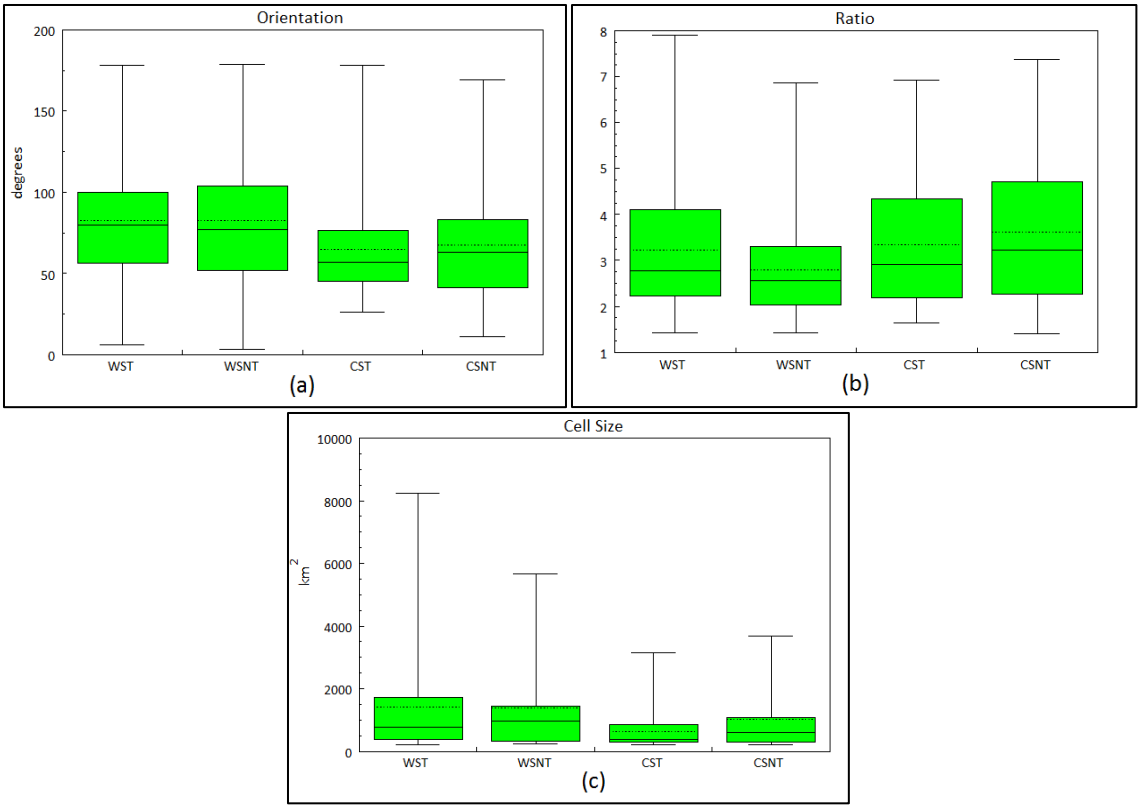

Figure A.16. Box and Whisker plots for the pre-event time step for 40 dBZ. a) orientation, b) ratio, c) cell size.

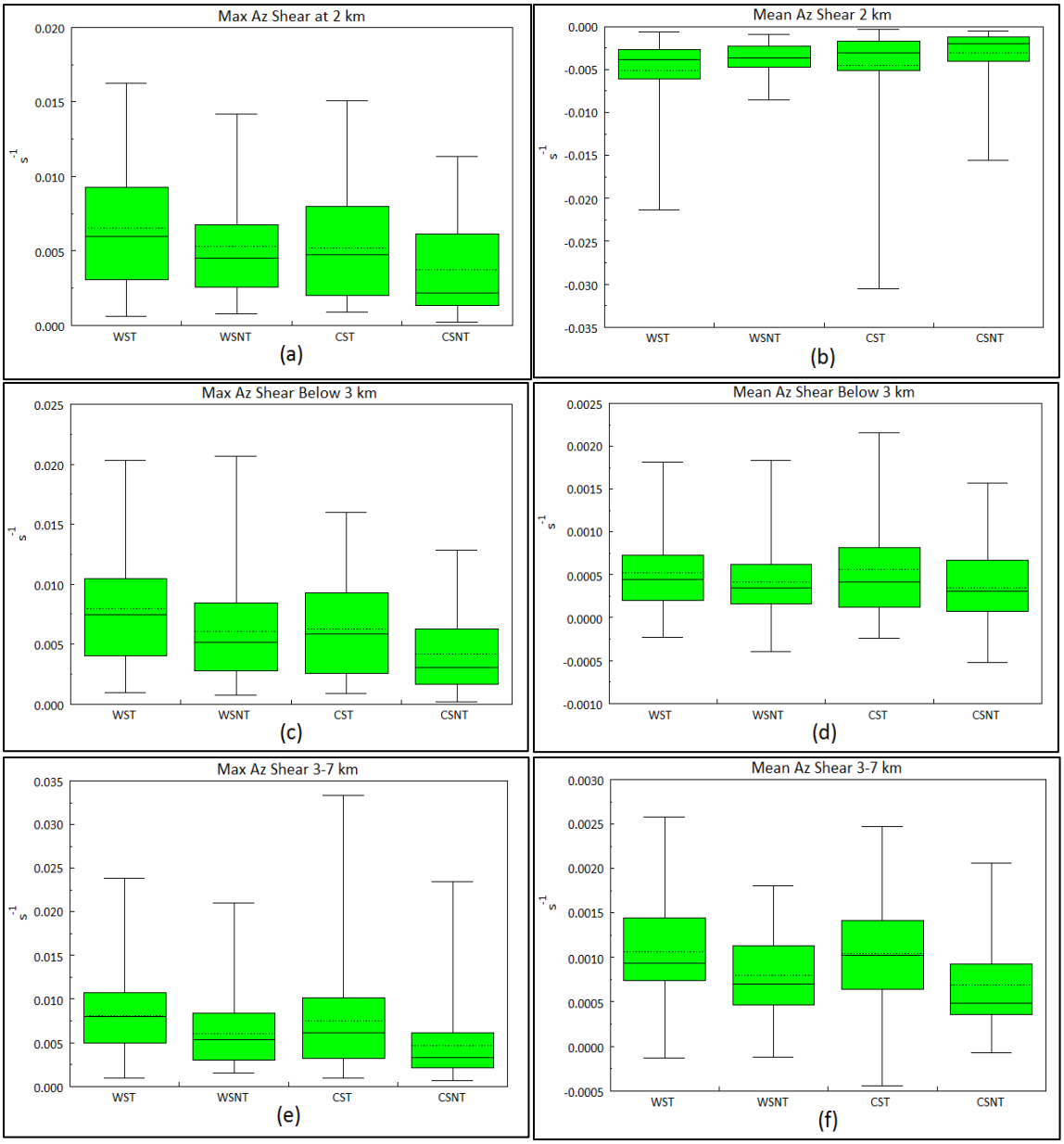

Figure A.17. Box and Whisker plots for the event time step for 40 dBZ. a) max azimuthal shear at 2 km, b) mean azimuthal shear at 2 km, c) max azimuthal shear below 3 km, d) mean azimuthal shear below 3 km, e) max azimuthal shear 3-7 km, f) mean azimuthal shear 3-7 km.

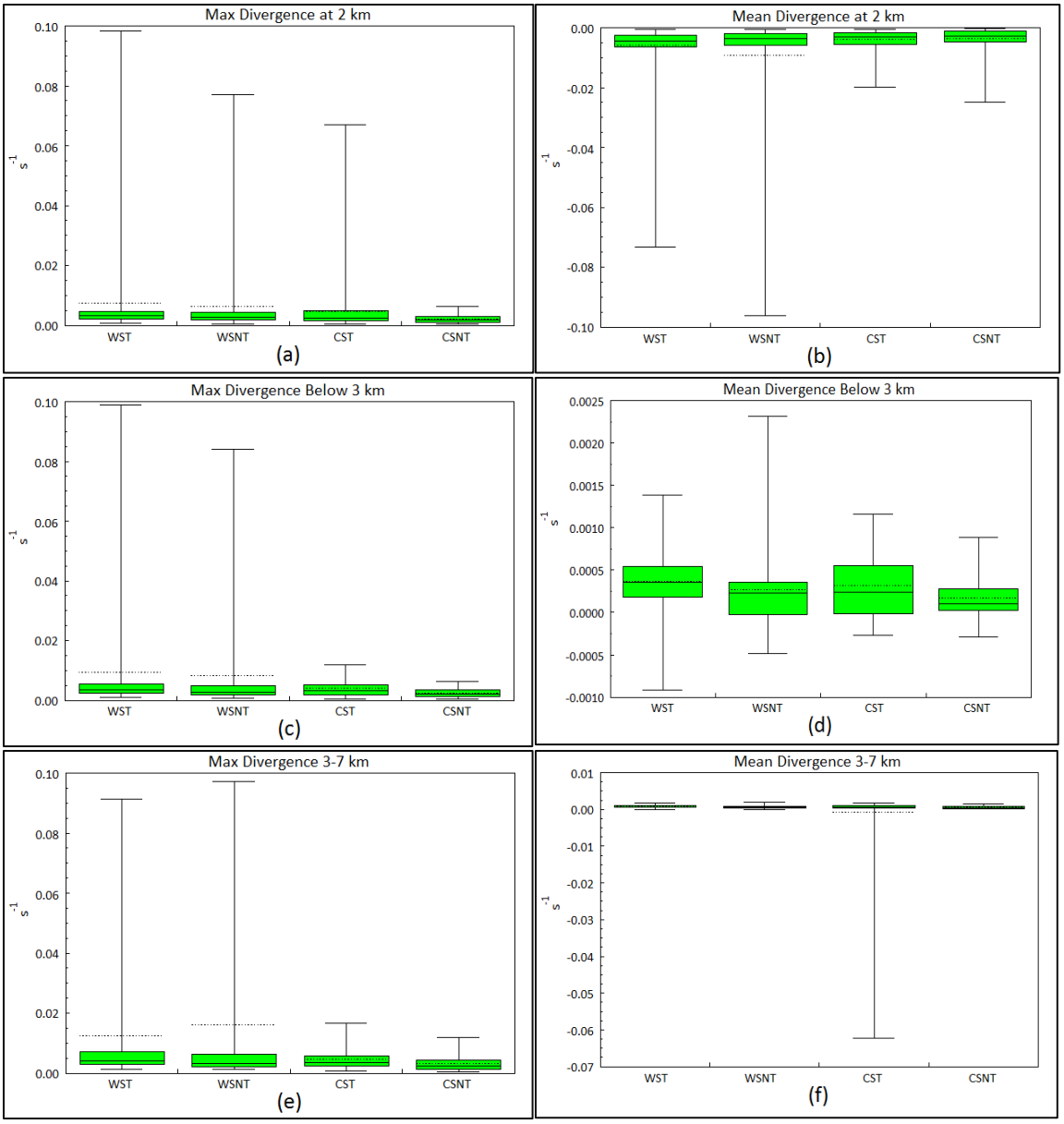

Figure A.18. Box and Whisker plots for the event time step for 40 dBZ. a) max divergence at 2 km, b) mean divergence at 2 km, c) max divergence below 3 km, d) mean divergence below 3 km, e) max divergence 3-7 km, f) mean divergence 3-7 km.

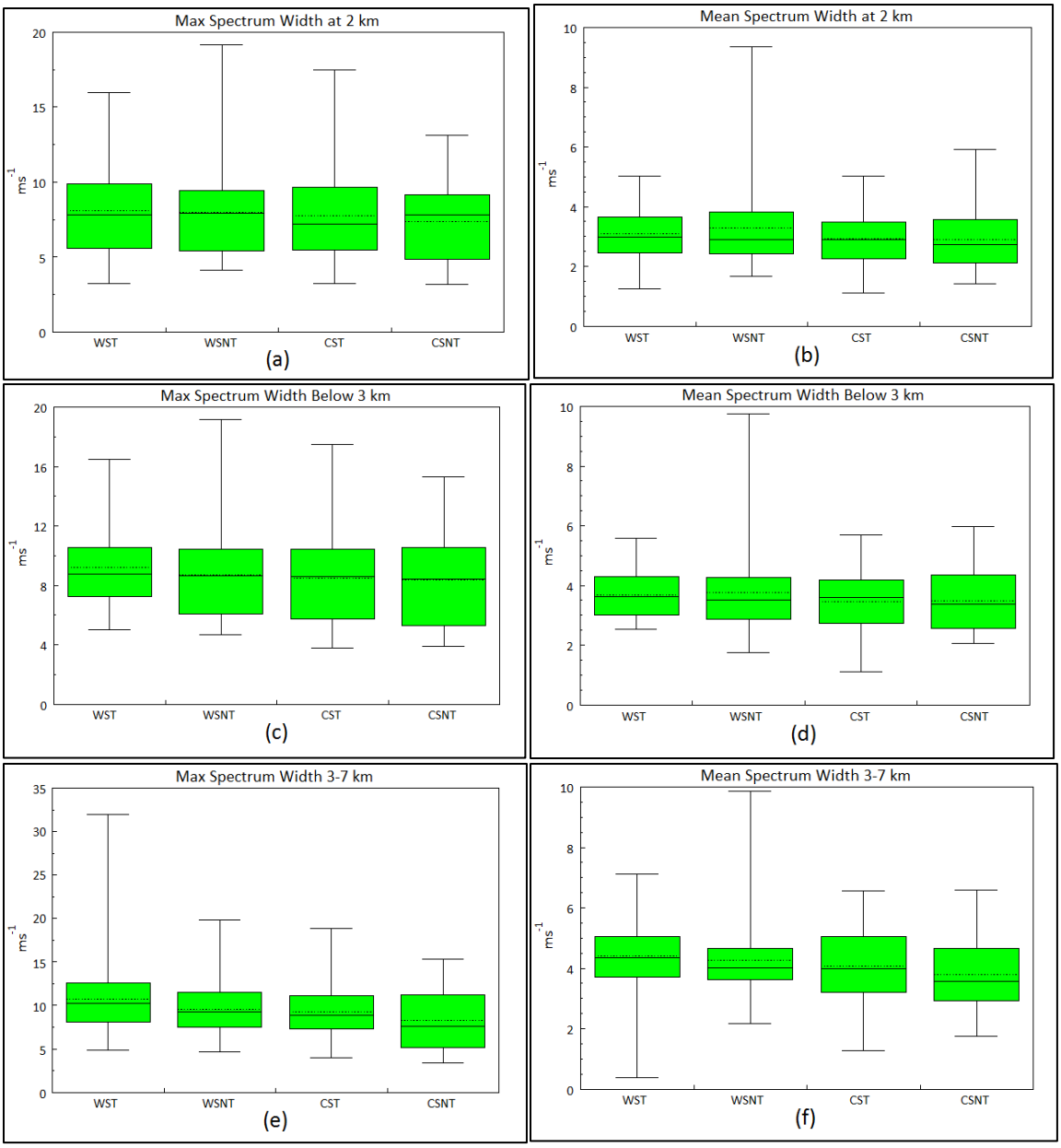

Figure A.19. Box and Whisker plots for the event time step for 40 dBZ. a) max spectrum width at 2 km, b) mean spectrum width at 2 km, c) max spectrum width below 3 km, d) mean spectrum width below 3 km, e) max spectrum width 3-7 km, f) mean spectrum width 3-7 km.

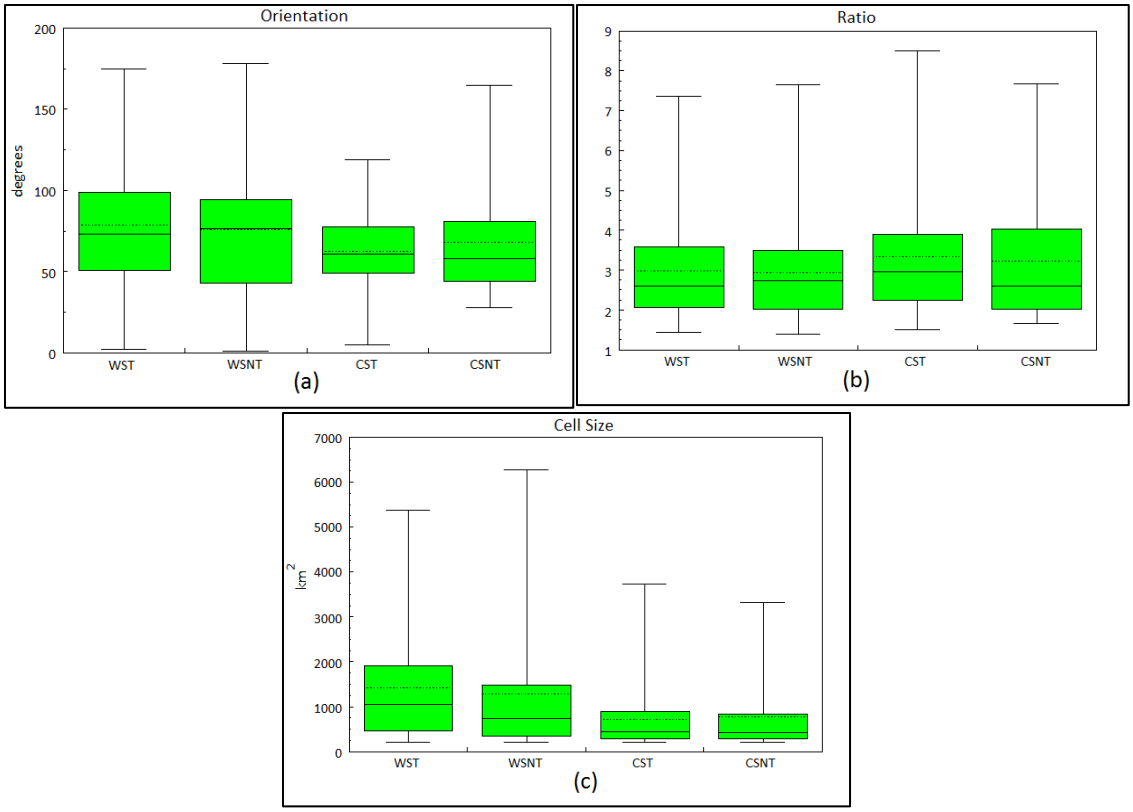

Figure A.20. Box and Whisker plots for the event time step for 40 dBZ. a) orientation, b) ratio, c) cell size.

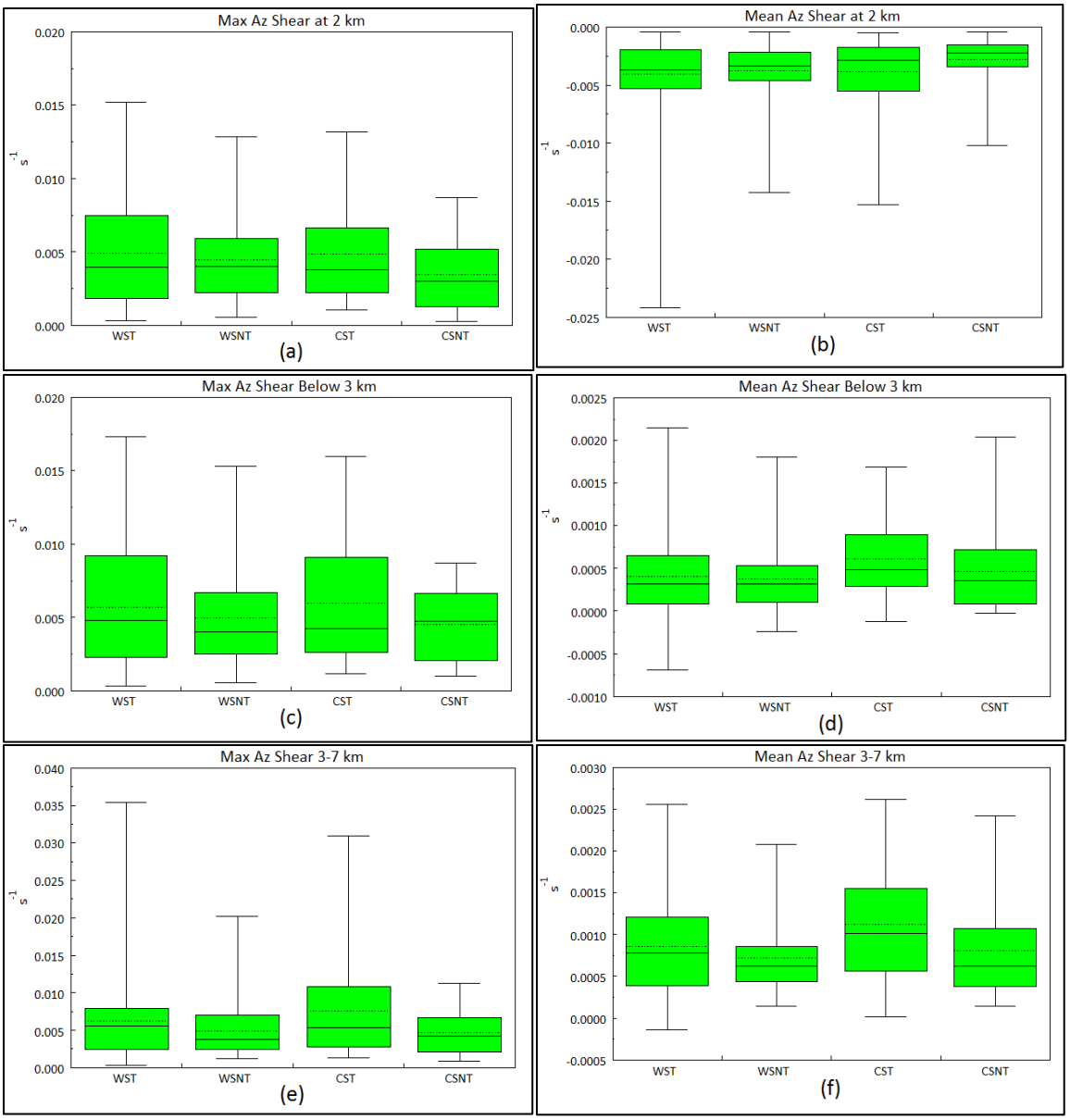

Figure A.21. Box and Whisker plots for the post-event time step for 40 dBZ. a) max azimuthal shear at 2 km, b) mean azimuthal shear at 2 km, c) max azimuthal shear below 3 km, d) mean azimuthal shear below 3 km, e) max azimuthal shear 3-7 km, f) mean azimuthal shear 3-7 km.

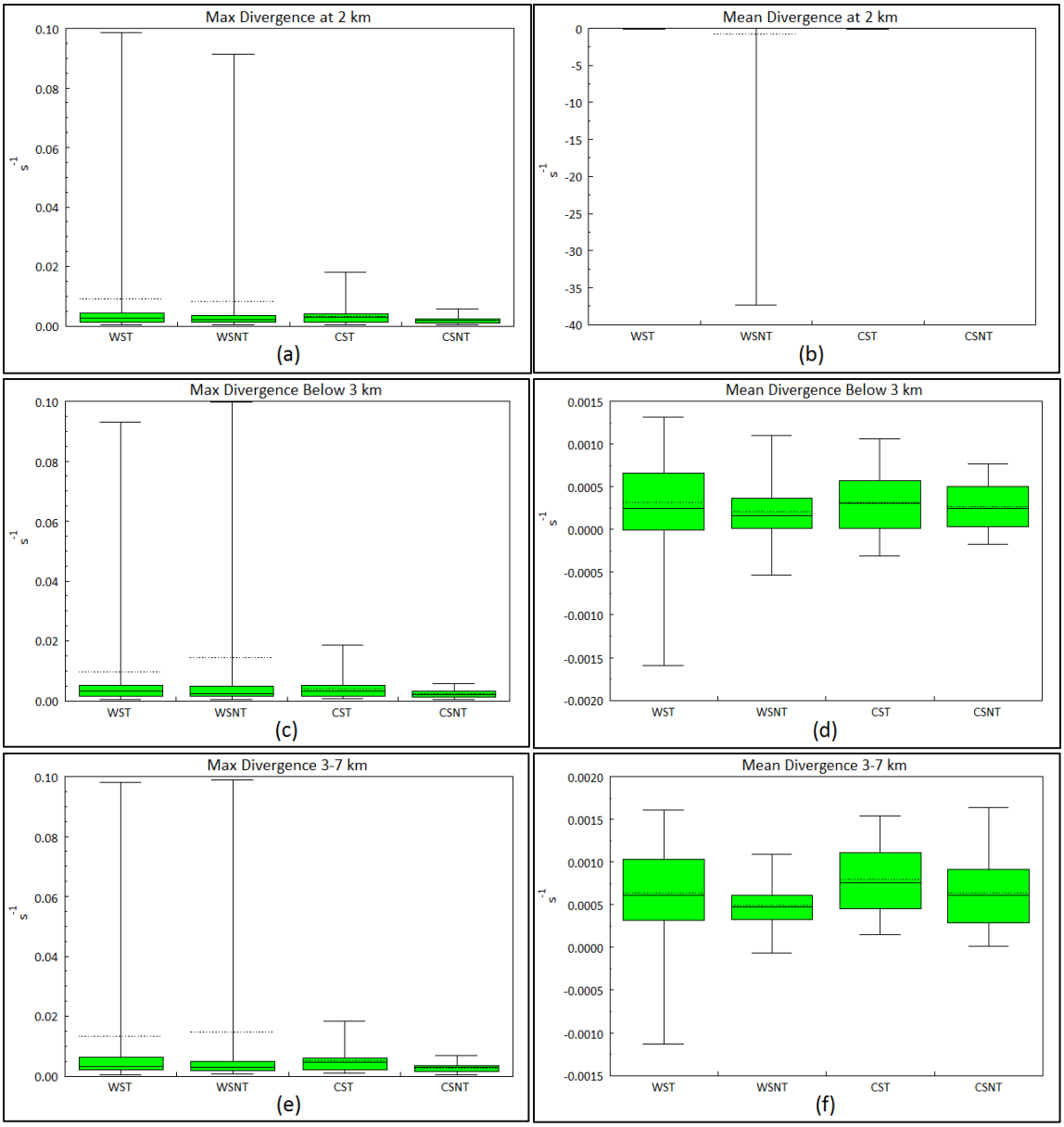

Figure A.22. Box and Whisker plots for the post-event time step for 40 dBZ. a) max divergence at 2 km, b) mean divergence at 2 km, c) max divergence below 3 km, d) mean divergence below 3 km, e) max divergence 3-7 km, f) mean divergence 3-7 km.

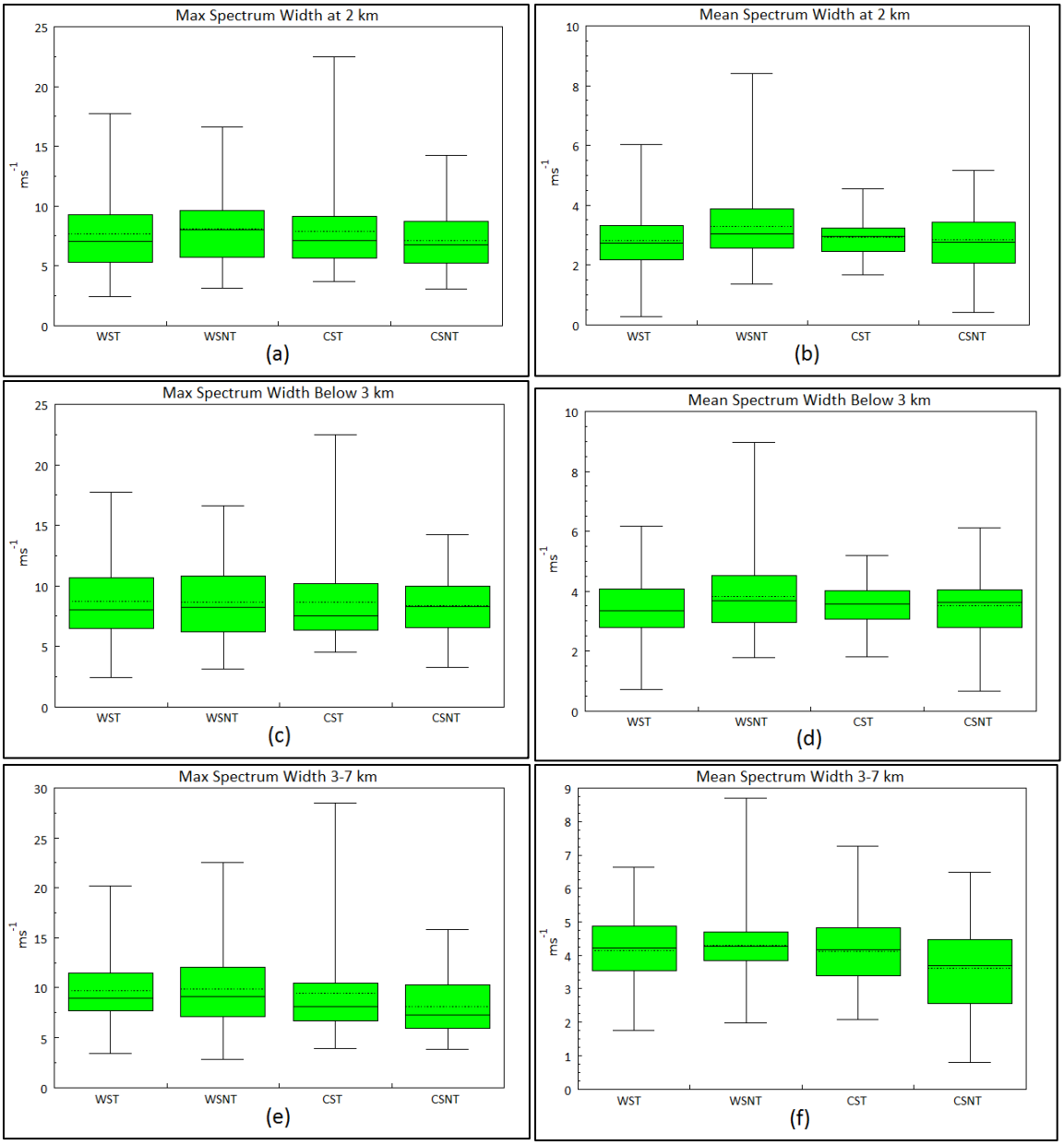

Figure A.23. Box and Whisker plots for the post-event time step for 40 dBZ. a) max spectrum width at 2 km, b) mean spectrum width at 2 km, c) max spectrum width below 3 km, d) mean spectrum width below 3 km, e) max spectrum width 3-7 km, f) mean spectrum width 3-7 km.

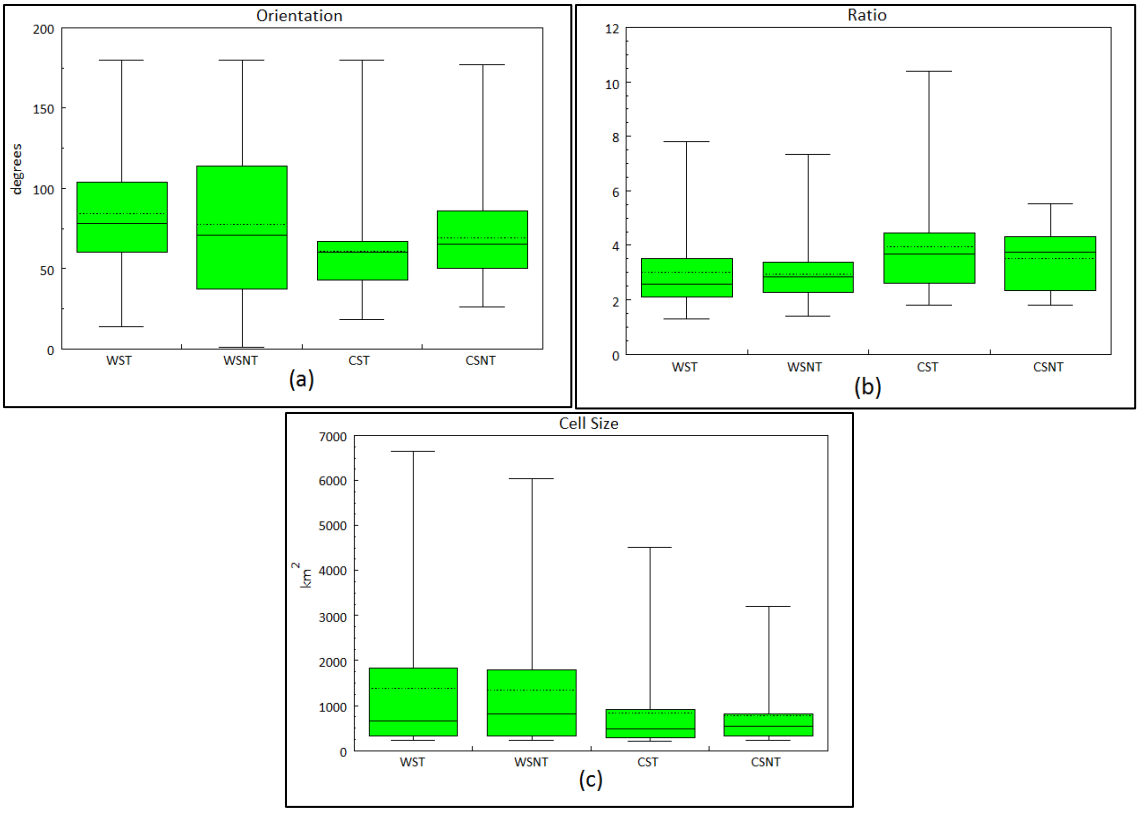

Figure A.24. Box and Whisker plots for the post-event time step for 40 dBZ. a) orientation, b) ratio, c) cell size.

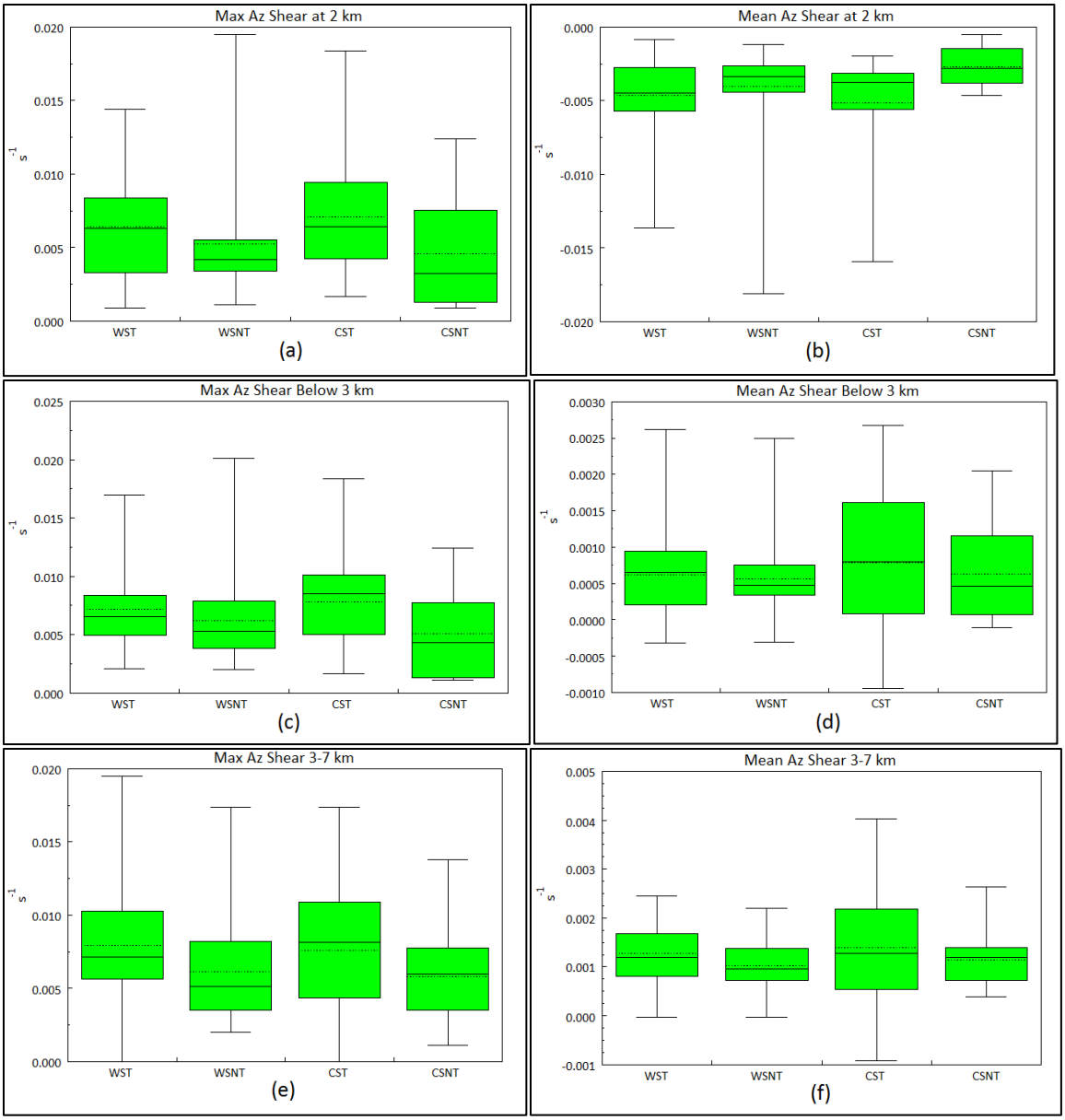

Figure A.25. Box and Whisker plots for the pre-event time step for 45 dBZ. a) max azimuthal shear at 2 km, b) mean azimuthal shear at 2 km, c) max azimuthal shear below 3 km, d) mean azimuthal shear below 3 km, e) max azimuthal shear 3-7 km, f) mean azimuthal shear 3-7 km.

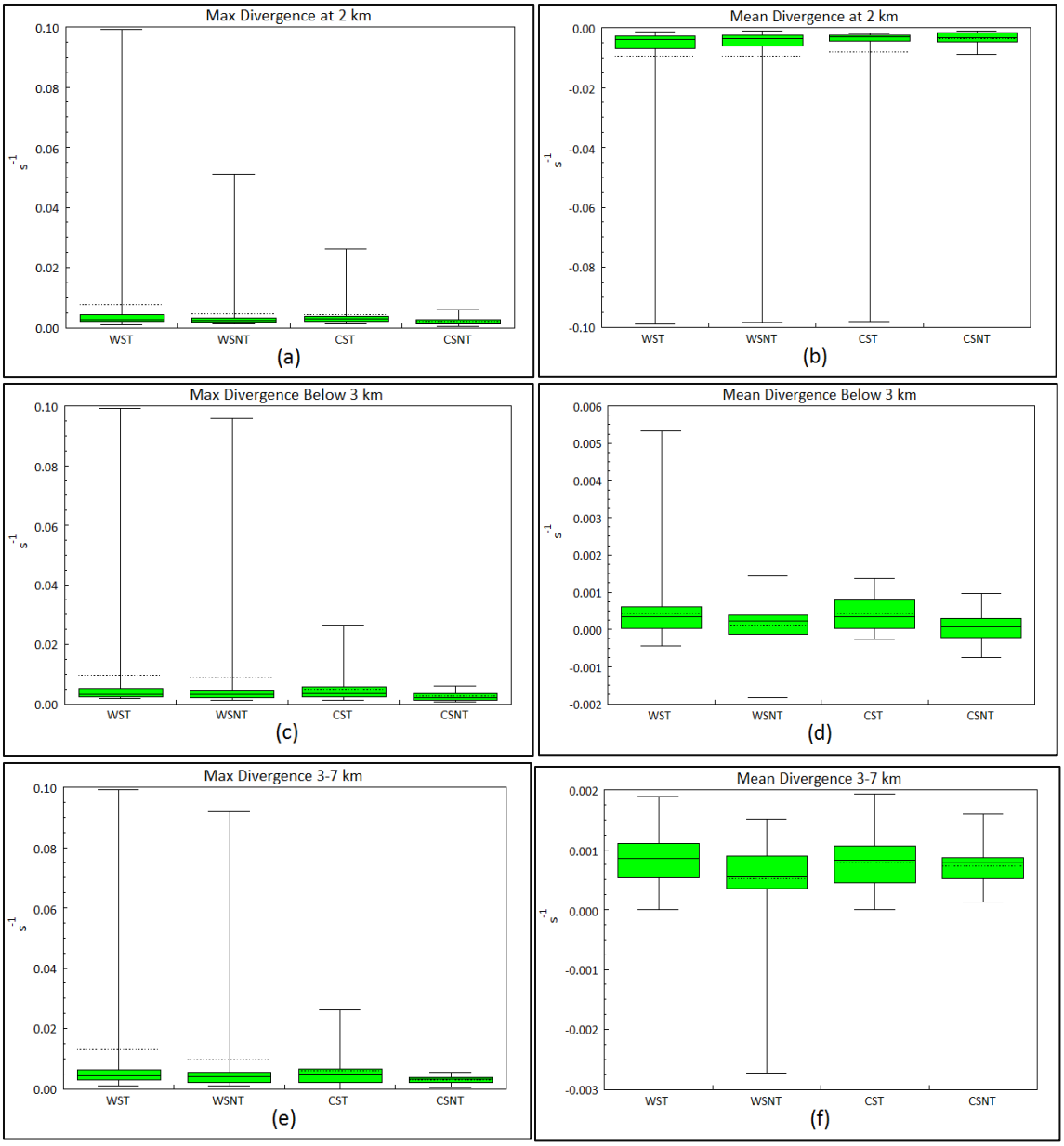

Figure A.26. Box and Whisker plots for the pre-event time step for 45 dBZ. a) max divergence at 2 km, b) mean divergence at 2 km, c) max divergence below 3 km, d) mean divergence below 3 km, e) max divergence 3-7 km, f) mean divergence 3-7 km.

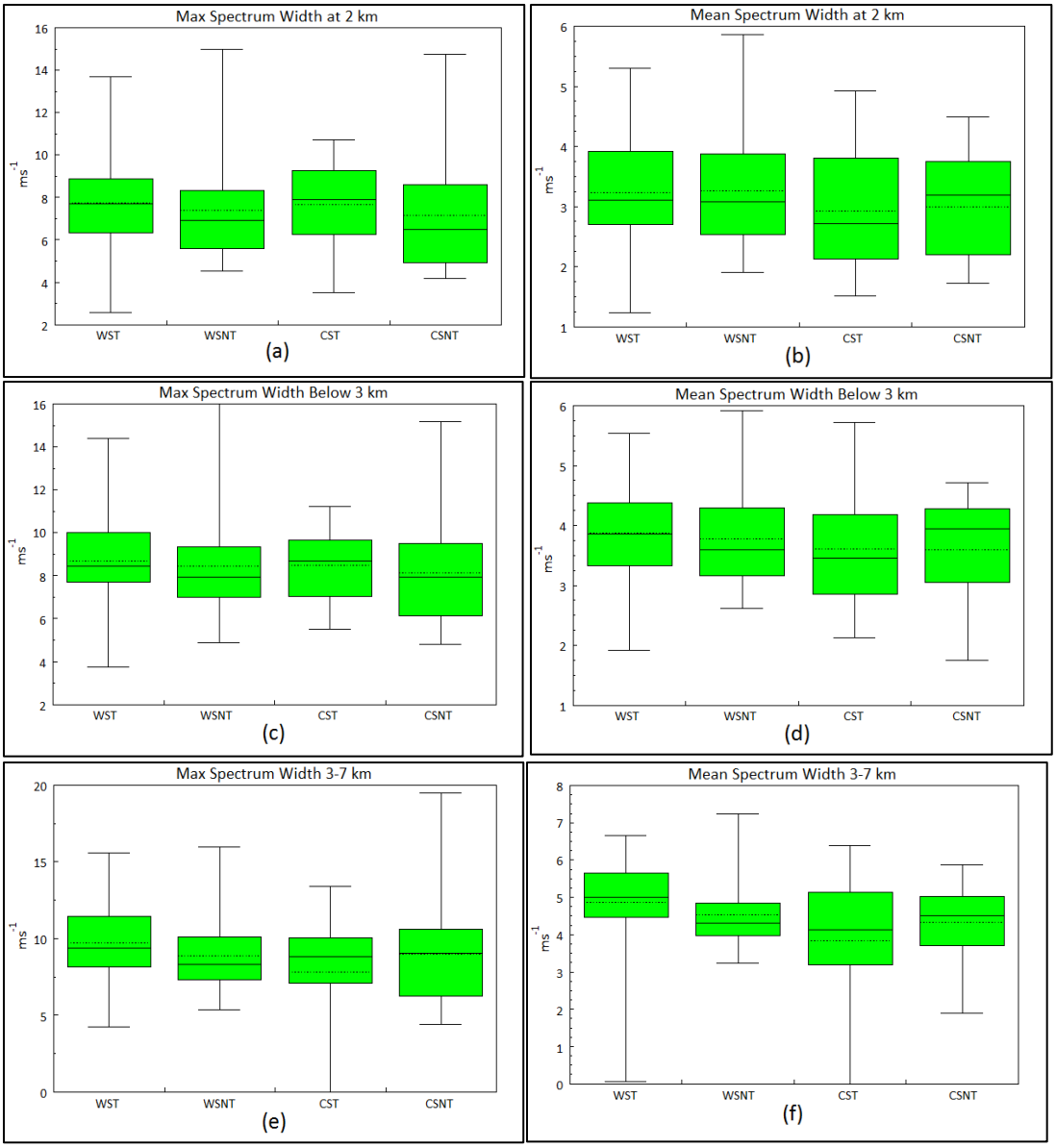

Figure A.27. Box and Whisker plots for the pre-event time step for 45 dBZ. a) max spectrum width at 2 km, b) mean spectrum width at 2 km, c) max spectrum width below 3 km, d) mean spectrum width below 3 km, e) max spectrum width 3-7 km, f) mean spectrum width 3-7 km.

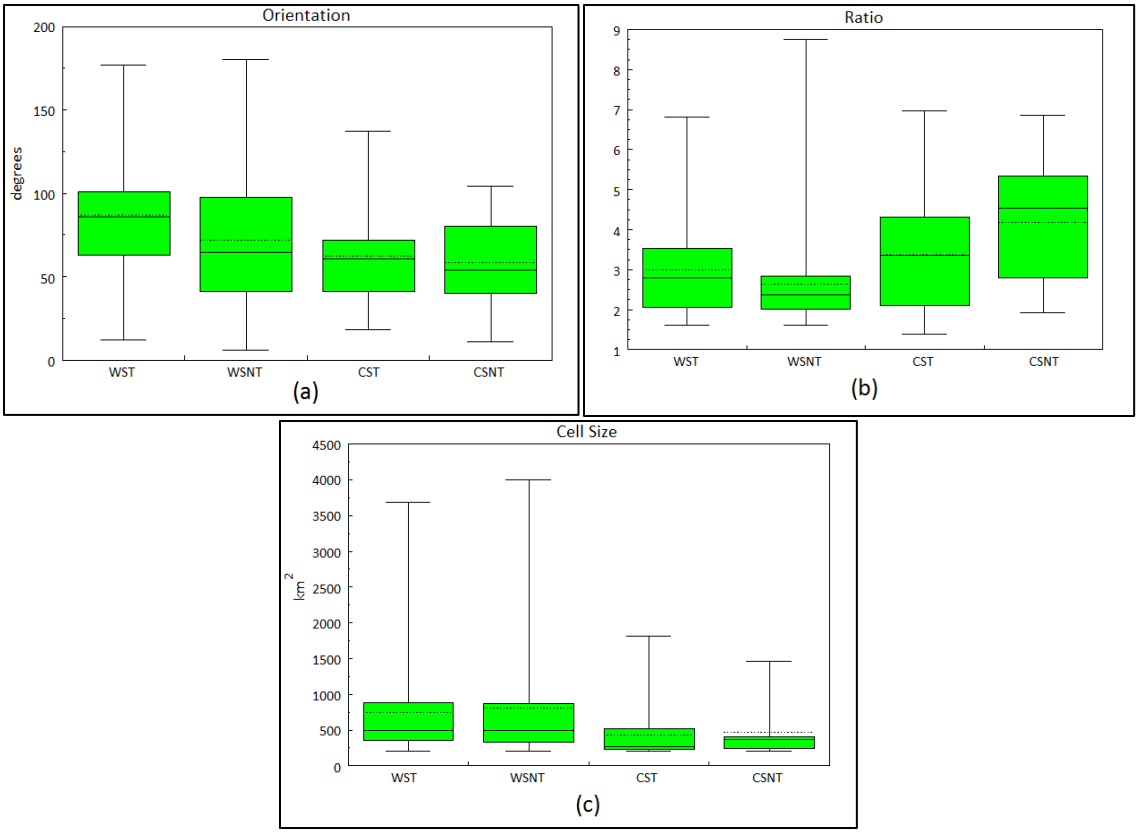

Figure A.28. Box and Whisker plots for the pre-event time step for 45 dBZ. a) orientation, b) ratio, c) cell size.

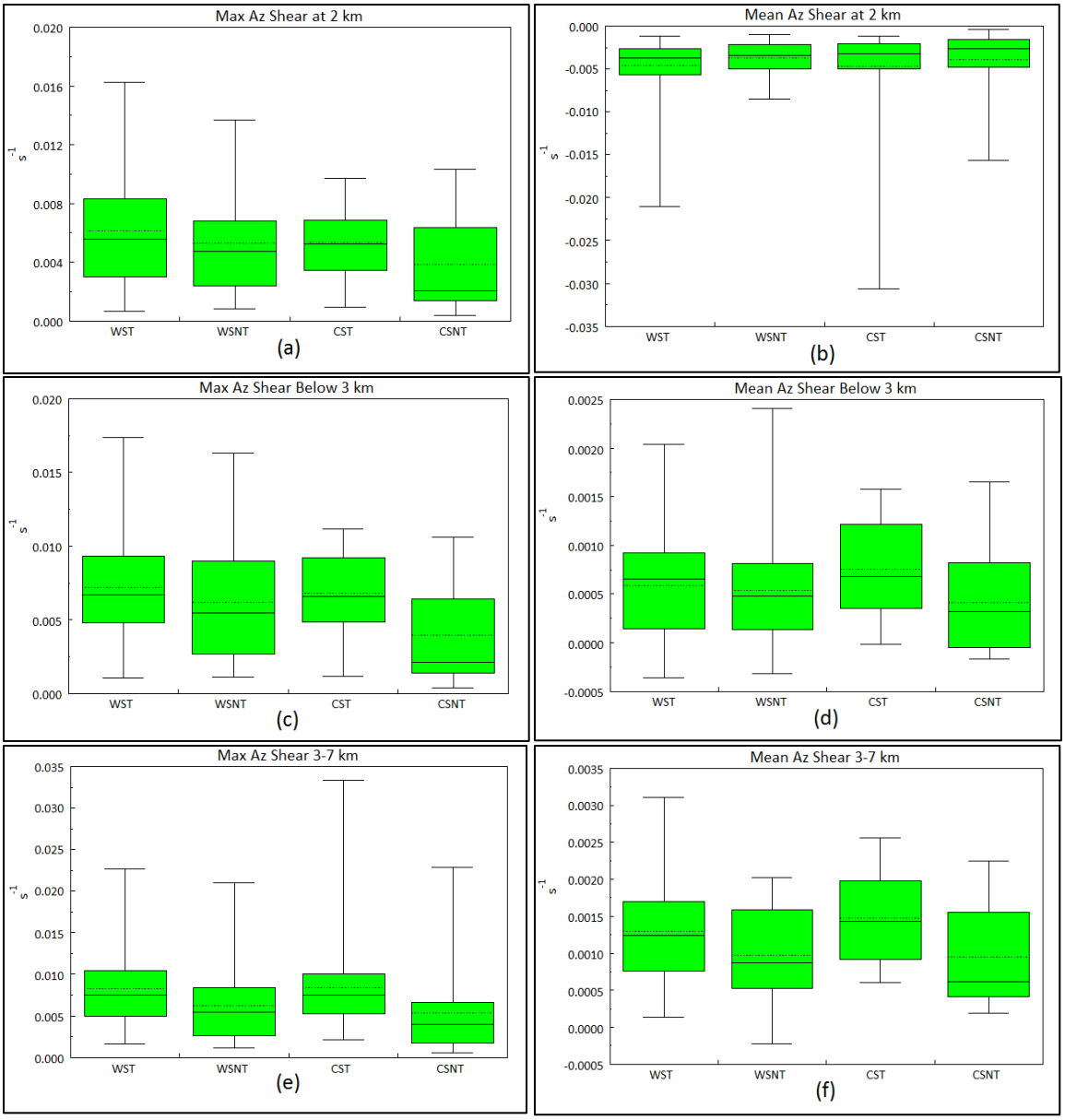

Figure A.29. Box and Whisker plots for the event time step for 45 dBZ. a) max azimuthal shear at 2 km, b) mean azimuthal shear at 2 km, c) max azimuthal shear below 3 km, d) mean azimuthal shear below 3 km, e) max azimuthal shear 3-7 km, f) mean azimuthal shear 3-7 km.

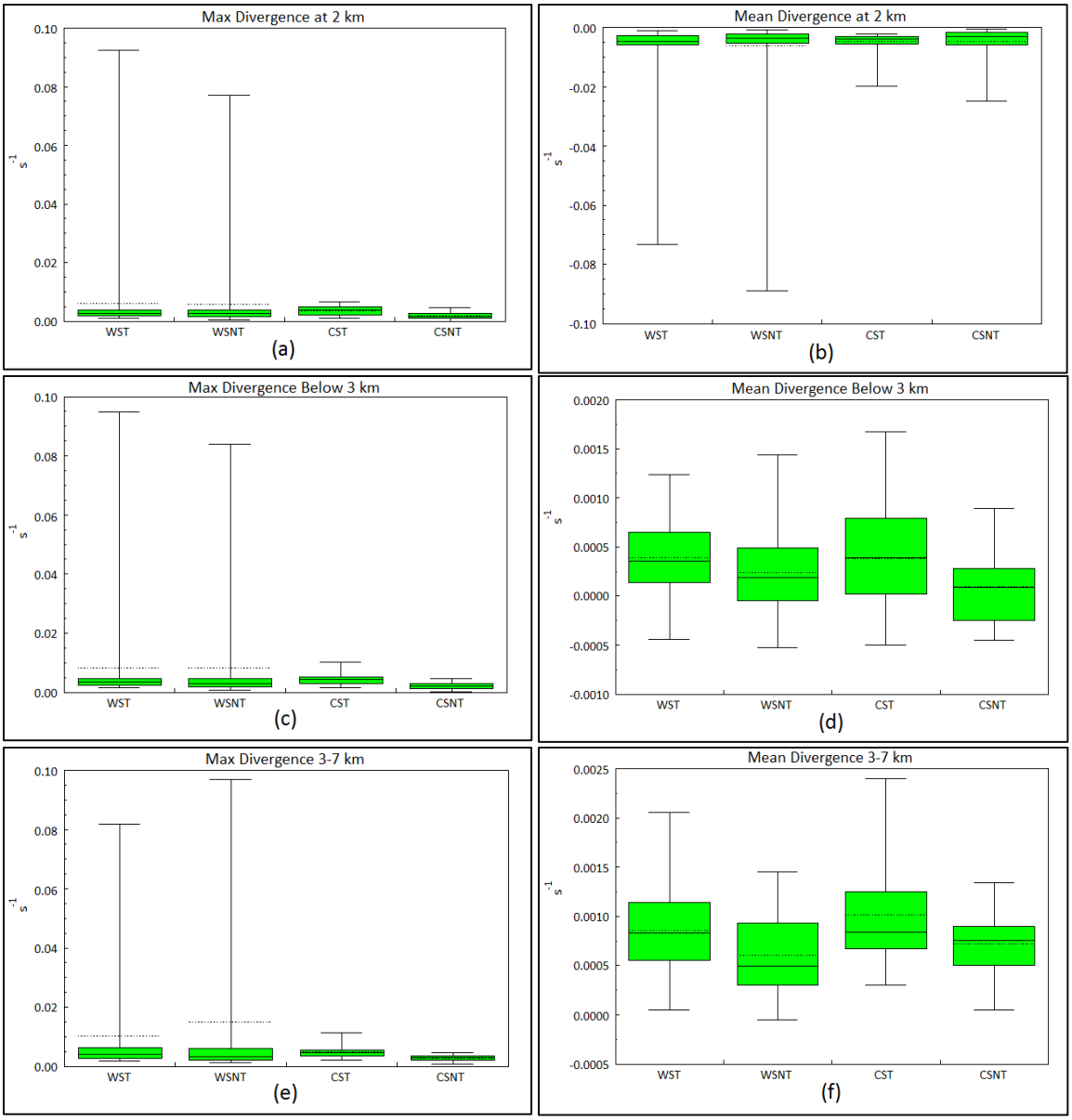

Figure A.30. Box and Whisker plots for the event time step for 45 dBZ. a) max divergence at 2 km, b) mean divergence at 2 km, c) max divergence below 3 km, d) mean divergence below 3 km, e) max divergence 3-7 km, f) mean divergence 3-7 km.

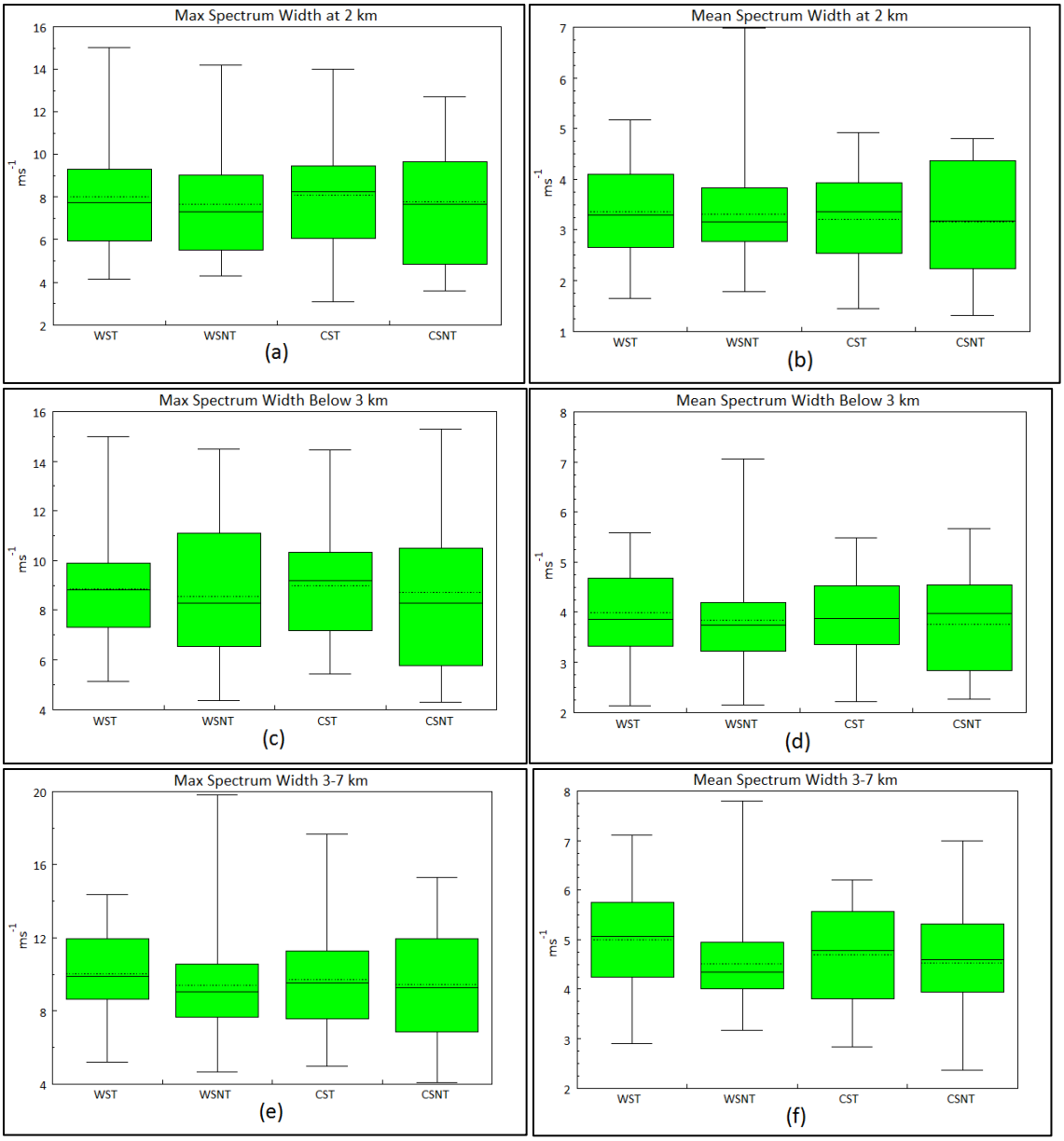

Figure A.31. Box and Whisker plots for the event time step for 45 dBZ. a) max spectrum width at 2 km, b) mean spectrum width at 2 km, c) max spectrum width below 3 km, d) mean spectrum width below 3 km, e) max spectrum width 3-7 km, f) mean spectrum width 3-7 km.

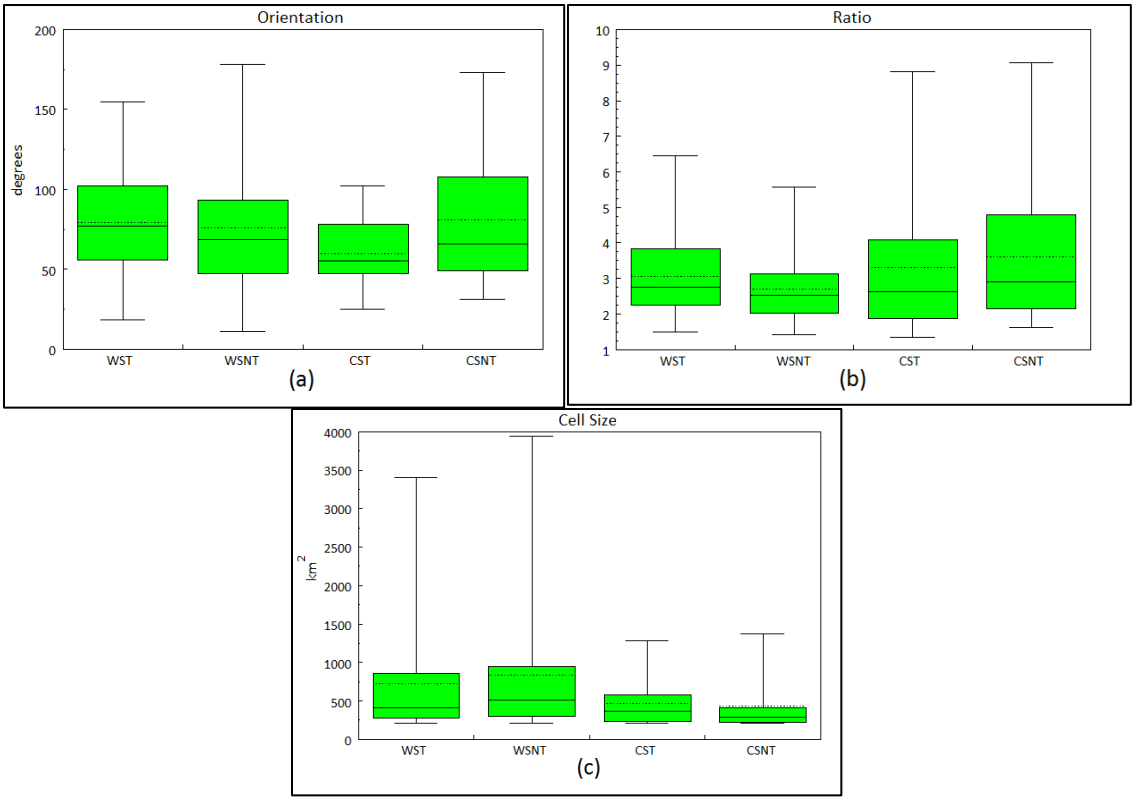

Figure A.32. Box and Whisker plots for the event time step for 45 dBZ. a) orientation, b) ratio, c) cell size.

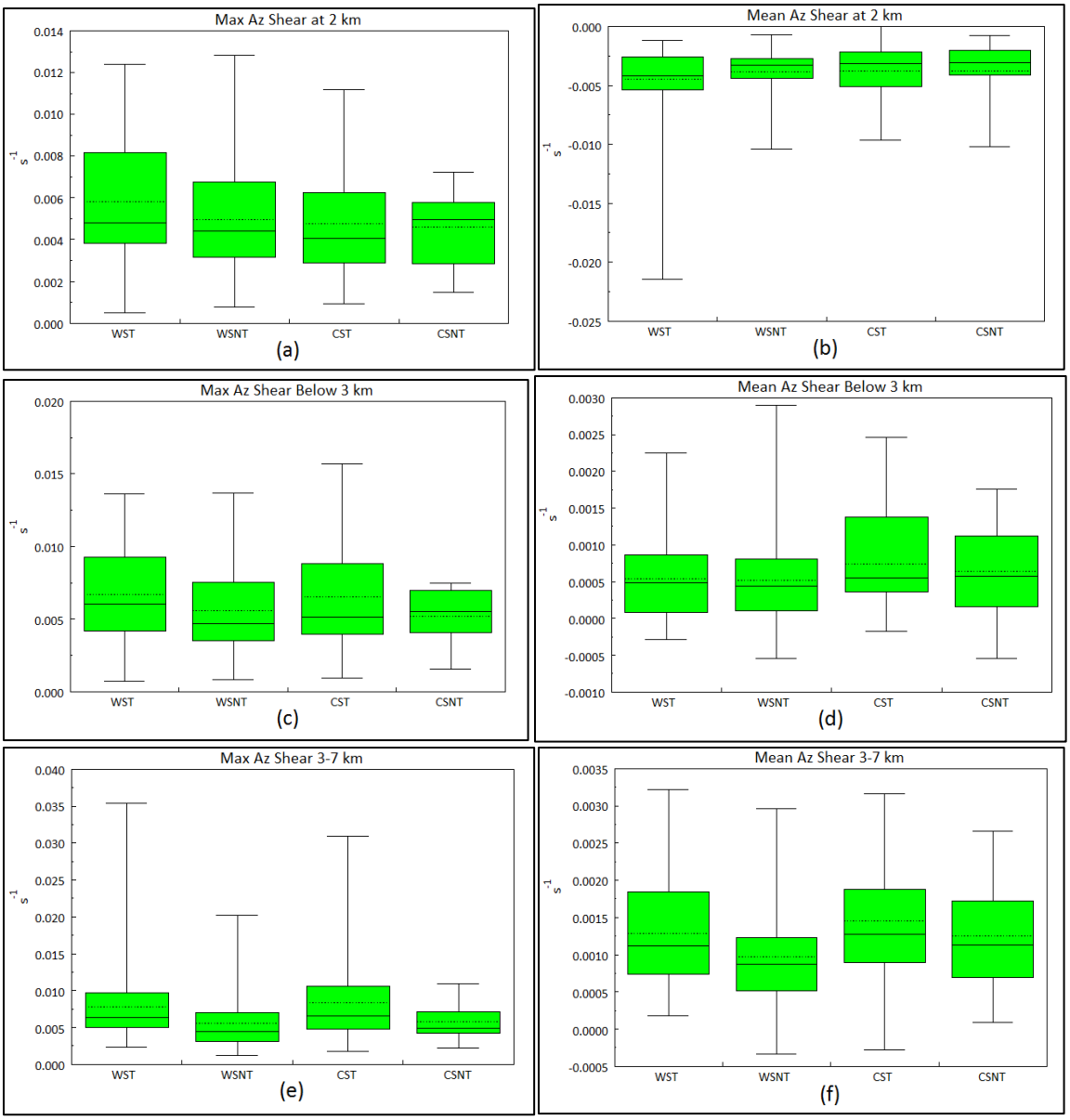

Figure A.33. Box and Whisker plots for the post-event time step for 45 dBZ. a) max azimuthal shear at 2 km, b) mean azimuthal shear at 2 km, c) max azimuthal shear below 3 km, d) mean azimuthal shear below 3 km, e) max azimuthal shear 3-7 km, f) mean azimuthal shear 3-7 km.

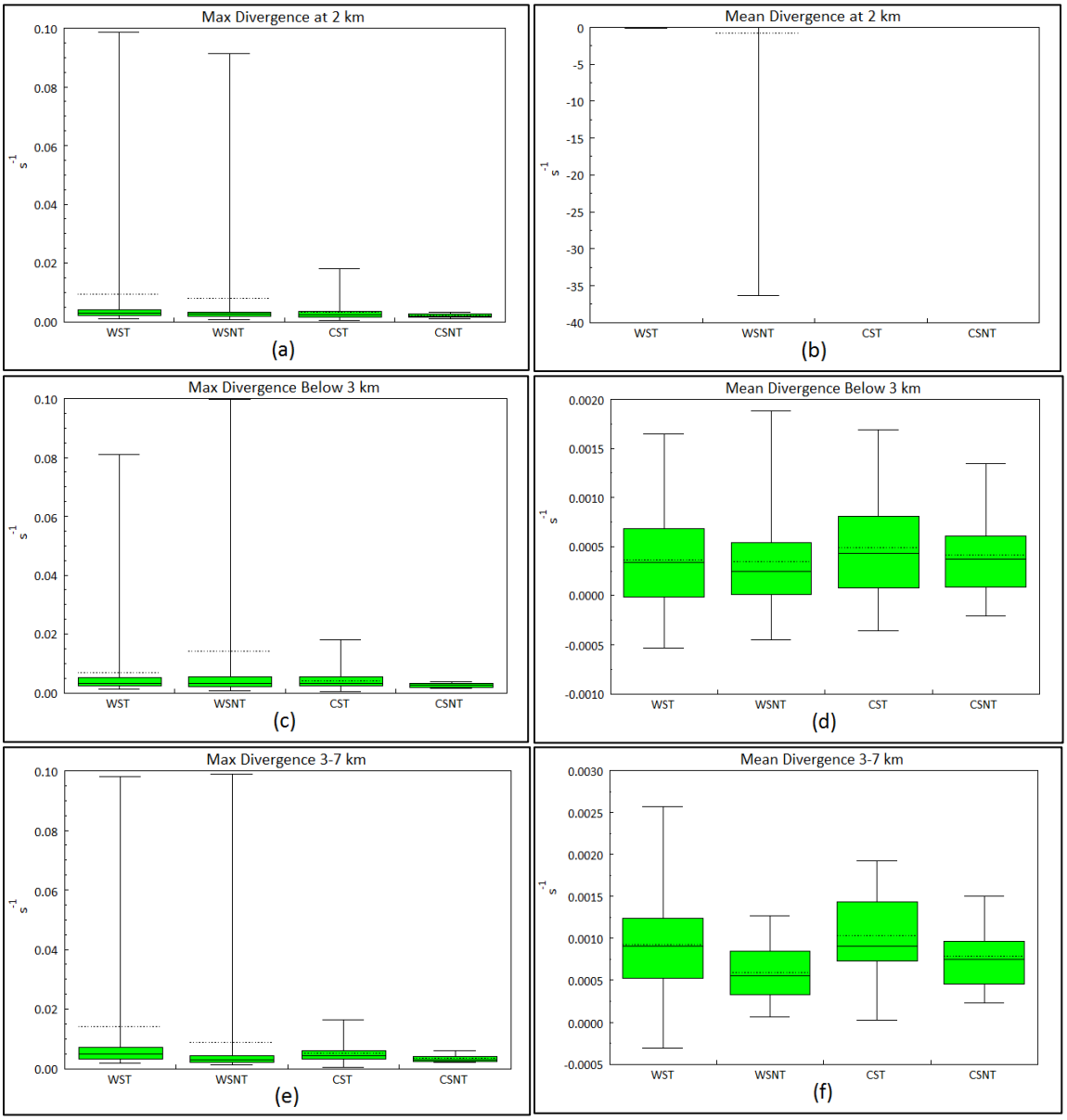

Figure A.34. Box and Whisker plots for the post-event time step for 45 dBZ. a) max divergence at 2 km, b) mean divergence at 2 km, c) max divergence below 3 km, d) mean divergence below 3 km, e) max divergence 3-7 km, f) mean divergence 3-7 km.

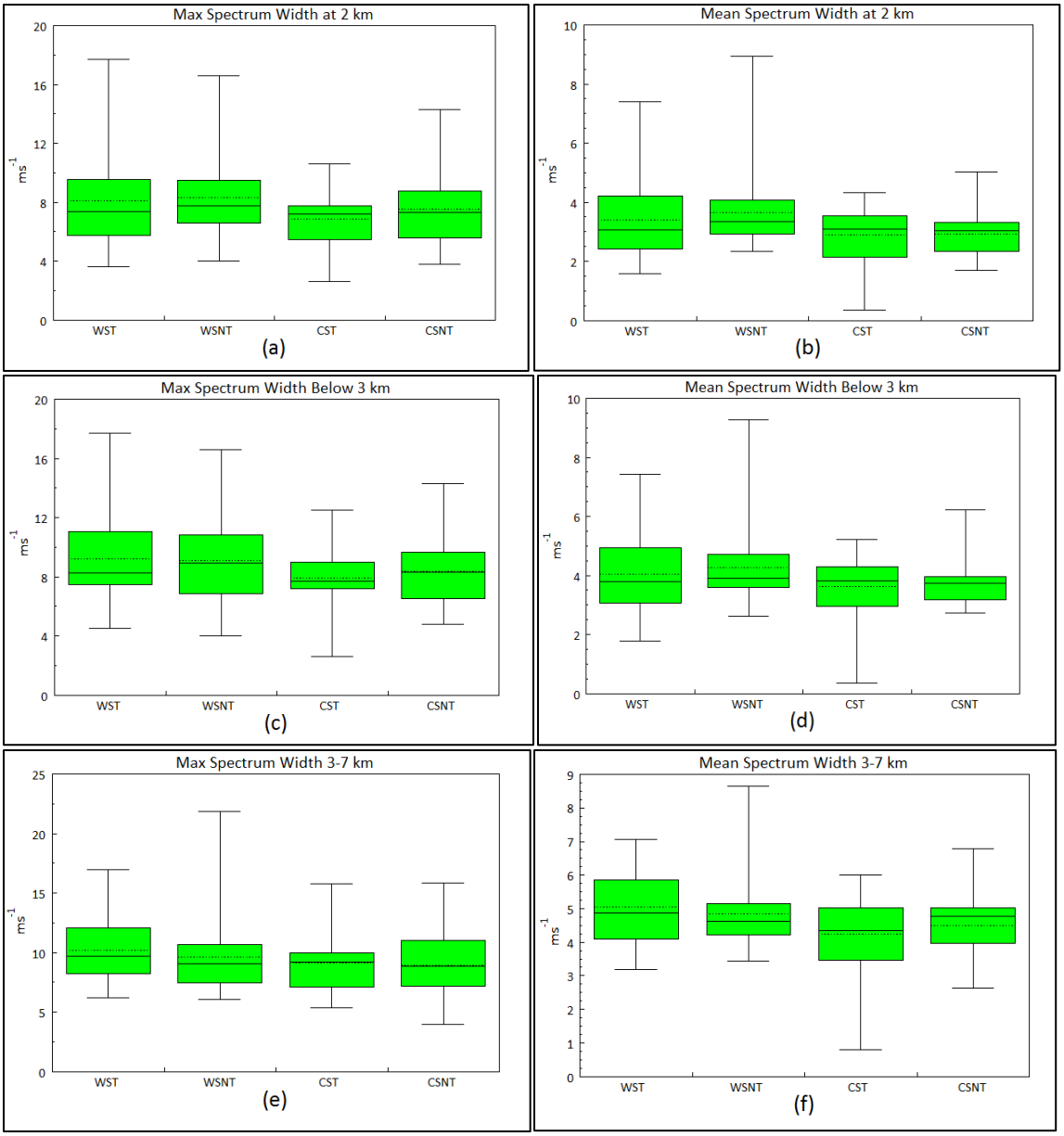

Figure A.35. Box and Whisker plots for the post-event time step for 45 dBZ. a) max spectrum width at 2 km, b) mean spectrum width at 2 km, c) max spectrum width below 3 km, d) mean spectrum width below 3 km, e) max spectrum width 3-7 km, f) mean spectrum width 3-7 km.

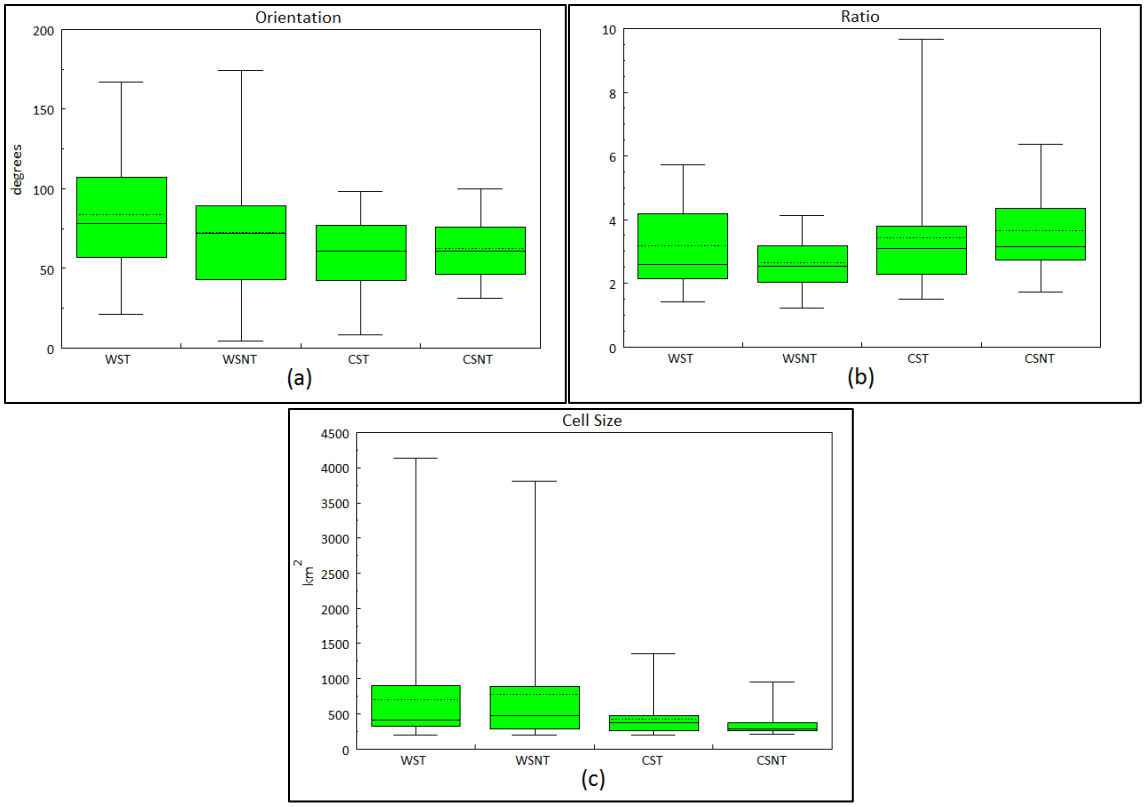

Figure A.36. Box and Whisker plots for the post-event time step for 45 dBZ. a) orientation, b) ratio, c) cell size.

Appendix B

The following are figures that include the reflectivity image of the event time for each warm season tornadic and non-tornadic case and each cold season tornadic and non-tornadic cases.

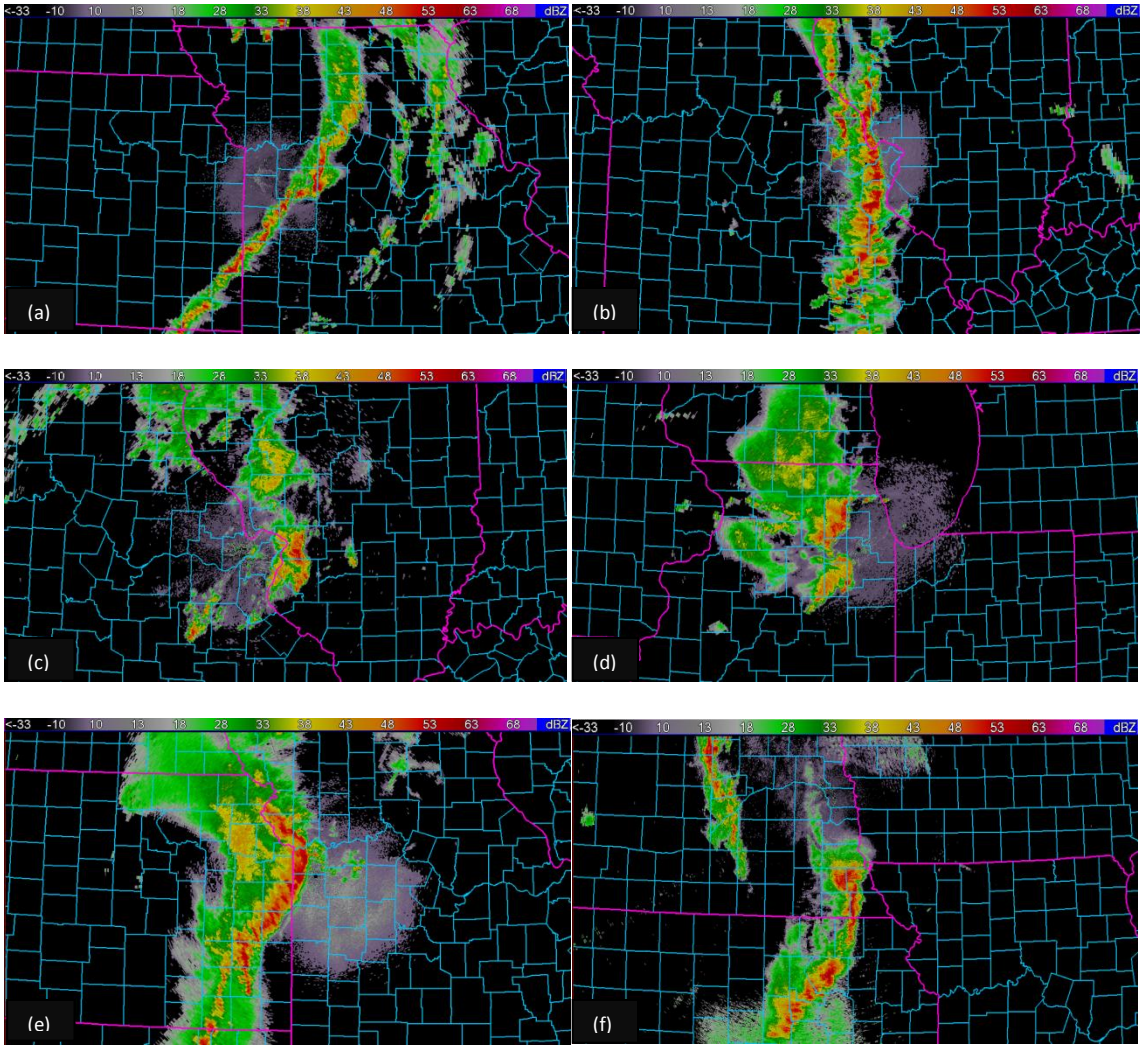

Figure B.1. Event time for warm season tornadic cases. a) 03/31/2006, b) 04/02/2006, c) 07/21/2006, d) 08/23/2007, e) 05/02/2008, f) 06/06/2008.

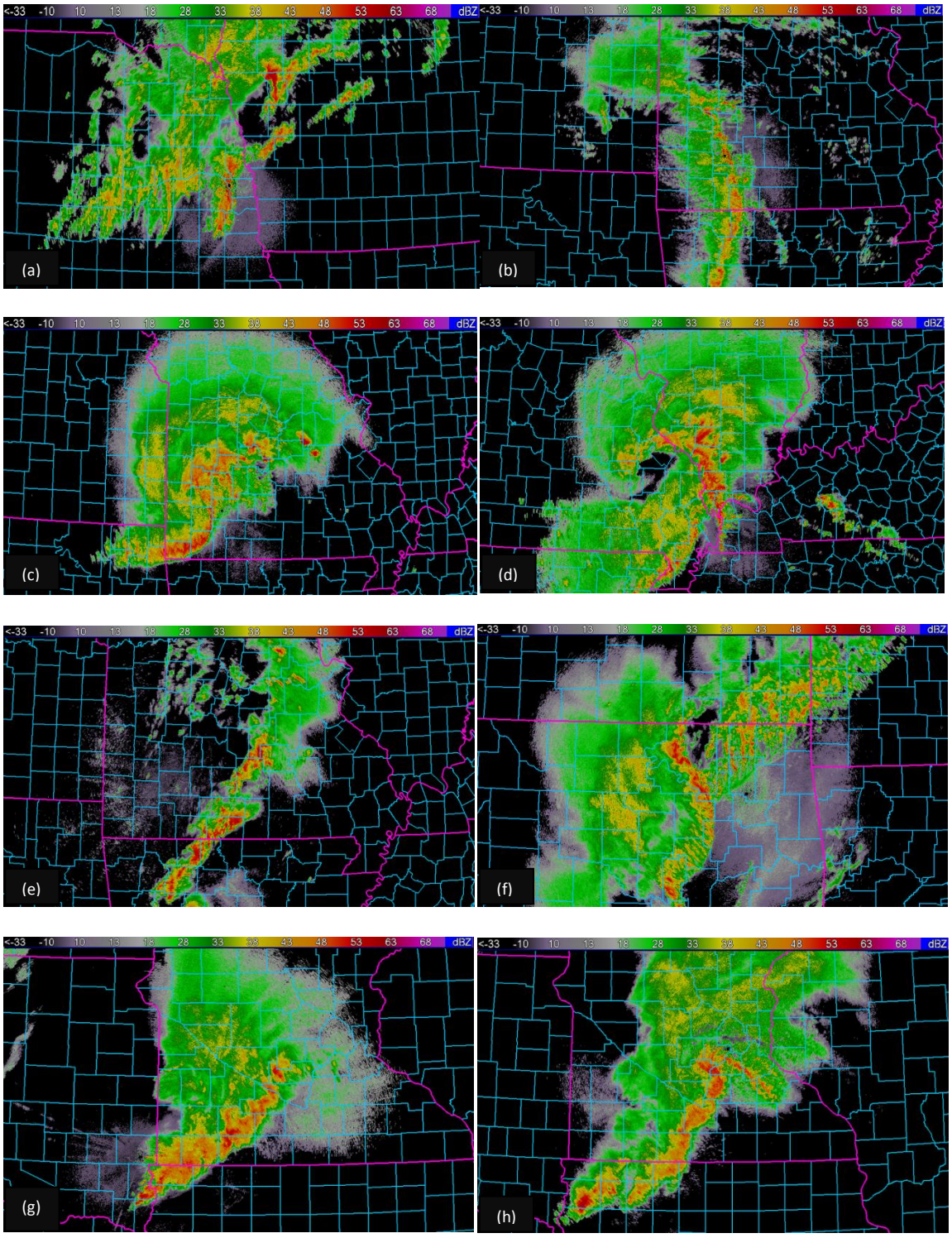

Figure B.2. Event time for warm season tornadic cases. a) 06/08/2008, b) 04/10/2009, c) 05/08/2009 – KSGF, d) 05/08/2009 – KPAH, e) 04/30/2010, f) 05/13/2010, g) 06/27/2010 – KFSD, h) 06/27/2010 – KMPX.

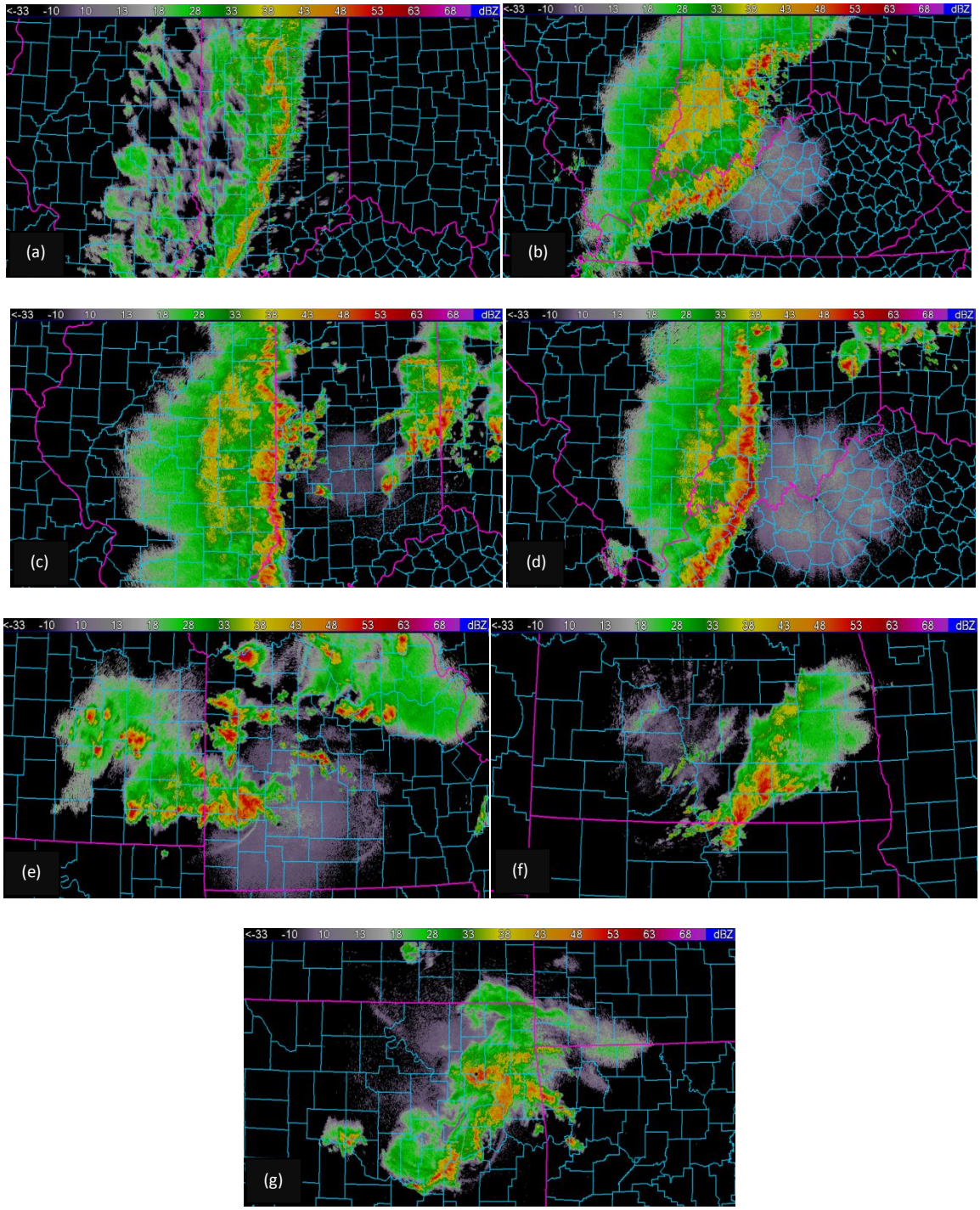

Figure B.3. Event time for warm season tornadic cases. a) 10/26/2010, b) 04/20/2011, c) 05/26/2011 – KIND, d) 05/26/2011 – KLVX, e) 06/19/2011, f) 07/10/2011, g) 08/10/2011.

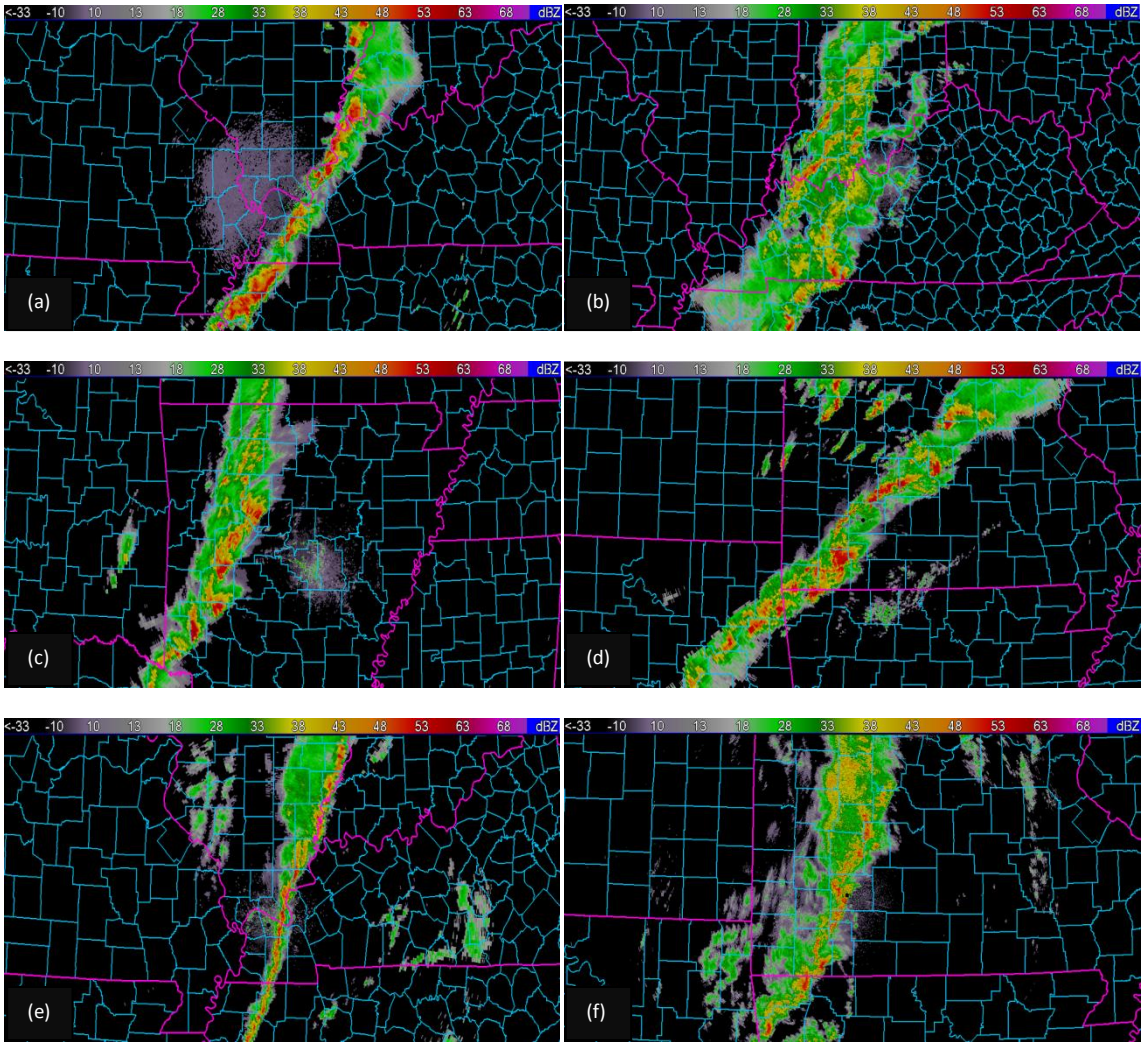

Figure B.4. Event time for cold season tornadic cases. a) 11/06/2005, b) 11/15/2005, c) 11/27/2005, d) 01/08/2008, e) 01/29/2008, f) 11/06/2008.

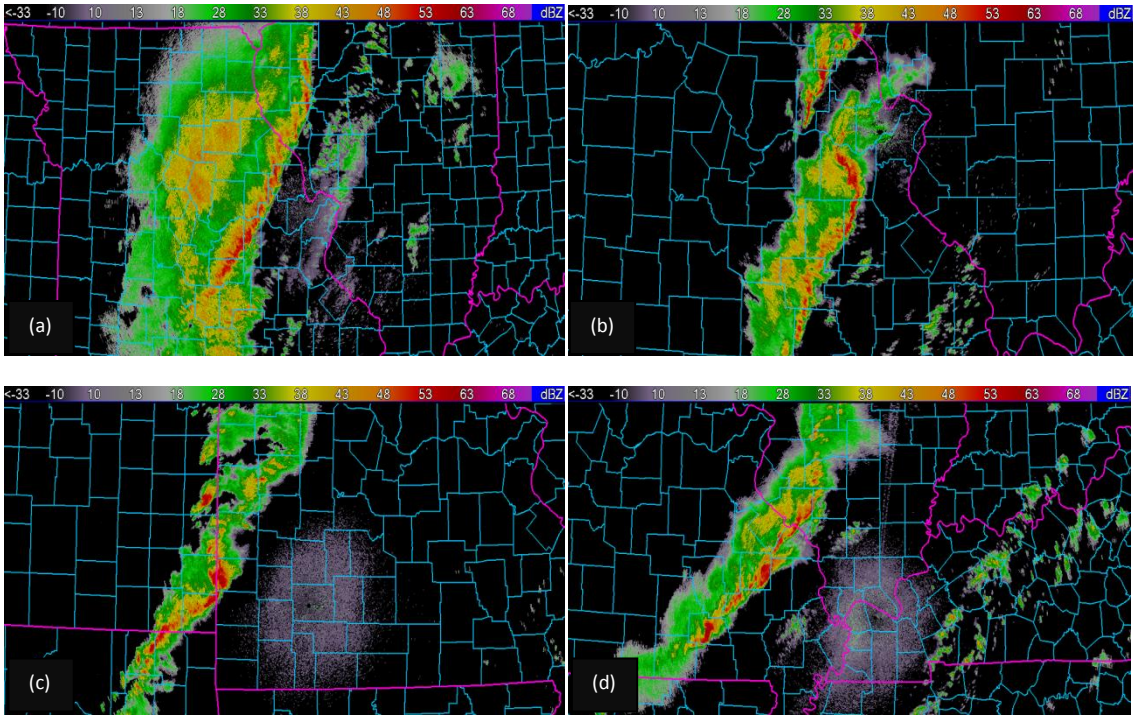

Figure B.5. Event time for cold season tornadic cases. a) 12/27/2008, b) 12/31/2010, c) 02/29/2012 – KSGF, d) 02/29/2012 – KPAH.

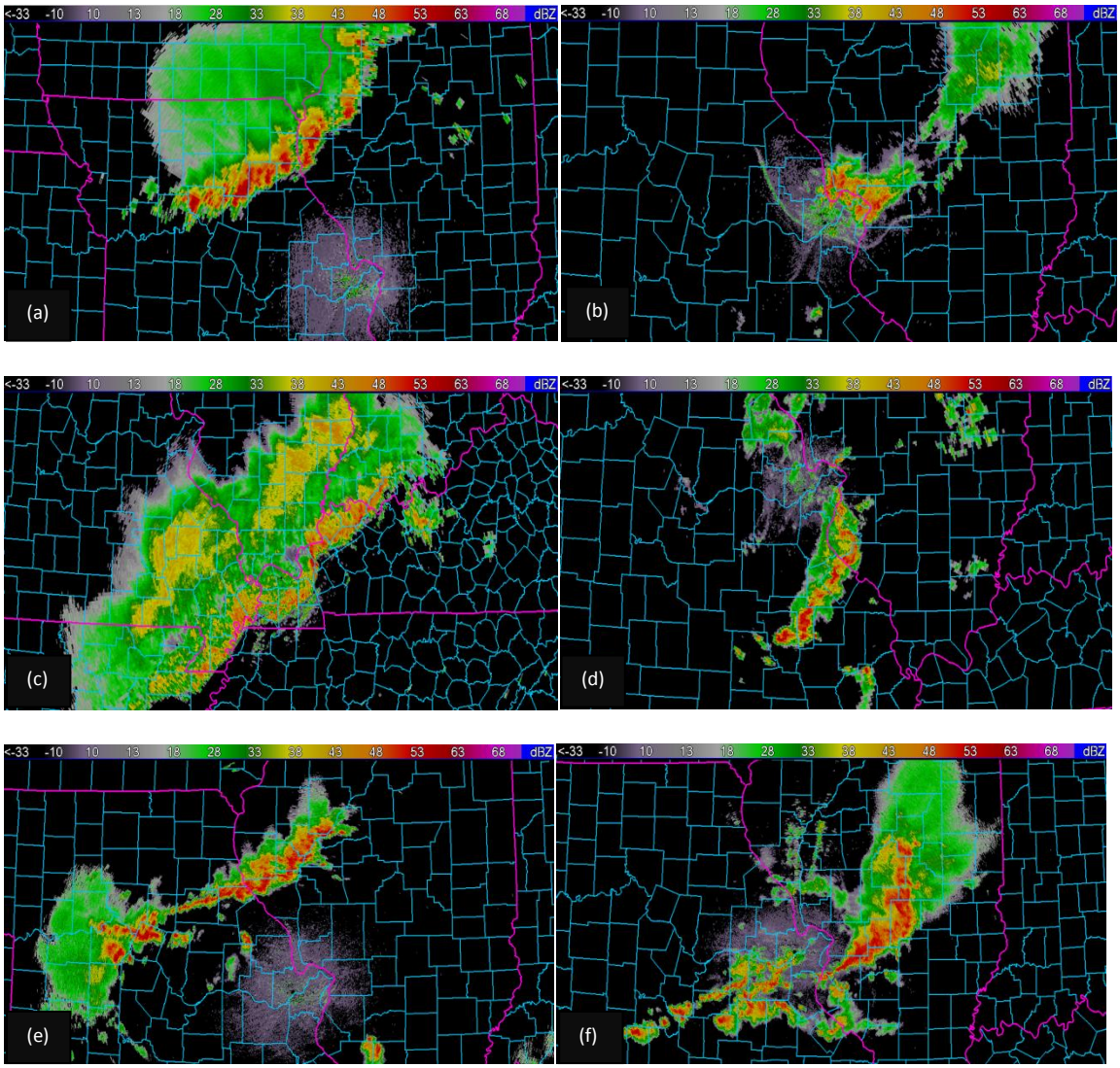

Figure B.6. Event time for warm season non-tornadic cases. a) 06/08/2005, b) 07/20/2006, c) 09/23/2006, d) 09/06/2007, e) 07/08/2008, f) 08/06/2008.

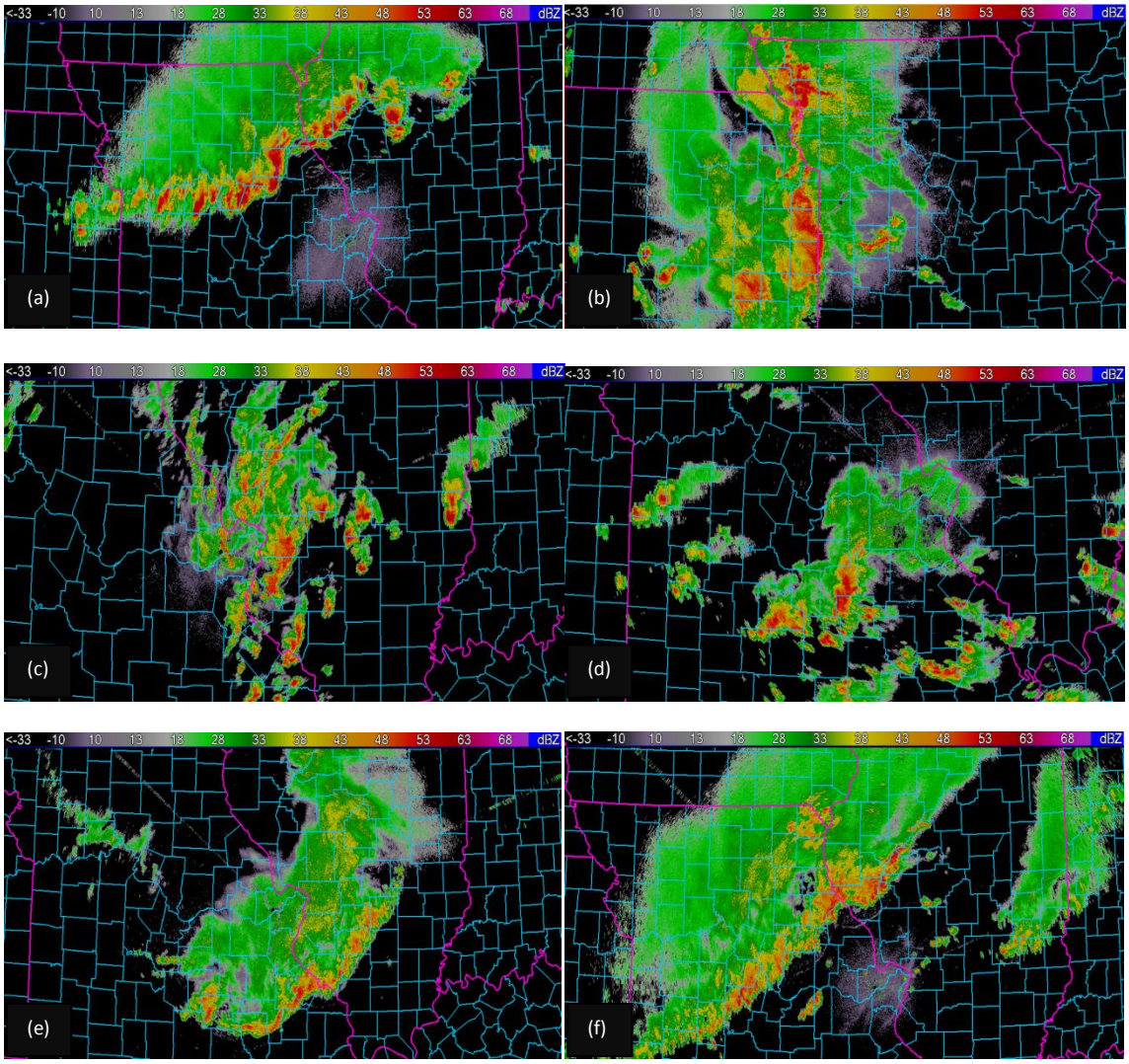

Figure B.7. Event time for warm season non-tornadic cases. a) 05/15/2009, b) 06/16/2009, c) 06/15/2010, d) 07/11/2010, e) 07/18/2010, f) 07/25/2010.

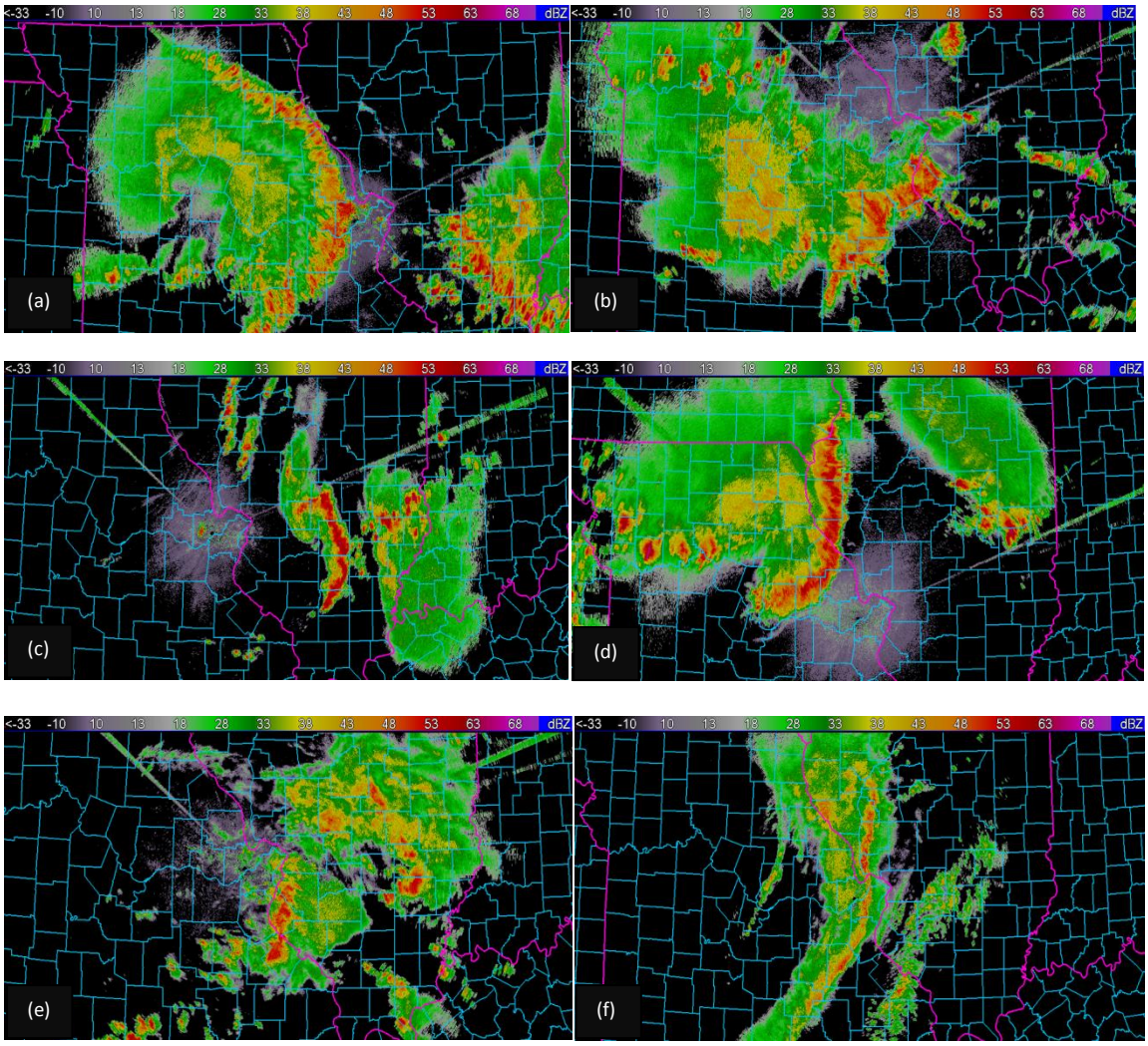

Figure B.8. Event time for warm season non-tornadic cases. a) 06/18/2011, b) 06/19/2011, c) 06/21/2011, d) 06/27/2011, e) 07/08/2011, f) 10/17/2012.

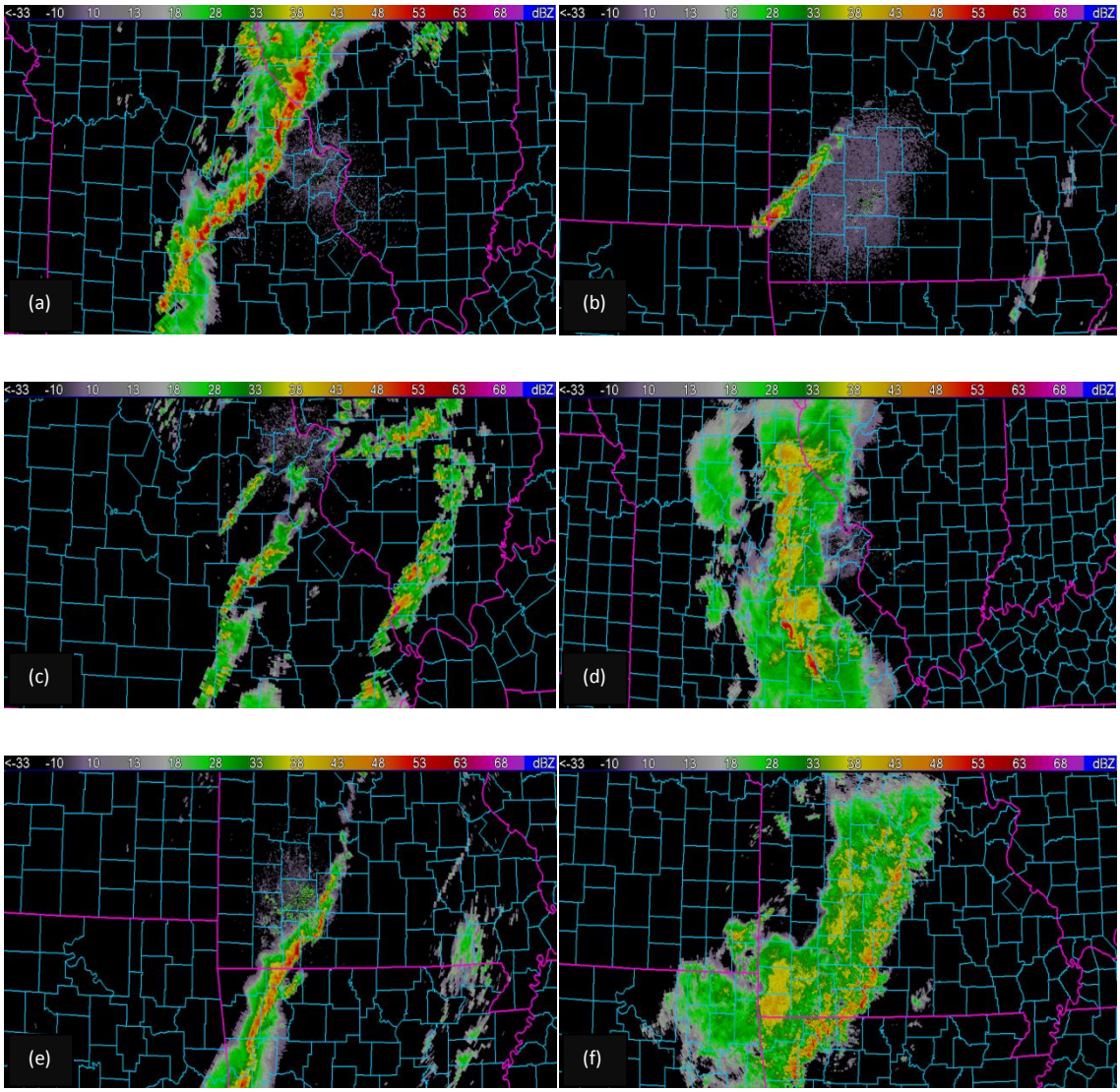

Figure B.9. Event time for cold season non-tornadic cases. a) 11/06/2005, b) 11/13/2005, c) 11/15/2005, d) 11/28/2005, e) 01/13/2006, f) 11/30/2006.

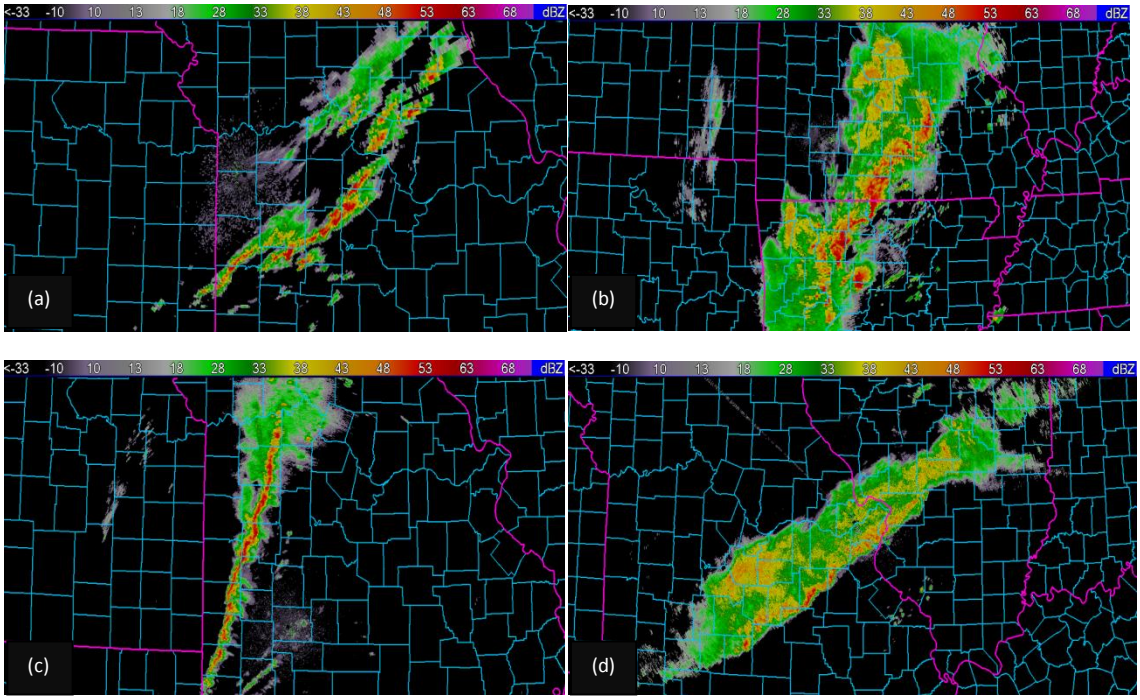

Figure B.10. Event time for cold season non-tornadic cases. a) 01/07/2008, b) 02/05/2008, c) 03/08/2009, d) 11/25/2010.

Appendix C

The following are tables that include the mean, median, and standard deviation for the warm season tornadic and non-tornadic events, and the cold season tornadic and non-tornadic events. They are divided up by time step (pre-event, event, and post-event) and reflectivity threshold hold (35 dBZ, 40 dBZ, and 45 dBZ).

Table C.1. Mean, median, and standard deviations of all radar parameters at the pre-event time for 35 dBZ for warm season tornadic and non-tornadic QLCS cases.

Parameter	Tornadic			Non-tornadic		
35 dBZ	**Mean**	**Median**	**Standard Deviation**	**Mean**	**Median**	**Standard Deviation**
Max Az at 2 km (s^{-1})	0 .0065	0.0043	0.00502	0.0047	0.0041	0.00359
Mean Az at 2 km (s^{-1})	-0.0049	-0.0037	0.00427	-0.0038	-0.0037	0.00297
Max Div at 2 km (s^{-1})	0.0086	0.0028	0.02061	0.0146	0.0022	0.02840
Mean Div at 2 km (s^{-1})	-0.0135	-0.0035	0.02060	-0.0107	-0.0030	0.02246
Max SW at 2 km (ms^{-1})	8.23	8.07	3.08542	7.03	6.77	2.87615
Mean SW at 2 km (ms^{-1})	2.88	2.85	0.91212	2.88	2.69	0.89384
Max Az below 3 km (s^{-1})	0.0075	0.0057	0.00620	0.0054	0.0053	0.00396
Mean Az below 3 km (s^{-1})	0.0004	0.0004	0.00033	0.0040	0.0029	0.00028
Max Div below 3 km (s^{-1})	0.0173	0.0033	0.03246	0.0142	0.0028	0.02820
Mean Div below 3 km (s^{-1})	0.0003	0.0003	0.00028	0.0003	0.0002	0.00049
Max SW below 3 km (ms^{-1})	9.11	9.20	3.23756	7.89	7.59	2.90429
Mean SW below 3 km (ms^{-1})	3.44	3.37	0.92643	3.32	3.17	0.84684
Max Az 3-7 km (s^{-1})	0.0073	0.0063	0.00552	0.0054	0.0049	0.00350
Mean Az 3-7 km (s^{-1})	0.0008	0.0008	0.00045	0.0007	0.0007	0.00035
Max Div 3-7 km (s^{-1})	0.0160	0.0041	0.03008	0.0160	0.0031	0.02790
Mean Div 3-7 km (s^{-1})	0.0006	0.0006	0.00032	0.0005	0.0004	0.00026
Max SW 3-7 km (ms^{-1})	10.2	9.79	4.27608	8.20	7.68	2.71162
Mean SW 3-7 km (ms^{-1})	4.07	4.1	1.07910	3.74	3.78	0.92534
Orientation (deg)	77.5	69.5	44.7975	79.6	70.0	49.08069
Ratio	2.85	2.58	1.31239	2.71	2.43	1.05834
Cell Size (km^2)	2,660	1,240	3257.64	2,140	1,100	2710.626

Table C.2. Mean, median, and standard deviations of all radar parameters at the pre-event time for 40 dBZ for warm season tornadic and non-tornadic QLCS cases.

Parameter	Tornadic			Non-tornadic		
40 dBZ	**Mean**	**Median**	**Standard Deviation**	**Mean**	**Median**	**Standard Deviation**
Max Az at 2 km (s^{-1})	0.0062	0.0062	0.00414	0.0054	0.0049	0.00347
Mean Az at 2 km (s^{-1})	-0.0045	-0.0033	0.00363	-0.0042	-0.0039	0.00292
Max Div at 2 km (s^{-1})	0.0072	0.0030	0.01807	0.0112	0.0031	0.02248
Mean Div at 2 km (s^{-1})	-0.0092	-0.0037	0.02032	-0.0128	-0.0039	0.02409
Max SW at 2 km (ms^{-1})	7.75	7.60	2.53868	7.69	7.17	2.58377
Mean SW at 2 km (ms^{-1})	3.07	3.02	0.84616	3.26	2.93	1.01192
Max Az below 3 km (s^{-1})	0.0073	0.0068	0.00499	0.0062	0.0057	0.00360
Mean Az below 3 km (s^{-1})	0.0006	0.0005	0.00052	0.0005	0.0005	0.00042
Max Div below 3 km (s^{-1})	0.0111	0.0036	0.02366	0.0129	0.0034	0.02565
Mean Div below 3 km (s^{-1})	0.0004	0.0004	0.00031	0.0003	0.0002	0.00056
Max SW below 3 km (ms^{-1})	8.95	8.63	2.63039	8.43	7.96	2.64762
Mean SW below 3 km (ms^{-1})	3.73	3.77	0.77484	3.73	3.52	0.91918
Max Az 3-7 km (s^{-1})	0.0074	0.0064	0.00504	0.0062	0.0056	0.00321
Mean Az 3-7 km (s^{-1})	0.001	0.0010	0.00054	0.0009	0.0008	0.00043
Max Div 3-7 km (s^{-1})	0.0141	0.0041	0.02842	0.0121	0.0039	0.02288
Mean Div 3-7 km (s^{-1})	0.0007	0.0007	0.00034	0.0006	0.0005	0.00028
Max SW 3-7 km (ms^{-1})	9.75	9.04	4.03995	8.78	8.41	2.62592
Mean SW 3-7 km (ms^{-1})	4.29	4.34	1.1564	4.24	4.07	0.91463
Orientation (deg)	82.4	80.0	36.318	82.3	77.0	48.2273
Ratio	3.23	2.78	1.4588	2.79	2.57	1.11007
Cell Size (km^2)	1,400	775	1582.9	1,380	978	1,469.97

Table C.3. Mean, median, and standard deviations of all radar parameters at the pre-event time for 45 dBZ for warm season tornadic and non-tornadic QLCS cases.

Parameter	Tornadic			Non-tornadic		
45 dBZ	**Mean**	**Median**	**Standard Deviation**	**Mean**	**Median**	**Standard Deviation**
Max Az at 2 km (s^{-1})	0.0064	0.0063	0.00347	0.0052	0.0042	0.00346
Mean Az at 2 km (s^{-1})	-0.0047	-0.0045	0.00243	-0.0041	-0.0033	0.00294
Max Div at 2 km (s^{-1})	0.0078	0.0027	0.01954	0.0048	0.0026	0.00885
Mean Div at 2 km (s^{-1})	-0.0096	-0.0038	0.01974	-0.0096	-0.0037	0.01952
Max SW at 2 km (ms^{-1})	7.73	7.69	2.25470	7.40	6.93	2.49835
Mean SW at 2 km (ms^{-1})	3.23	3.10	0.89823	3.26	3.07	0.90176
Max Az below 3 km (s^{-1})	0.0072	0.0065	0.00344	0.0062	0.0053	0.00355
Mean Az below 3 km (s^{-1})	0.0006	0.0007	0.00055	0.0006	0.0005	0.00045
Max Div below 3 km (s^{-1})	0.0098	0.0034	0.02054	0.0089	0.0032	0.01821
Mean Div below 3 km (s^{-1})	0.0004	0.0003	0.00080	0.0001	0.0002	0.00063
Max SW below 3 km (ms^{-1})	8.66	8.44	2.18252	8.43	7.92	2.48284
Mean SW below 3 km (ms^{-1})	3.88	3.87	0.86122	3.78	3.59	0.79522
Max Az 3-7 km (s^{-1})	0.0080	0.0071	0.00373	0.0061	0.0051	0.00334
Mean Az 3-7 km (s^{-1})	0.0013	0.0012	0.00054	0.0010	0.0095	0.00049
Max Div 3-7 km (s^{-1})	0.0131	0.0044	0.02667	0.0097	0.0040	0.01925
Mean Div 3-7 km (s^{-1})	0.0009	0.0009	0.00040	0.0005	0.0005	0.00063
Max SW 3-7 km (ms^{-1})	9.74	9.38	2.39253	8.87	8.30	2.37323
Mean SW 3-7 km (ms^{-1})	4.87	5.00	1.16495	4.52	4.31	0.81890
Orientation (deg)	87.2	86	36.91361	71.6	64.5	44.2776
Ratio	2.99	2.79	1.15714	2.64	2.38	1.18732
Cell Size (km^2)	746	494	691.090	810	487	886.5624

Table C.4. Mean, median, and standard deviations of all radar parameters at the event time for 35 dBZ for warm season tornadic and non-tornadic QLCS cases.

Parameter	Tornadic			Non-tornadic		
35 dBZ	**Mean**	**Median**	**Standard Deviation**	**Mean**	**Median**	**Standard Deviation**
Max Az at 2 km (s^{-1})	0.0065	0.0060	0.00436	0.0046	0.0034	0.00357
Mean Az at 2 km (s^{-1})	-0.0054	-0.0040	0.00521	-0.0035	-0.0032	0.00207
Max Div at 2 km (s^{-1})	0.0097	0.0031	0.02198	0.0091	0.0024	0.02081
Mean Div at 2 km (s^{-1})	-0.0072	-0.0040	0.01400	-0.0224	-0.0029	0.09177
Max SW at 2 km (ms^{-1})	8.36	7.46	3.12605	7.61	7.09	3.17769
Mean SW at 2 km (ms^{-1})	3.08	3.08	0.74241	3.06	2.64	1.26567
Max Az below 3 km (s^{-1})	0.0079	0.0067	0.00595	0.0054	0.0041	0.00423
Mean Az below 3 km (s^{-1})	0.0004	0.0003	0.00037	0.0003	0.0003	0.00031
Max Div below 3 km (s^{-1})	0.0125	0.0036	0.02461	0.0089	0.0028	0.02058
Mean Div below 3 km (s^{-1})	0.0003	0.0003	0.00028	0.0002	0.0002	0.00053
Max SW below 3 km (ms^{-1})	9.28	9.06	2.95739	8.34	8.35	3.14299
Mean SW below 3 km (ms^{-1})	3.60	3.54	0.71452	3.50	3.10	1.23242
Max Az 3-7 km (s^{-1})	0.0076	0.0069	0.00553	0.0053	0.0038	0.00415
Mean Az 3-7 km (s^{-1})	0.0008	0.0009	0.00048	0.0006	0.0006	0.00036
Max Div 3-7 km (s^{-1})	0.0133	0.0039	0.02288	0.0185	0.0028	0.03365
Mean Div 3-7 km (s^{-1})	0.0006	0.0006	0.00032	0.0006	0.0005	0.00046
Max SW 3-7 km (ms^{-1})	10.6	9.96	4.60481	9.22	8.61	3.81892
Mean SW 3-7 km (ms^{-1})	3.98	4.07	1.11731	3.90	3.75	1.15763
Orientation (deg)	80.4	70.5	40.90754	71.7	67.5	43.9982
Ratio	2.82	2.45	1.21906	2.70	2.39	1.03175
Cell Size (km^2)	2,630	1,390	3441.348	1,970	1,030	2203.733

Table C.5. Mean, median, and standard deviations of all radar parameters at the event time for 40 dBZ for warm season tornadic and non-tornadic QLCS cases.

Parameter	Tornadic			Non-tornadic		
40 dBZ	**Mean**	**Median**	**Standard Deviation**	**Mean**	**Median**	**Standard Deviation**
Max Az at 2 km (s^{-1})	0.0065	0.0060	0.003913	0.0053	0.0045	0.00357
Mean Az at 2 km (s^{-1})	-0.0051	-0.0039	0.003696	-0.0037	-0.0037	0.00176
Max Div at 2 km (s^{-1})	0.0075	0.0033	0.018367	0.0062	0.0026	0.01326
Mean Div at 2 km (s^{-1})	-0.0059	-0.0046	0.009155	-0.0092	-0.0036	0.02082
Max SW at 2 km (ms^{-1})	8.09	7.80	2.94917	7.97	7.90	3.08416
Mean SW at 2 km (ms^{-1})	3.09	2.99	0.78942	3.29	2.90	1.41856
Max Az below 3 km (s^{-1})	0.0080	0.0074	0.00475	0.0061	0.0052	0.00434
Mean Az below 3 km (s^{-1})	0.0005	0.0004	0.00046	0.0004	0.0003	0.00041
Max Div below 3 km (s^{-1})	0.0095	0.0036	0.02001	0.0083	0.0028	0.01843
Mean Div below 3 km (s^{-1})	0.0004	0.0004	0.00035	0.0003	0.0002	0.00046
Max SW below 3 km (ms^{-1})	9.21	8.75	2.72730	8.70	8.63	3.02390
Mean SW below 3 km (ms^{-1})	3.69	3.61	0.74082	3.77	3.51	1.36812
Max Az 3-7 km (s^{-1})	0.0081	0.0080	0.00479	0.0061	0.0054	0.00424
Mean Az 3-7 km (s^{-1})	0.0011	0.0093	0.00058	0.0008	0.0007	0.00045
Max Div 3-7 km (s^{-1})	0.0123	0.0040	0.02205	0.0160	0.0033	0.03142
Mean Div 3-7 km (s^{-1})	0.0008	0.0007	0.00035	0.0006	0.0006	0.00040
Max SW 3-7 km (ms^{-1})	10.7	10.2	4.11833	9.53	9.24	3.12381
Mean SW 3-7 km (ms^{-1})	4.41	4.36	1.13579	4.27	4.03	1.24600
Orientation (deg)	78.4	73.0	41.1831	75.6	76.5	45.1382
Ratio	2.97	2.59	1.14211	2.94	2.73	1.28039
Cell Size (km^2)	1,430	1,050	1338.54	1,290	734	1,421.39

Table C.6. Mean, median, and standard deviations of all radar parameters at the event time for 45 dBZ for warm season tornadic and non-tornadic QLCS cases.

Parameter	Tornadic			Non-tornadic		
45 dBZ	**Mean**	**Median**	**Standard Deviation**	**Mean**	**Median**	**Standard Deviation**
Max Az at 2 km (s^{-1})	0.0061	0.0056	0.003627	0.0053	0.0048	0.00343
Mean Az at 2 km (s^{-1})	-0.0046	-0.0037	0.00326	-0.0037	-0.0034	0.00191
Max Div at 2 km (s^{-1})	0.0061	0.0028	0.01638	0.0058	0.0026	0.01395
Mean Div at 2 km (s^{-1})	-0.0059	-0.0047	0.00951	-0.0061	-0.0036	0.01394
Max SW at 2 km (ms^{-1})	8.00	7.76	2.42578	7.64	7.32	2.49268
Mean SW at 2 km (ms^{-1})	3.36	3.30	0.88954	3.31	3.16	0.96314
Max Az below 3 km (s^{-1})	0.0072	0.0067	0.00407	0.0062	0.0055	0.00416
Mean Az below 3 km (s^{-1})	0.0006	0.0007	0.00054	0.0005	0.0005	0.00052
Max Div below 3 km (s^{-1})	0.0082	0.0034	0.01895	0.0083	0.0028	0.01904
Mean Div below 3 km (s^{-1})	0.0004	0.0004	0.00038	0.0002	0.0002	0.00043
Max SW below 3 km (ms^{-1})	8.85	8.82	2.27359	8.55	8.28	2.60882
Mean SW below 3 km (ms^{-1})	4.00	3.86	0.84734	3.84	3.73	0.95821
Max Az 3-7 km (s^{-1})	0.0083	0.0075	0.00431	0.0063	0.0055	0.00414
Mean Az 3-7 km (s^{-1})	0.0013	0.0012	0.00067	0.0010	0.0009	0.00060
Max Div 3-7 km (s^{-1})	0.0103	0.0041	0.01932	0.0149	0.0033	0.02993
Mean Div 3-7 km (s^{-1})	0.0009	0.0008	0.00037	0.0006	0.0005	0.00039
Max SW 3-7 km (ms^{-1})	10.0	9.91	2.22872	9.42	9.05	2.81005
Mean SW 3-7 km (ms^{-1})	5.00	5.06	1.00816	4.51	4.35	0.87110
Orientation (deg)	79.1	77.0	33.6631	76.1	68.5	41.2788
Ratio	3.05	2.75	1.13106	2.71	2.52	0.91599
Cell Size (km^2)	720	405	678.949	835	514	864.720

Table C.7. Mean, median, and standard deviations of all radar parameters at the post-event time for 35 dBZ for warm season tornadic and non-tornadic QLCS cases.

Parameter	Tornadic			Non-tornadic		
35 dBZ	**Mean**	**Median**	**Standard Deviation**	**Mean**	**Median**	**Standard Deviation**
Max Az at 2 km (s^{-1})	0.0050	0.0038	0.00397	0.0036	0.0028	0.00280
Mean Az at 2 km (s^{-1})	-0.0042	-0.0036	0.00384	-0.0033	-0.0027	0.00269
Max Div at 2 km (s^{-1})	0.0114	0.0028	0.02553	0.0098	0.0021	0.02355
Mean Div at 2 km (s^{-1})	-0.0158	-0.0029	0.03087	-0.0551	-0.0026	4.50012
Max SW at 2 km (ms^{-1})	8.21	7.69	3.31521	7.32	6.72	3.16555
Mean SW at 2 km (ms^{-1})	2.82	2.70	0.89975	2.86	2.61	1.09513
Max Az below 3 km (s^{-1})	0.0061	0.0038	0.00561	0.0041	0.0030	0.00329
Mean Az below 3 km (s^{-1})	0.0003	0.0003	0.00035	0.0003	0.0002	0.00029
Max Div below 3 km (s^{-1})	0.0136	0.0033	0.02737	0.0152	0.0026	0.03057
Mean Div below 3 km (s^{-1})	0.0003	0.0002	0.00051	-0.0001	0.0002	0.00290
Max SW below 3 km (ms^{-1})	9.24	8.60	3.56002	7.94	7.20	3.22534
Mean SW below 3 km (ms^{-1})	3.28	3.30	0.93688	3.31	3.14	1.14676
Max Az 3-7 km (s^{-1})	0.0063	0.0048	0.00531	0.0042	0.0030	0.00343
Mean Az 3-7 km (s^{-1})	0.0007	0.0006	0.00048	0.0005	0.0004	0.00033
Max Div 3-7 km (s^{-1})	0.0158	0.0034	0.02981	0.0159	0.0028	0.03089
Mean Div 3-7 km (s^{-1})	0.0005	0.0004	0.00038	0.0005	0.0004	0.00026
Max SW 3-7 km (ms^{-1})	10.5	9.63	4.90169	8.81	7.74	4.48145
Mean SW 3-7 km (ms^{-1})	3.80	3.81	0.95141	3.55	3.66	1.18827
Orientation (deg)	82.9	75.0	41.0505	75.5	65.0	50.7861
Ratio	2.75	2.35	1.38104	2.60	2.42	0.81014
Cell Size (km^2)	2,760	1,430	3264.81	2,120	847	2992.19

Table C.8. Mean, median, and standard deviations of all radar parameters at the post-event time for 40 dBZ for warm season tornadic and non-tornadic QLCS cases.

Parameter	Tornadic			Non-tornadic		
40 dBZ	**Mean**	**Median**	**Standard Deviation**	**Mean**	**Median**	**Standard Deviation**
Max Az at 2 km (s^{-1})	0.0049	0.0039	0.00368	0.0045	0.0040	0.00284
Mean Az at 2 km (s^{-1})	-0.0040	-0.0037	0.00335	-0.0038	-0.0034	0.00267
Max Div at 2 km (s^{-1})	0.0091	0.0027	0.02202	0.0084	0.0021	0.02015
Mean Div at 2 km (s^{-1})	-0.0142	-0.0035	0.02928	-0.0741	-0.0030	5.23444
Max SW at 2 km (ms^{-1})	7.68	7.00	3.44068	8.08	8.00	2.83447
Mean SW at 2 km (ms^{-1})	2.82	2.73	1.05183	3.29	3.04	1.11177
Max Az below 3 km (s^{-1})	0.0057	0.0048	0.00427	0.0050	0.0040	0.00331
Mean Az below 3 km (s^{-1})	0.0004	0.0003	0.00049	0.0004	0.0003	0.00040
Max Div below 3 km (s^{-1})	0.0096	0.0031	0.02205	0.0143	0.0025	0.02988
Mean Div below 3 km (s^{-1})	0.0003	0.0002	0.00046	0.0002	0.0002	0.00034
Max SW below 3 km (ms^{-1})	8.68	8.00	3.35139	8.61	8.19	2.91753
Mean SW below 3 km (ms^{-1})	3.36	3.34	1.07785	3.82	3.69	1.18306
Max Az 3-7 km (s^{-1})	0.0062	0.0055	0.00528	0.0049	0.0038	0.00366
Mean Az 3-7 km (s^{-1})	0.0009	0.0008	0.00056	0.0007	0.0006	0.00042
Max Div 3-7 km (s^{-1})	0.0132	0.0034	0.02693	0.0146	0.0030	0.03002
Mean Div 3-7 km (s^{-1})	0.0006	0.0006	0.00049	0.0005	0.0005	0.00029
Max SW 3-7 km (ms^{-1})	9.68	8.95	3.22983	9.86	9.08	3.90839
Mean SW 3-7 km (ms^{-1})	4.14	4.23	1.06343	4.30	4.27	1.05926
Orientation (deg)	84.2	78.0	36.0037	77.4	71.0	53.6957
Ratio	3.01	2.59	1.43261	2.94	2.83	1.15210
Cell Size (km^2)	1,390	666	1507.831	1,350	823	1354.51

Table C.9. Mean, median, and standard deviations of all radar parameters at the post-event time for 45 dBZ for warm season tornadic and non-tornadic QLCS cases.

Parameter	Tornadic			Non-tornadic		
45 dBZ	**Mean**	**Median**	**Standard Deviation**	**Mean**	**Median**	**Standard Deviation**
Max Az at 2 km (s^{-1})	0.0058	0.0048	0.00308	0.0050	0.0044	0.00263
Mean Az at 2 km (s^{-1})	-0.0045	-0.0042	0.00310	-0.0038	-0.0033	0.00206
Max Div at 2 km (s^{-1})	0.0094	0.0030	0.02191	0.0081	0.0026	0.01951
Mean Div at 2 km (s^{-1})	-0.0097	-0.0040	0.02014	-0.0815	-0.0030	5.42445
Max SW at 2 km (ms^{-1})	8.11	7.37	3.33496	8.32	7.75	2.50943
Mean SW at 2 km (ms^{-1})	3.41	3.06	1.36656	3.64	3.33	1.12720
Max Az below 3 km (s^{-1})	0.0067	0.0060	0.00336	0.0056	0.0047	0.00310
Mean Az below 3 km (s^{-1})	0.0005	0.0005	0.00059	0.0005	0.0004	0.00066
Max Div below 3 km (s^{-1})	0.0069	0.0031	0.01543	0.0140	0.0033	0.02770
Mean Div below 3 km (s^{-1})	0.0004	0.0003	0.00049	0.0003	0.0002	0.00051
Max SW below 3 km (ms^{-1})	9.19	8.23	3.16881	9.07	8.90	2.61621
Mean SW below 3 km (ms^{-1})	4.05	3.78	1.23450	4.26	3.91	1.14169
Max Az 3-7 km (s^{-1})	0.0078	0.0063	0.00520	0.0055	0.0044	0.00361
Mean Az 3-7 km (s^{-1})	0.0013	0.0011	0.00075	0.0010	0.0009	0.00066
Max Div 3-7 km (s^{-1})	0.0141	0.0048	0.02641	0.0087	0.0031	0.02088
Mean Div 3-7 km (s^{-1})	0.0009	0.0009	0.00056	0.0006	0.0006	0.00032
Max SW 3-7 km (ms^{-1})	10.2	9.69	2.64597	9.59	9.08	2.88162
Mean SW 3-7 km (ms^{-1})	5.04	4.88	1.11737	4.48	4.62	0.93040
Orientation (deg)	83.6	78.0	35.273	72.4	72.0	43.7853
Ratio	3.18	2.58	1.2938	2.65	2.52	0.73898
Cell Size (km^2)	704	414	682.14	774	475	805.702

Table C.10. Mean, median, and standard deviations of all radar parameters at the pre-event time for 35 dBZ for cold season tornadic and non-tornadic QLCS cases.

Parameter	Tornadic			Non-tornadic		
35 dBZ	**Mean**	**Median**	**Standard Deviation**	**Mean**	**Median**	**Standard Deviation**
Max Az at 2 km (s^{-1})	0.0068	0.0054	0.00498	0.0038	0.0024	0.00321
Mean Az at 2 km (s^{-1})	-0.0046	-0.0037	0.00420	-0.0033	-0.0019	0.00378
Max Div at 2 km (s^{-1})	0.0039	0.0025	0.00442	0.0022	0.0017	0.00166
Mean Div at 2 km (s^{-1})	-0.1670	-0.0038	0.94828	-0.0033	-0.0021	0.00342
Max SW at 2 km (ms^{-1})	9.57	8.93	6.23258	7.04	6.50	2.95558
Mean SW at 2 km (ms^{-1})	2.81	2.73	0.76172	2.66	2.54	0.76842
Max Az below 3 km (s^{-1})	0.0077	0.0068	0.00557	0.0052	0.0030	0.00597
Mean Az below 3 km (s^{-1})	0.0005	0.0005	0.00052	0.0004	0.0002	0.00073
Max Div below 3 km (s^{-1})	0.0046	0.0030	0.00530	0.0058	0.0020	0.01522
Mean Div below 3 km (s^{-1})	0.0005	0.0002	0.00144	0.0002	0.0002	0.00033
Max SW below 3 km (ms^{-1})	11.0	10.0	7.48465	8.21	7.30	2.95561
Mean SW below 3 km (ms^{-1})	3.33	3.30	0.86654	3.27	3.15	0.76203
Max Az 3-7 km (s^{-1})	0.0077	0.0070	0.00517	0.0066	0.0038	0.00741
Mean Az 3-7 km (s^{-1})	0.0009	0.0009	0.00068	0.0008	0.0005	0.00091
Max Div 3-7 km (s^{-1})	0.0068	0.0043	0.00746	0.0059	0.0024	0.01282
Mean Div 3-7 km (s^{-1})	0.0006	0.0006	0.00038	0.0005	0.0004	0.00034
Max SW 3-7 km (ms^{-1})	10.7	9.50	5.34205	9.02	7.53	3.91535
Mean SW 3-7 km (ms^{-1})	3.93	3.93	1.30478	3.49	3.23	1.02511
Orientation (deg)	56.2	50.0	28.8373	58.6	54.0	33.23440
Ratio	3.44	3.45	1.30231	3.41	2.71	1.57553
Cell Size (km^2)	1,570	1,100	1445.75	1,810	521	3,039.875

Table C.11. Mean, median, and standard deviations of all radar parameters at the pre-event time for 40 dBZ for cold season tornadic and non-tornadic QLCS cases.

Parameter	Tornadic			Non-tornadic		
40 dBZ	**Mean**	**Median**	**Standard Deviation**	**Mean**	**Median**	**Standard Deviation**
Max Az at 2 km (s^{-1})	0.0061	0.0054	0.00397	0.0040	0.0023	0.00324
Mean Az at 2 km (s^{-1})	-0.0040	-0.0031	0.00320	-0.0038	0.0034	0.00360
Max Div at 2 km (s^{-1})	0.0035	0.0026	0.00419	0.0021	0.0019	0.00123
Mean Div at 2 km (s^{-1})	-0.0058	-0.0032	0.01568	-0.0033	-0.0028	0.00219
Max SW at 2 km (ms^{-1})	8.09	7.65	2.73535	7.66	7.30	2.82958
Mean SW at 2 km (ms^{-1})	2.90	2.71	1.05558	2.96	2.93	0.85183
Max Az below 3 km (s^{-1})	0.0066	0.0064	0.00438	0.0050	0.0028	0.00485
Mean Az below 3 km (s^{-1})	0.0007	0.0006	0.00065	0.0004	0.0003	0.00047
Max Div below 3 km (s^{-1})	0.0518	0.0034	0.28906	0.0025	0.0022	0.00138
Mean Div below 3 km (s^{-1})	0.0004	0.0003	0.00056	0.0002	0.0001	0.00029
Max SW below 3 km (ms^{-1})	9.45	8.63	5.19957	8.37	8.30	2.85766
Mean SW below 3 km (ms^{-1})	3.47	3.37	1.11983	3.56	3.63	0.79471
Max Az 3-7 km (s^{-1})	0.0074	0.0064	0.00490	0.0068	0.0049	0.00666
Mean Az 3-7 km (s^{-1})	0.0012	0.0011	0.00089	0.0009	0.0007	0.00081
Max Div 3-7 km (s^{-1})	0.0057	0.0042	0.00640	0.0063	0.0034	0.01479
Mean Div 3-7 km (s^{-1})	0.0007	0.0007	0.00051	0.0006	0.0005	0.00047
Max SW 3-7 km (ms^{-1})	9.38	8.59	5.32844	9.78	9.50	3.76039
Mean SW 3-7 km (ms^{-1})	3.99	3.95	1.34833	3.94	3.89	1.11011
Orientation (deg)	64.8	57.0	32.1050	67.6	63.0	34.80901
Ratio	3.34	2.91	1.35686	3.61	3.23	1.70171
Cell Size (km^2)	620	394	571.319	1,010	595	1,093.97

Table C.12. Mean, median, and standard deviations of all radar parameters at the pre-event time for 45 dBZ for cold season tornadic and non-tornadic QLCS cases.

Parameter	Tornadic			Non-tornadic		
45 dBZ	**Mean**	**Median**	**Standard Deviation**	**Mean**	**Median**	**Standard Deviation**
Max Az at 2 km (s^{-1})	0.0071	0.0064	0.00431	0.0046	0.0032	0.00354
Mean Az at 2 km (s^{-1})	-0.0051	0.0036	0.00356	-0.0027	-0.0028	0.00132
Max Div at 2 km (s^{-1})	0.0044	0.0030	0.00538	0.0022	0.0017	0.00141
Mean Div at 2 km (s^{-1})	-0.0082	-0.0032	0.02118	-0.0037	-0.0035	0.00240
Max SW at 2 km (ms^{-1})	7.66	7.92	1.80180	7.17	6.50	2.91532
Mean SW at 2 km (ms^{-1})	2.93	2.71	1.01387	3.00	3.19	0.85411
Max Az below 3 km (s^{-1})	0.0078	0.0085	0.00417	0.0051	0.0043	0.00358
Mean Az below 3 km (s^{-1})	0.0008	0.0008	0.00098	0.0006	0.0005	0.00062
Max Div below 3 km (s^{-1})	0.0050	0.0036	0.00533	0.0027	0.0022	0.00161
Mean Div below 3 km (s^{-1})	0.0004	0.0003	0.00047	0.00008	0.00008	0.00040
Max SW below 3 km (ms^{-1})	8.48	8.69	1.58680	8.12	7.94	2.89061
Mean SW below 3 km (ms^{-1})	3.61	3.45	0.92457	3.60	3.94	0.83351
Max Az 3-7 km (s^{-1})	0.0076	0.0081	0.00483	0.0058	0.0059	0.00343
Mean Az 3-7 km (s^{-1})	0.0014	0.0013	0.00119	0.0011	0.0012	0.00056
Max Div 3-7 km (s^{-1})	0.0060	0.0045	0.00638	0.0030	0.0032	0.00140
Mean Div 3-7 km (s^{-1})	0.0008	0.0008	0.00053	0.0007	0.0008	0.00038
Max SW 3-7 km (ms^{-1})	7.82	8.79	3.40316	8.99	9.01	3.69209
Mean SW 3-7 km (ms^{-1})	3.84	4.14	1.86258	4.33	4.50	1.07876
Orientation (deg)	62.5	60.5	28.3317	58.3	54.0	24.8351
Ratio	3.38	3.35	1.46574	4.18	4.53	1.54068
Cell Size (km^2)	427	265	379.729	472	372	378.165

Table C.13. Mean, median, and standard deviations of all radar parameters at the event time for 35 dBZ for cold season tornadic and non-tornadic QLCS cases.

Parameter	Tornadic			Non-tornadic		
35 dBZ	**Mean**	**Median**	**Standard Deviation**	**Mean**	**Median**	**Standard Deviation**
Max Az at 2 km (s^{-1})	0.0071	0.0059	0.00562	0.0046	0.0033	0.00423
Mean Az at 2 km (s^{-1})	-0.0058	-0.0039	0.00601	-0.0034	-0.0025	0.00319
Max Div at 2 km (s^{-1})	0.0077	0.0043	0.14261	0.0025	0.0021	0.00160
Mean Div at 2 km (s^{-1})	-0.0076	-0.0047	0.01652	-0.0043	-0.0024	0.00546
Max SW at 2 km (ms^{-1})	9.35	9.00	3.21561	7.56	7.06	3.20219
Mean SW at 2 km (ms^{-1})	2.88	2.78	0.79956	2.76	2.70	0.89272
Max Az below 3 km (s^{-1})	0.0080	0.0066	0.00557	0.0053	0.0037	0.00486
Mean Az below 3 km (s^{-1})	0.0005	0.0004	0.00045	0.0005	0.0003	0.00060
Max Div below 3 km (s^{-1})	0.0052	0.0048	0.00296	0.0050	0.0026	0.01288
Mean Div below 3 km (s^{-1})	0.0002	0.0002	0.00034	0.0003	0.0002	0.00027
Max SW below 3 km (ms^{-1})	9.99	10.2	3.24977	8.87	8.47	3.21770
Mean SW below 3 km (ms^{-1})	3.45	3.22	0.82834	3.35	3.25	0.90656
Max Az 3-7 km (s^{-1})	0.0090	0.0080	0.00629	0.0065	0.0041	0.00670
Mean Az 3-7 km (s^{-1})	0.0010	0.0009	0.00049	0.0008	0.0005	0.00089
Max Div 3-7 km (s^{-1})	0.0090	0.0047	0.00132	0.0082	0.0031	0.01762
Mean Div 3-7 km (s^{-1})	-0.0009	0.0006	0.00861	0.0006	0.0006	0.00035
Max SW 3-7 km (ms^{-1})	11.1	10.5	3.66960	8.88	8.08	3.36626
Mean SW 3-7 km (ms^{-1})	4.11	4.12	1.35680	3.58	3.55	1.14809
Orientation (deg)	59.9	62.0	23.98014	63.6	57.0	40.10101
Ratio	3.59	3.15	1.85656	3.45	2.92	1.54394
Cell Size (km^2)	2,120	1,260	2,496.43	2,090	786	3,378.097

Table C.14. Mean, median, and standard deviations of all radar parameters at the event time for 40 dBZ for cold season tornadic and non-tornadic QLCS cases.

Parameter	Tornadic			Non-tornadic		
40 dBZ	**Mean**	**Median**	**Standard Deviation**	**Mean**	**Median**	**Standard Deviation**
Max Az at 2 km (s^{-1})	0.0052	0.0048	0.00334	0.0037	0.0022	0.00327
Mean Az at 2 km (s^{-1})	-0.0045	-0.0031	0.00514	-0.0030	-0.0020	0.00308
Max Div at 2 km (s^{-1})	0.0047	0.0025	0.00966	0.0022	0.0019	0.00157
Mean Div at 2 km (s^{-1})	-0.0039	-0.0031	0.00321	-0.0037	-0.0027	0.00421
Max SW at 2 km (ms^{-1})	7.77	7.17	3.03715	7.36	7.82	2.80678
Mean SW at 2 km (ms^{-1})	2.93	2.90	0.91941	2.89	2.73	0.99356
Max Az below 3 km (s^{-1})	0.0063	0.0059	0.00380	0.0042	0.0031	0.00343
Mean Az below 3 km (s^{-1})	0.0006	0.0004	0.00057	0.0003	0.0003	0.00042
Max Div below 3 km (s^{-1})	0.0042	0.0033	0.00297	0.0025	0.0021	0.00167
Mean Div below 3 km (s^{-1})	0.0003	0.0002	0.00040	0.0002	0.0001	0.00024
Max SW below 3 km (ms^{-1})	8.47	8.58	2.91476	8.35	8.40	3.02245
Mean SW below 3 km (ms^{-1})	3.46	3.59	1.00937	3.49	3.36	1.02668
Max Az 3-7 km (s^{-1})	0.0076	0.0061	0.00571	0.0047	0.0033	0.00430
Mean Az 3-7 km (s^{-1})	0.0011	0.0010	0.00064	0.0007	0.0005	0.00052
Max Div 3-7 km (s^{-1})	0.0045	0.0036	0.00325	0.0032	0.0025	0.00250
Mean Div 3-7 km (s^{-1})	-0.0006	0.0006	0.00931	0.0006	0.0005	0.00042
Max SW 3-7 km (ms^{-1})	9.25	8.90	3.24104	8.28	7.56	3.25265
Mean SW 3-7 km (ms^{-1})	4.08	3.98	1.26930	3.81	3.56	1.17696
Orientation (deg)	62.4	61.0	23.76793	67.9	58.0	32.5652
Ratio	3.34	2.96	1.6089	3.21	2.61	1.50273
Cell Size (km^2)	715	444	688.611	764	425	760.438

Table C.15. Mean, median, and standard deviations of all radar parameters at the event time for 45 dBZ for cold season tornadic and non-tornadic QLCS cases.

Parameter	Tornadic			Non-tornadic		
45 dBZ	**Mean**	**Median**	**Standard Deviation**	**Mean**	**Median**	**Standard Deviation**
Max Az at 2 km (s^{-1})	0.0053	0.0053	0.00218	0.0038	0.0021	0.00305
Mean Az at 2 km (s^{-1})	-0.0047	-0.0032	0.00572	-0.0040	0.0027	0.00419
Max Div at 2 km (s^{-1})	0.0036	0.0037	0.00175	0.0018	0.0017	0.00118
Mean Div at 2 km (s^{-1})	-0.0048	-00040	0.00334	-0.0048	-0.0031	0.00582
Max SW at 2 km (ms^{-1})	8.08	8.25	2.59487	7.76	7.65	2.80237
Mean SW at 2 km (ms^{-1})	3.20	3.36	0.87042	3.16	3.17	1.13746
Max Az below 3 km (s^{-1})	0.0068	0.0066	0.00268	0.0040	0.0021	0.00318
Mean Az below 3 km (s^{-1})	0.0008	0.0007	0.00050	0.0004	0.0003	0.00054
Max Div below 3 km (s^{-1})	0.0042	0.0042	0.00189	0.0021	0.0021	0.00124
Mean Div below 3 km (s^{-1})	0.0004	0.0004	0.00054	0.0001	0.00009	0.00039
Max SW below 3 km (ms^{-1})	8.98	9.20	2.13171	8.71	8.28	3.38106
Mean SW below 3 km (ms^{-1})	3.87	3.87	0.75949	3.76	3.97	1.02215
Max Az 3-7 km (s^{-1})	0.0084	0.0075	0.00604	0.0053	0.0040	0.00544
Mean Az 3-7 km (s^{-1})	0.0015	0.0014	0.00059	0.0010	0.0006	0.00066
Max Div 3-7 km (s^{-1})	0.0048	0.0046	0.00184	0.0028	0.0029	0.00112
Mean Div 3-7 km (s^{-1})	0.0010	0.0008	0.00051	0.0007	0.0008	0.00035
Max SW 3-7 km (ms^{-1})	9.71	9.51	2.92824	9.43	9.25	3.41248
Mean SW 3-7 km (ms^{-1})	4.70	4.78	0.95380	4.52	4.60	1.11104
Orientation (deg)	59.9	55.0	20.0797	80.7	66.0	44.94547
Ratio	3.29	2.62	1.76918	3.60	2.89	2.01302
Cell Size (km^2)	463	368	299.982	433	285	379.193

Table C.16. Mean, median, and standard deviations of all radar parameters at the post-event time for 35 dBZ for cold season tornadic and non-tornadic QLCS cases.

Parameter	Tornadic			Non-tornadic		
35 dBZ	**Mean**	**Median**	**Standard Deviation**	**Mean**	**Median**	**Standard Deviation**
Max Az at 2 km (s^{-1})	0.0047	0.0037	0.00356	0.0040	0.0028	0.00496
Mean Az at 2 km (s^{-1})	-0.0042	-0.0036	0.00354	-0.0032	-0.0021	00.0034
Max Div at 2 km (s^{-1})	0.0091	0.0033	0.02036	0.0022	0.0021	0.00160
Mean Div at 2 km (s^{-1})	-0.0057	-0.0031	0.01247	-0.0041	-0.0031	0.00584
Max SW at 2 km (ms^{-1})	8.68	7.67	4.61814	6.94	6.80	3.09506
Mean SW at 2 km (ms^{-1})	2.78	2.80	0.68474	2.62	2.51	1.09036
Max Az below 3 km (s^{-1})	0.0057	0.0054	0.00393	0.0049	0.0042	0.00511
Mean Az below 3 km (s^{-1})	0.0004	0.0004	0.00043	0.0004	0.0002	0.00061
Max Div below 3 km (s^{-1})	0.0078	0.0036	0.01545	0.0027	0.0023	0.00166
Mean Div below 3 km (s^{-1})	0.0003	0.0003	0.00027	0.0002	0.0002	0.00025
Max SW below 3 km (ms^{-1})	9.40	8.14	4.59010	8.64	8.30	3.10860
Mean SW below 3 km (ms^{-1})	3.32	3.39	0.77105	3.37	3.35	1.18791
Max Az 3-7 km (s^{-1})	0.0070	0.0050	0.00653	0.0055	0.0036	0.00514
Mean Az 3-7 km (s^{-1})	0.0082	0.0065	0.00066	0.0006	0.0005	0.00056
Max Div 3-7 km (s^{-1})	0.0071	0.0049	0.00888	0.0032	0.0031	0.00184
Mean Div 3-7 km (s^{-1})	0.0006	0.0007	0.00031	0.0006	0.0006	0.00038
Max SW 3-7 km (ms^{-1})	11.6	10.4	6.04833	9.28	8.26	5.02134
Mean SW 3-7 km (ms^{-1})	3.72	3.69	1.16711	3.28	3.26	1.17505
Orientation (deg)	55.7	58.0	21.94479	65.8	60.5	33.01242
Ratio	3.60	3.17	1.83676	3.20	3.00	1.27470
Cell Size (km^2)	1,860	1,010	2,560.43	1,980	687	3,594.688

Table C.17. Mean, median, and standard deviations of all radar parameters at the post-event time for 40 dBZ for cold season tornadic and non-tornadic QLCS cases.

Parameter	Tornadic			Non-tornadic		
40 dBZ	**Mean**	**Median**	**Standard Deviation**	**Mean**	**Median**	**Standard Deviation**
Max Az at 2 km (s^{-1})	0.0048	0.0038	0.00321	0.0035	0.0030	0.00229
Mean Az at 2 km (s^{-1})	-0.0038	-0.0029	0.00311	-0.0028	-0.0022	0.00200
Max Div at 2 km (s^{-1})	0.0032	0.0029	0.00288	0.0019	0.0018	0.00113
Mean Div at 2 km (s^{-1})	-0.0056	-0.0029	0.01231	-0.0030	-0.0026	0.00216
Max SW at 2 km (ms^{-1})	7.84	7.11	3.59882	7.09	6.75	2.58694
Mean SW at 2 km (ms^{-1})	2.94	2.94	0.65973	2.85	2.75	0.98881
Max Az below 3 km (s^{-1})	0.0060	0.0042	0.00392	0.0045	0.0048	0.00237
Mean Az below 3 km (s^{-1})	0.0006	0.0005	0.00046	0.0005	0.0004	0.00049
Max Div below 3 km (s^{-1})	0.0042	0.0034	0.00374	0.0024	0.0023	0.00126
Mean Div below 3 km (s^{-1})	0.0003	0.0003	0.00035	0.0003	0.0003	0.00029
Max SW below 3 km (ms^{-1})	8.65	7.55	3.63015	8.37	8.30	2.71005
Mean SW below 3 km (ms^{-1})	3.56	3.58	0.74638	3.51	3.63	1.03950
Max Az 3-7 km (s^{-1})	0.0076	0.0053	0.00651	0.0047	0.0042	0.00289
Mean Az 3-7 km (s^{-1})	0.0011	0.0010	0.00067	0.0008	0.0006	0.00057
Max Div 3-7 km (s^{-1})	0.0051	0.0047	0.00379	0.0028	0.0030	0.00159
Mean Div 3-7 km (s^{-1})	0.0008	0.0008	0.00038	0.0006	0.0006	0.00039
Max SW 3-7 km (ms^{-1})	9.48	8.08	4.41121	8.14	7.30	3.14088
Mean SW 3-7 km (ms^{-1})	4.11	4.17	0.97787	3.61	3.70	1.14425
Orientation (deg)	60.7	60.0	25.58737	68.9	65.0	28.1622
Ratio	3.93	3.68	1.86676	3.50	3.74	1.10292
Cell Size (km^2)	834	475	932.738	771	539	723.299

Table C.18. Mean, median, and standard deviations of all radar parameters at the post-event time for 45 dBZ for cold season tornadic and non-tornadic QLCS cases.

Parameter	Tornadic			Non-tornadic		
45 dBZ	**Mean**	**Median**	**Standard Deviation**	**Mean**	**Median**	**Standard Deviation**
Max Az at 2 km (s^{-1})	0.0048	0.0041	0.00240	0.0046	0.0050	0.00185
Mean Az at 2 km (s^{-1})	-0.0038	-0.0032	0.00206	-0.0038	-0.0030	0.00245
Max Div at 2 km (s^{-1})	0.0033	0.0026	0.00314	0.0021	0.0019	0.00069
Mean Div at 2 km (s^{-1})	-0.0047	-0.0038	0.00436	-0.0033	-0.0025	0.00183
Max SW at 2 km (ms^{-1})	6.87	7.20	1.86638	7.53	7.28	2.86111
Mean SW at 2 km (ms^{-1})	2.91	3.09	0.87285	2.94	3.04	0.82084
Max Az below 3 km (s^{-1})	0.0065	0.0051	0.00359	0.0052	0.0055	0.00191
Mean Az below 3 km (s^{-1})	0.0007	0.0005	0.00063	0.0006	0.0006	0.00066
Max Div below 3 km (s^{-1})	0.0042	0.0033	0.00326	0.0027	0.0028	0.00073
Mean Div below 3 km (s^{-1})	0.0005	0.0004	0.00047	0.0004	0.0004	0.00042
Max SW below 3 km (ms^{-1})	7.92	7.71	1.99757	8.38	8.30	2.68647
Mean SW below 3 km (ms^{-1})	3.62	3.81	1.01506	3.75	3.74	0.88153
Max Az 3-7 km (s^{-1})	0.0083	0.0065	0.00578	0.0058	0.0049	0.00240
Mean Az 3-7 km (s^{-1})	0.0014	0.0013	0.00087	0.0013	0.0011	0.00073
Max Div 3-7 km (s^{-1})	0.0051	0.0045	0.00297	0.0034	0.0030	0.00122
Mean Div 3-7 km (s^{-1})	0.0010	0.0009	0.00047	0.0008	0.0007	0.00037
Max SW 3-7 km (ms^{-1})	9.13	9.21	2.56658	8.90	8.82	3.05036
Mean SW 3-7 km (ms^{-1})	4.23	4.34	1.11666	4.51	4.77	1.04780
Orientation (deg)	60.9	61.0	22.35823	62.3	61.0	22.2475
Ratio	3.42	3.09	1.69024	3.66	3.15	1.42752
Cell Size (km^2)	420	367	238.716	369	291	202.515

References

Atkins, N. T., and M. St. Laurent, 2009a: Bow Echo Mesovortices. Part I: Processes That Influence Their Damaging Potential. *Mon. Wea. Rev.*,**137**, 1497–1513.

Atkins, N. T., and M. St. Laurent, 2009b: Bow Echo Mesovortices. Part II: Their Genesis. *Mon. Wea. Rev.*, **137**, 1514–1532.

Atkins, N. T., C. S. Bouchard, R. W. Przybylinski, R. J. Trapp, G. Schmocker, 2005: Damaging Surface Wind Mechanisms within the 10 June 2003 Saint Louis Bow Echo during BAMEX. *Mon. Wea. Rev.*, **133**, 2275–2296.

Atkins, N. T., J. M. Arnott, R. W. Przybylinski, R. A. Wolf, and B. D. Ketcham, 2004: Vortex structure and evolution within bow echoes. Part I: Single-Doppler and damage analysis of the 29 June 1998 derecho. *Mon. Wea. Rev.*, **132**, 2224–2242.

DeWald, V. L., and T. W. Funk, 2000: WSR-88D reflectivity and velocity trends of a damaging squall line event on 20 April 1996 over south-central Indiana and central Kentucky. Preprints, *20th Conf. on Severe Local Storms*, Orlando, FL, Amer. Meteor. Soc., 177–180.

Doswell, C. A., H. E. Brooks, M. P. Kay, 2005: Climatological Estimates of Daily Local Nontornadic Severe Thunderstorm Probability for the United States. *Wea. Forecasting*, **20**, 577–595.

Droegemeier, K. K., 1985: The numerical simulation of thunderstorm outflow dynamics. Ph.D. thesis. University of Illinois at Urbana-Champaign, 659pp. [Available from University Microfilms, Ann Arbor, MI, Order No. AAD86-00166.]

Duda, J. D., W. A. Gallus, 2010: Spring and Summer Midwestern Severe Weather Reports in Supercells Compared to Other Morphologies.*Wea. Forecasting*, **25**, 190–206.

Emanuel, K. A., 1986: Overview and definition of mesoscale meteorology. *Mesoscale Meteorology and Forecasting*, P. S. Ray, Ed., Amer. Meteor. Soc., 1–17.

Fovell, R. G., and P. S. Dailey, 1995: The temporal behavior of numerically simulated multicell-type storms. Part I: Modes of behavior. *J. Atmos. Sci.*, **52,** 2073–2095.

Funk, T. W., K. E. Darmofal, J. D. Kirkpatrick, V. L. Dewald, R. W. Przybylinski, G. K. Schmocker, and Y.-J Lin, 1999: Storm reflectivity and mesocyclone evolution associated with the 15 April 1994 squall line over Kentucky and southern Indiana. *Wea. Forecasting*, **14,** 976–993.

Fujita, T. T.,1979: Objective, operation, and results of Project NIMROD. Preprints, *11th Conf. on Severe Local Storms*, Kansas City, MO, Amer. Meteor. Soc., 259–266.

Gallus, W. A., N. A. Snook, and E. V. Johnson, 2008: Spring and Summer Severe Weather Reports over the Midwest as a Function of Convective Mode: A Preliminary Study. *Wea. Forecasting*, **23**, 101–113.

Grams, J. S., R. L. Thompson, D. V. Snively, J. A. Prentice, G. M. Hodges, L. J. Reames, 2012: A Climatology and Comparison of Parameters for Significant Tornado Events in the United States. *Wea. Forecasting*, **27**, 106–123.

Houze, R. A., Jr., 1993: *Cloud Dynamics.* Academic Press, 573 pp.

Houze, R. A., Jr., 2004: Mesoscale convective systems, *Rev. Geophys.*, **42**, RG4003.

Houze, R. A., Jr., B. F. Smull, and P. Dodge, 1990: Mesoscale organization of springtime rainstorms in Oklahoma. *Mon. Wea. Rev.,* **118,** 613– 654.

Houze, R. A., Jr., S. A. Rutledge, M. I. Biggerstaff, and B. F. Smull, 1989: Interpretation of Doppler weather radar displays of midlatitudes mesoscale convective systems. *Bull. Amer. Meteor. Soc.,* **70,** 608–619.

Klemp, J. B., 1987: Dynamics of tornadic thunderstorms. *Annu. Rev. Fluid Mech.,* **19,** 369–402.

Knupp, K. R., 2000: Narrow streaks of "straight-line" wind damage. Do tornadoes or microbursts produce them? Preprints, *20th Conf. on Severe Local Storms,* Orlando, FL, Amer. Meteor. Soc., 644–645.

Markowski, P., Y. Richardson 2010: Mesoscale Convective Systems. *In Mesoscale Meteorology in Midlatitudes,* Wiley-Blackwell, Ed., John Wiley & Sons, Ltd, 245-265.

Moncrieff, M. W., 1992: Organized convective systems: Archetypal dynamical models, mass and momentum flux theory, and parameterization. *Quart. J. Roy. Meteor. Soc.,* **118,** 819–850.

Newton, C. W., and J. C. Fankhauser, 1964: On the movements of convective storms, with emphasis on size discrimination in relation to waterbudget requirements. *J. Appl. Meteor.,* **3,** 651–668.

Orlanski, I., 1975: A rational subdivision of scales for atmospheric processes. *Bull. Amer. Meteor. Soc.*, **56**, 527–530.

Parker, M. D., 1999: May 1996 and May 1997 linear mesoscale convective systems of the Central Plains: Synoptic meteorology and a reflectivity-based taxonomy. Dept. of Atmospheric Science Paper No. 675, Colorado State University, Fort

Collins, CO, 185 pp. [Available from Dept. of Atmospheric Science, Colorado State University, Fort Collins, CO 80523.]

Parker, M. D., and R. H. Johnson, 2000: Organizational modes of midlatitude mesoscale convective systems. *Mon. Wea. Rev.*, **128**, 3413–3436.

Parker, M. D., and R. H. Johnson, 2004: Structures and dynamics of quasi-2D mesoscale convective systems. *J. Atmos. Sci.*, **61**, 545–567.

Pettet, C. R., and R. H. Johnson, 2003: Airflow and precipitation structure of two leading stratiform mesoscale convective systems determined from operational datasets. *Wea. Forecasting,* **18,** 685–699.

Rotunno, R., and J. B. Klemp, 1985: On the rotation and propagation of simulated supercell thunderstorms. *J. Atmos. Sci.,* **42,** 271–292.

Rotunno, R., J. B. Klemp, and M. L. Weisman, 1988: A Theory for Strong, Long-Lived Squall Lines. *J. Atmos. Sci.*, **45**, 463–485.

Schiesser, H. H., R. A. Houze Jr., and H. Huntrieser, 1995: The mesoscale structure of severe precipitation systems in Switzerland. *Mon. Wea. Rev.*, **123,** 2070–2097.

Smith, B. T., R. L. Thompson, J. S. Grams, C. Broyles, and H. E. Brooks, 2012: Convective modes for significant thunderstorms in the contiguous United States. Part I: Storm classification and climatology. *Wea. Forecasting*, **27**, 1114-1135.

Thorpe, A. J., M. J. Miller and M. W. Moncrieff, 1982: Two-dimensional convection in nonconstant shear: a model of midlatitude squall lines. *Quart*. J. Roy, Meteor. Soc., **108**, 739-762.

Trapp, R. J., 1999: Observations of nontornadic low-level mesocyclones and attendant tornadogenesis failure during VORTEX. *Mon. Wea. Rev.*, **127,** 1693–1705.

Trapp, R. J., E. D. Mitchell, G. A. Tipton, D. W. Effertz, A. I. Watson, D. L. Andra Jr., and M. A. Magsig, 1999: Descending and nondescending tornadic vortex signatures detected by WSR-88Ds. *Wea. Forecasting,* **14,** 625–639.

Trapp, R. J., and M. L. Weisman, 2003: Low-level mesovortices within squall lines and bow echoes. Part II: Their genesis and implications. *Mon. Wea. Rev.*, **131**, 2804–2823.

Trapp, R. J., D. M. Wheatley, N. T. Atkins, R. W. Przybylinski, and R. Wolf, 2006: Buyer beware: Some words of caution on the use of severe wind reports in postevent assessment and research. *Wea. Forecasting*, 21, 408–415.

Trapp, R. J., S. A. Tessendorf, E. S. Godfrey, and H. E. Brooks, 2005: Tornadoes from squall lines and bow echoes. Part I: Climatological distribution. *Wea. Forecasting*, **20**, 23–34.

Wakimoto, R. M., and H. Cai, 2000: Analysis of a nontornadic storm during VORTEX 95. *Mon. Wea. Rev.,* **128,** 565–592.

Weisman, M. L., 1992: The role of convectively generated rear-inflow jets in the evolution of long-lived meso-convective systems. *J. Atmos. Sci.* 49, 1827-1847.

Weisman, M. L., 1993: The Genesis of Severe, Long-Lived Bow Echoes. *J. Atmos. Sci.*, **50**, 645–670.

Weisman, M. L., R. J. Trapp, 2003: Low-Level Mesovortices within Squall Lines and Bow Echoes. Part I: Overview and Dependence on Environmental Shear. *Mon. Wea. Rev.*, **131**, 2779–2803.

Weiss, S. J., J. A. Hart, and P. R. Janish, 2002: An examination of severe thunderstorm wind report climatology: 1970–1999. Preprints, 21st Conf. Severe Local Storms, San Antonio, TX, Amer. Meteor. Soc., 446–449.